Resource allocation in multicarrier cognitive radio networks

Xin Jin

THESE DE DOCTORAT CONJOINT TELECOM SUDPARIS et L'UNIVERSITE PIERRE ET MARIE CURIE

Spécialité :
Télécommunications et Informatique

Ecole Doctorale EDITE :
Informatique, Télécommunications et Electronique de Paris

Présentée par

Xin Jin

Pour obtenir le grade de

DOCTEUR DE TELECOM SUDPARIS

Allocation des Ressources dans les Réseaux Radio Cognitives basée sur la Modulation Multi-porteuses

13 Juin 2014

Jury composé de :

Laurent Clavier	Rapporteur	Professeur, Télécom Lille 1, France
Mourad Gueroui	Rapporteur	Maître de Conférences, HDR, UVSQ, France
Marcelo Dias de Amorim	Président	Professeur, UPMC-LIP6-EDITE, France
Michel Terre	Examinateur	Professeur, CNAM-EDITE, France
Salah Eddine Elayoubi	Examinateur	Maître de Conférences, Orange labs, France
Mohamad Assaad	Examinateur	Maître de Conférences, SUPELEC, France
Abdelwaheb Marzouki	Encadrant	Maître de Conférences, Télécom SudParis, France
Djamal Zeghlache	Directeur de Thèse	Professeur, Télécom SudParis, France

Thèse n° 2014TELE0014

THESIS OF JOINT DOCTORATE OF TELECOM SUDPARIS AND PIERRE & MARIE CURIE UNIVERSITY

Speciality:
Telecommunications and Information Technology

Doctoral School EDITE:
Computer Science, Telecommunications and Electronics (Paris)

presented by

Xin Jin

To obtain the Degree of

DOCTORATE OF TELECOM SUDPARIS

Resource Allocation in Multicarrier Cognitive Radio Networks

13 June 2014

Commitee:

Laurent Clavier	Rapporteur	Professeur, Télécom Lille 1, France
Mourad Gueroui	Rapporteur	Maître de Conférences, HDR, UVSQ, France
Marcelo Dias de Amorim	Président	Professeur, UPMC-LIP6-EDITE, France
Michel Terre	Examinateur	Professeur, CNAM-EDITE, France
Salah Eddine Elayoubi	Examinateur	Maître de Conférences, Orange labs, France
Mohamad Assaad	Examinateur	Maître de Conférences, SUPELEC, France
Abdelwaheb Marzouki	Encadrant	Maître de Conférences, Télécom SudParis, France
Djamal Zeghlache	Directeur de Thèse	Professeur, Télécom SudParis, France

Thèse n° **2014TELE0014**

Acknowledgements

I deeply acknowledge Professor Djamal Zeghlache, my thesis director, Dr. Abdelwaheb Marzouki, my thesis advisor and Mrs. Valérie Mateus, for all of their kindness and help in these years.

I express my gratitude to all my colleagues in the department RS2M. Their comments, suggestions and kindness also help me to complete this work.

Finally, I would like to thank my parents for their love and encouragement.

Thesis Publications

- Xin Jin, Abdelwaheb Marzouki, Djamal Zeghlache, and Mathew Goonewardena, "Resource Allocation and Routing in MIMO-WPM Cognitive Radio Ad-Hoc Networks," in *Proc. IEEE Vehicular Technology Conference (VTC)-Fall*, Quebec City, Canada, Sep. 2012, pp. 1-5.

- Xin Jin, Abdelwaheb Marzouki, Li-Chuan Tseng, Mathew Goonewardena and Djamal Zeghlache, "Adaptive Resource Allocation Using Kalman Filters in Busy and Idle Bands for WPM-based Cognitive Radio Systems," in *Proc. IEEE Symposium on Communications and Vehicular Technology (SCVT)*, Ghent, Belgium, Nov. 2011, pp. 1-5.

- Mathew Goonewardena, Xin Jin, Wessam Ajib, and Halima Elbiazey, "Competition vs. Cooperation: A Game-Theoretic Decision Analysis for MIMO HetNets," in *Proc. IEEE International Conference on Communications (ICC)*, Sydney, Australia, Jun. 2014, accepted.

- Li-Chuan Tseng, Xin Jin, Abdelwaheb Marzouki, and ChingYao Huang, "Downlink Scheduling in Network MIMO Using Two-Stage Channel State Feedback," in *Proc. IEEE Vehicular Technology Conference (VTC)-Fall*, Quebec City, Canada, Sep. 2012, pp. 1-5.

- Abdelwaheb Marzouki and Xin Jin, "Precoder Design for Orthogonal Space-Time Block Coding based Cognitive Radio with Polarized Antennas," in *Proc. IEEE International Symposium on Wireless Communication Systems (ISWCS)*, Paris, France, Aug. 2012, pp. 691-695.

Abstract

In view of the wide usage of multicarrier modulation in wireless communications and the prominent contribution of Cognitive Radio (CR) to deal with critical shortage of spectrum resource, we focus on multicarrier based cognitive radio networks to investigate general resource allocation issues: subcarrier allocation, power allocation, routing, and beamforming in this thesis.

We investigate two types of multicarrier modulation: Wavelet-based Orthogonal Frequency Division Multiplexing (WOFDM) and Fourier-based Orthogonal Frequency Division Multiplexing (OFDM). WOFDM adopts Wavelet Packet Modulation (WPM). Compared with fourier-based OFDM, wavelet-based OFDM achieves much lower side lobe in the transmitted signal. Wavelet-based OFDM excludes Cyclic Prefix (CP) which is used in fourier-based OFDM systems. Wavelet-based OFDM turns to exploit equalization to combat Inter-Symbol Interference (ISI). We evaluate the performance of WOFDM under different channel conditions. We compare the performance of wavelet-based OFDM using equalization in the time domain to that of fourier-based OFDM with CP and the equalization in the frequency domain.

In chapter 3, we consider the resource allocation and routing problem in multi-hop Multiple-Input Multiple-Output (MIMO) WPM CR ad-hoc networks. We comply with four principles to design our resource allocation scheme with the goal to maximize the capacity of entire network. First, Primary Users (PUs) have higher priority to access to the subcarrier in private bands, while PUs and Secondary Users (SUs) have the equal opportunity in public bands. Second, the MIMO channel of each link on each subcarrier in each time slot is decomposed by Block Diagonal Geometric Mean Decomposition (BD-GMD) into multiple sub-channels with identical gains. In addition, the sub-channel gain of one link is determined by the channel matrices of all links sharing the same source node on the same subcarrier in the same time slot. Third, PUs have the privilege of higher Signal to Interference and Noise Ratio (SINR) threshold for the successful decoding in private bands, but PUs and SUs have the same SINR threshold in public bands. Fourth, the interference caused by one link to all other links having the same destination node should be avoided, moreover, the power of all other links is not assumed to be known but also need to be allocated at the same time. Based on our proposed resource allocation scheme, we investigate a multicast routing strategy that aims to maximize network throughput.

In chapter 4, we propose a user scheduling scheme which is based merely on the ergodic rate. We derive the ergodic rate of each user in our network MIMO system from the average Signal-to-Noise Ratio (SNR) and the covariance of prediction error. Further more, we design a joint precoding for the selected users. The precoding matrices are contrived according to the predicted Channel State Information at Transmitter (CSIT) in the future time slot to reduce the deviation caused by delay. Such a network MIMO system is under consideration, where the users are cooperatively served by multiple Base Stations (BSs). User scheduling and joint precoding are executed by a central unit connected to all

BSs. Both the above functions require the CSIT which is acquired by an uplink feedback overhead.

In chapter 5, we investigate the core issue in the spectrum sharing CR strategy: interference mitigation at Primary Receiver (PR). For the spectrum sharing which has recently passed into a mainstream CR strategy, We propose a linear precoder design which aims at alleviating the interference caused by SU from the source for Orthogonal Space-Time Block Coding (OSTBC) based CR. We resort to Minimum Variance (MV) approach to contrive the precoding matrix at Secondary Transmitter (ST) in order to maximize the Signal to Noise Ratio (SNR) at Secondary Receiver (SR) on the premise that the orthogonality of OSTBC is kept, the interference introduced to Primary Link (PL) by Secondary Link (SL) is maintained under a tolerable level and the total transmitted power constraint at ST is satisfied. Moreover, the selection of polarization mode for SL is incorporated in the precoder design. In order to provide an analytic solution with low computational cost, we put forward an original precoder design algorithm which exploits an auxiliary variable to treat the optimization problem with a mixture of linear and quadratic constraints.

In chapter 6, we propound a solution named Cognitive Sub-Small Cell for Sojourners (CSCS) in allusion to a broadly representative small cell scenario, where users can be categorized into two groups: sojourners and inhabitants. CSCS contributes to save energy, enhance the number of concurrently supportable users and enshield inhabitants. We consider two design issues in CSCS: i) determining the number of transmit antennas on sub-small cell APs; ii) controlling downlink inter-sub-small cell interference. For issue i), we excogitate an algorithm helped by the probability distribution of the number of concurrent sojourners. For issue ii), we propose an interference control scheme named BDBF: Block Diagonalization (BD) Precoding based on uncertain channel state information in conjunction with auxiliary optimal Beamformer (BF). In the simulation, we delve into the issue: how the factors impact the number of transmit antennas on sub-small cell APs. Moreover, we verify a significant conclusion: Using BDBF gains more capacity than using optimal BF alone within a bearably large radius of uncertainty region.

In chapter 7, we address the issue of competition vs. cooperation in the downlink, between base stations (BSs), of a multiple input multiple output (MIMO) interference, heterogeneous wireless network (HetNet). We present a scenario where a macrocell base station (MBS) and a cochannel femtocell base station (FBS) each simultaneously serving their own user equipment (UE), has to choose to act as individual systems or to cooperate in *coordinated multipoint transmission* (CoMP). We employ both the theories of non-cooperative and cooperative games in a unified procedure to analyze the decision making process. The BSs, of the competing uncoordinated system, are assumed to operate at the *maximum expected sum rate* (MESR) *correlated equilibrium* (CE) which we compare against the coalition value to establish the stability of the *core* of the coordinated system. We prove that there exists a threshold geographical separation, d_{th}, between the macrocell user equipment (MUE) and FBS, under which the region of coordination is non-empty. Theoretical results are verified through simulation.

Keywords

Cognitive radio networks, multicarrier modulation, resource allocation, routing, beamforming, heterogeneous wireless network, and game theory.

Résumé

Vu que la modulation multi-porteuses est largement utilisée dans les communications sans-fil et la radio cognitive (CR pour “Cognitive Radio”) améliore l'utilisation des ressources radio et du spectre, nous nous concentrons sur les réseaux radio cognitifs (CR) pour faire progresser l'allocation des ressources, le routage, et l'ajustement de la puissance d'émission vers les récepteurs (synthèse de faisceaux ou beamforming) dans cette thèse.

Nous étudions deux types de modulations multi-porteuses :Orthogonal Frequency-Division Multiplexing (OFDM) à base d'ondelettes (WOFDM pour Wavelet OFDM) et OFDM dans sa forme classique ou traditionnelle (OFDM s'appuyant sur la transformation de Fourier pour partager les ressources). WOFDM adopte Wavelet Packet Modulation (WPM) pour obtenir des lobes secondaires beaucoup plus faibles dans la densité spectrale de puissance du signal transmis en comparaison à OFDM. WPM permet de surcroit à WOFDM de s'affranchir du Préfixe Cyclique (indispensable à OFDM) et d'exploiter l'égalisation pour combattre l'Interférence entre Symboles (ISI).

Nous évaluons la performance de WOFDM sous différentes conditions du canal radio. Nous comparons la performance de WOFDM, qui s'appuie sur l'égalisation dans le domaine temporel, à celle de OFDM, qui requiert l'utilisation du Préfixe Cyclique et opère dans le domaine fréquentiel.

Dans le chapitre 3, nous considérons l'allocation de ressources et le routage dans le contexte des réseaux à entrées et sorties multiples (MIMO), et ce pour des réseaux Ad Hoc de type WPM et cognitifs (CR).

Nous nous conformons à quatre principes de coexistence entre utilisateurs primaires (prioritaires) et secondaires (partagent le spectre de manière opportuniste avec les utilisateurs primaires à condition de ne pas dégrader la qualité de service des primaires) pour concevoir notre schéma d'allocation de ressources dans le but de maximiser la capacité de l'ensemble du réseau :

- Premièrement, les utilisateurs primaires (PUs) ont une plus grande priorité d'accès aux sous porteuses dans la bande privée tandis que les utilisateurs primaires et secondaires ont le même niveau de priorité dans les bandes publiques.

- Deuxièmement, le canal MIMO de chaque liaison de chaque sous porteuse dans chaque intervalle de temps est décomposé en en plusieurs sous-canaux avec des gains identiques via la méthode BD-GMD (Block Diagonal-Geometric Mean Decomposition). De plus, le gain du sous-canal d'une liaison est déterminé par les matrices de canal de tous les liens partageant le même noeud source sur la même sous-porteuse dans le même intervalle de temps.

- Troisièmement, une différenciation entre primaires et secondaires s'appuyant sur leurs rapports signal à interférences (SINR). Les utilisateurs primaires (ou PU) ont un seuil de SINR plus élevé (que les utilisateurs secondaires ou SU) pour le décodage dans les

bandes privées. Les PU et SU ont en revanche les mêmes seuils SINR dans les bandes publiques.

- Quatrièmement, nous évitons l'interférence causée par une liaison à toutes les autres liaisons ayant le même noeud de destination. Bien que les puissances de toutes les autres liaisons ne soient pas connues, elles doivent également être attribuées en même temps. Nous associons à notre système d'allocation de ressource une stratégie de routage multicast pour maximiser le débit du réseau.

Dans le chapitre 4, nous proposons un schéma d'ordonnancement (scheduling) de l'utilisateur qui s'appuie uniquement sur le taux ergodique. Nous mesurons le taux ergodique de chaque utilisateur dans notre réseau MIMO en utilisant le rapport signal à bruit (SNR) et la covariance de l'erreur de prédiction. Nous concevons, de surcroît, un schéma de pré-codage pour les utilisateurs sélectionnés. Les matrices de pré-codage sont calculées selon l'état du canal au niveau de l'émetteur (CSIT) dans l'intervalle de temps futur ou à venir pour réduire l'écart causé par le retard. Dans le système MIMO élaboré, les utilisateurs sont servis en collaboration par plusieurs stations de base (BSs). L'ordonnancement de l'utilisateur et le pré-codage conjoint sont exécutés par une unité centrale reliée à toutes les stations de base. Les deux fonctions ci-dessus nécessitent la connaissance du CSIT qui est acquis par un en-tête de paquet sur la liaison montante.

Le chapitre 5 étudie un aspect important dans la stratégie du partage du spectre : l'atténuation des interférences au niveau du récepteur primaire (PR). Nous proposons un pré-codeur linéaire pour atténuer cette interférence, causée par le SU de la source pour CR lorsque des codes en blocs orthogonaux sont codés en espace et en temps (OSTBC). Nous recourons à l'approche de Minimum Variance (MV) pour concevoir la matrice de pré-codage de l'émetteur secondaire (ST) afin de maximiser le rapport signal sur bruit (SNR) au récepteur secondaire (SR) avec l'hypothèse que l'orthogonalité des OSTBC est conservée, avec comme objectif de maintenir l'interférence introduite sur un lien primaire (PL) par la liaison secondaire (SL) sous un niveau tolérable avec la contrainte que la puissance totale émise à ST est satisfaite. La sélection du mode de polarisation pour SL est incorporée dans la conception du pré-codeur. Afin de fournir une solution analytique avec un coût de calcul faible, nous avons proposé un algorithme original pour le pré-codeur. L'algorithme exploite une variable auxiliaire pour traiter le problème d'optimisation avec un mélange de contraintes linéaires et quadratiques.

Nous proposons, dans le chapitre 6, une solution nommée "Cognitive Sub-Small Cell for Sojourners (CSCS)"pour un scénario représentatif de petites cellules où les utilisateurs peuvent être classés en deux groupes : les visiteurs et les habitants. CSCS économise l'énergie, augmente le nombre d'utilisateurs (visiteurs en plus des habitants) acceptés ou accueillis simultanément et protége les habitants.

Nous considérons deux problèmes de conception CSCS :

- la détermination du nombre d'antennes d'émission sur le point d'accès d'une petite cellule ;

- le contrôle de l'interférence entre deux petites cellules.

Pour le problème i), nous concevons un algorithme aidé par la distribution de probabilité du nombre de visiteurs qui se présentent simultanément. Pour le problème ii), nous proposons un système de contrôle d'interférence nommé BDBF : Diagonalisation Block (BD) pré-codage utilisant des informations sur l'état du canal en combinaison avec un synthétiseur de faisceaux optimal auxiliaire (BF). Dans la simulation, nous étudions les facteurs qui influencent le choix du nombre d'antennes nombre d'antennes d'émission sur le point d'accès des petites cellules. Nous vérifions que BDBF peut augmenter la capacité si comparé qu'un simple beamforming optimal (BF).

Enfin dans le chaptire 7, nous étudions la question de la concurrence par rapport à la coopération sur la liaison descendante entre les stations de base (BS) pour des réseaux sans fil hétérogènes (HetNets) avec interférences MIMO. Nous présentons un scénario dans lequel une station de base de type macro-cellule (MBS) et une station de base co-canal de type femto cellule (FBS) desservant chacune simultanément leur propre terminaux (ou UE pour User Equipment). Les stations décident si elles agissent individuellement ou si elles coopèrent dans un cadre "Coordinated Multipoint Transmission"(connu sous l'acronyme CoMP). Nous utilisons à la fois la théorie des jeux non-coopératifs et coopératifs dans une procédure unifiée pour analyser le processus de prise de décision. Les stations de base de ce système unifié doivent fonctionner à un équilibre coordonné. Cet équilibre s'appuie sur la métrique Maximum Expected Sum Rate (MESR) Correlated Equilibrium (CE) qui est comparée à la valeur de la coalition pour établir ou assurer la stabilité de la coalition. Nous prouvons qu'il existe un seuil de séparation géographique, d_{th}, entre l'équipement utilisateur de la macro-cellule (MUE) et FBS, en vertu duquel la région de coordination est non vide. Les résultats théoriques sont vérifiés par simulation.

Introduction Générale

Généralités

La radio cognitive a suscité beaucoup d'attention de la part de la communauté scientifique pour mieux gérer la rareté du spectre en permettant notamment à plusieurs systèmes et services d'utiliser simultanément la ressource spectrale [1–4] avec la possibilité de rajouter de nouveaux systèmes à des réseaux déjà en opération. La radio cognitive permet à des utilisateurs sans licence d'accéder au spectre alloué à un système primaire à condition de s'assurer que la qualité de service des utilisateurs primaires, prioritaires, n'est pas dégradée [1, 2]. La radio cognitive a aussi fait son chemin en instances de normalisation, plus spécifiquement la 4G [3, 4]. La radio cognitive a par conséquent fait aussi l'objet de cette thèse pour améliorer les performances des réseaux mobiles en traitant des problèmes généraux de répartition et de partage de ressources comme l'allocation de sous-porteuse, l'allocation de puissance et la synthèse de faisceaux. Nous considérons de plus dans notre approche, des modulations multi-porteuses, et des systèmes de type MIMO. Deux types de modulations multi-porteuses font l'objet de nos investigations : OFDM à base d'ondelettes, WOFDM, et OFDM traditionnel. Trois types de réseaux sont pris en compte : réseaux ad hoc, réseaux cellulaires et réseaux hétérogènes. Les systèmes à antennes multiples comme MIMO améliore, grâce à la diversité démission et de réception, significativement la capacité

des réseaux et/ou la puissance d'émission ou la portée si on cherche à élargir la couverture radio. La formation de faisceaux, la configuration des antennes dans les systèmes MIMO sont des préoccupations centrales dans cette thèse. Nous considérons pour ces raisons tout d'abord un problème d'allocation des ressources dans les réseaux de type Wavelet Packet Modulation (WPM) ad-hoc s'appuyant sur la radio cognitive et plus spécifiquement. WOFDM qui adopte WPM [73]. Par rapport à OFDM, WOFDM permet d'obtenir des lobes secondaires beaucoup plus faibles du signal transmis et de s'affranchir du "cyclic prefix"indispensable à OFDM. WOFDM exploite l'égalisation pour lutter contre l'interférence entre symboles (ISI) [66, 70, 71, 73, 74]. Nous évaluons la performance de WOFDM qui agit dans le domaine temporel et fait appel à l'égalisation et la comparons avec celle d'OFDM qui s'appuie sur la transformée de Fourier et nécessite l'utilisation d'un préfixe cyclique pour le calage fréquentiel.

Les problèmes d'allocation des ressources dans les réseaux ad-hoc et cognitifs on fait l'objet de plusieurs travaux, notamment dans [5–10]. Les auteurs de [6,7]] traite ce problème pour des systèmes multi-porteuses. Les travaux de [8, 9] étudie l'apport du MIMO. Les algorithmes d'allocation de ressource dans les réseaux ad hoc peuvent être classés en deux types d'algorithmes : algorithmes distribués [5–8, 11] et algorithmes centralisés [12, 13].

L'étude de l'utilisation conjointe de la radio cognitive, des approches MIMO et de l'allocation de ressources n'est pas considérée dans la littérature. Nous proposons pour répondre à ce manque des algorithmes d'allocation de sous-porteuse et de puissance dans les réseaux Ad Hoc de type WPM faisant recours à la radio cognitive et nous fixons comme objectif de maximiser la capacité de l'ensemble du réseau dans le chapitre 3 [26]. La radio cognitive, les techniques de décomposition MIMO [81] pour gérer les interférences entre des utilisateurs primaires (prioritaires) et des utilisateurs secondaires (accès autorisé si et seulement s'ils ne perturbent pas le système primaire) sont prises en compte dans nos travaux. L'algorithme d'allocation de sous-porteuse est réalisé sous forme d'un algorithme distribué dans le noeud actif. Pour la gestion collective de la répartition de puissance sur l'ensemble des liaisons, l'algorithme d'allocation de puissance est implémenté dans un noeud balise.

Pour les réseaux MIMO multi-cellules, nous cherchons à annuler l'interférence multiutilisateurs via le pré-codage de type BD (Bloc Diagonalisation) évoqué précédemment et décrit dans [14, 15]. Le pré-codage BD dépend de l'information concernant l'état du canal à l'émetteur (plus communément appelé CSIT ,Äì Channel State Information at the Transmitter). L'algorithme d'allocation de sous-porteuse qui maximise la capacité s'appuie également sur l'information CSIT. La qualité et précision du paramètre ou de la métrique CSIT affecte directement le pré-codage et l'allocation de ressources et par conséquent le débit atteignable sur la voie radio. Une bonne précision du CSIT exige un retour (feedback) important et donc coûteux en présence de beaucoup d'utilisateurs. Nous consacrons le chapitre 4 (voir aussi [27]) à la réduction de ces coûts en proposant une allocation de sous porteuse moins gourmande en information de retour sur le CSIT et qui traite en même temps l'effet du fading (ou évanouissements). En effet, Small Scale Fading (SSF) a peu d'influence sur la répartition de la sous-porteuse alors qu'il est important pour le pré-codage. Nous proposons d'utiliser le taux ergodique asymptotique, qui dépend des phénomènes à large échelle (Large Scale Fading-LSF), pour effectuer l'allocation de sous porteuse. L'infor-

mation à long terme contient le gain de puissance qui reflète l'affaiblissement de parcours et le "shadowing"et peut donc être substituée à la disponibilité (ou l'élaboration) d'une matrice de canal précise mais trop coûteuse. L'évaluation à long terme permet de sélectionner les utilisateurs dans le régime d'attribution de sous porteuse que nous proposons. Le CSIT précis est contenu dans les évaluations courtes terme qui déterminent la matrice de pré-codage. Nous comparons le débit atteint par ces deux approches, celle qui alloue les sous porteuse et pré-code en s'appuyant sur une connaissance parfaite du CSIT et notre approche moins coûteuse fondée sur le taux ergodique asymptotique.

En partant de l'observation que les systèmes radio cognitifs utilisant un nombre important d'antennes avec Orthogonal Space-Time Block Code (OSTBC) améliorent nettement les performances, nous explorons une conception du pré-codeur de type OSTBC comme décrit dans le chapitre 5 ([16]) de ce manuscrit. La conception du pré-codeur proposé prend l'interférence causée par l'utilisateur secondaire (SU) et l'orthogonalité introduite par OSTBC en compte. La matrice de pré-codage est conçue à l'émetteur secondaire (ST) en utilisant le principe de Minimum Variance (MV) pour maximiser le rapport signal sur bruit (SNR) au récepteur secondaire (SR) en imposant l'orthogonalité des OSTBC soit maintenue et l'interférence introduite sur le lien primaire (PL ou Primary Link) par le lien secondaire (SL - Secondary Link) soit maitrisée sous la contrainte du respect du budget de puissance totale transmise au terminal secondaire (ST). De plus, la sélection du mode de polarisation pour SL est incorporée dans la conception du pré-codeur.

Le système du pré-codeur proposé peut être décrit comme un problème d'optimisation, avec un mélange des contraintes linéaires et quadratiques, qui consiste à trouver la matrice de pré-codage et le bon mode de polarisation. Afin d'obtenir une solution analytique exploitable et qui passe à l'échelle, une variable auxiliaire est introduite.

Enfin nous portons un intérêt aux évolutions des réseaux hétérogènes et plus spécifiquement à la densification et l'utilisation de cellules plus petites pour augmenter la capacité et/ou les débits [17]. Nous focalisons nos travaux au cas de petites cellules qui utilisent le même spectre que des macro-cellules qui couvre les mêmes zones géographiques. Les interférences entre macro cellules et petites cellules, et entre petites cellules sont le principal obstacle au développement de tels réseaux hétérogènes à haute capacité et plus hauts débits. Nous recourons naturellement à la radio cognitive pour coordonner ou maîtriser ces interférences comme [18–21].

Les chapitres 5 et 6 concernent ce problème de répartition de ressources entre macro et petites cellules. L'architecture de réseau hétérogène étudiée divise une petite cellule (small cell) en plusieurs encore plus petites cellules (ou sub-small cells en Anglais) et attribue des priorités d'utilisation du spectre aux cellules en fonction de leur statut avec le même type de priorités utilisées par des systèmes secondaires qui réutilisent un spectre dédié à un système primaire. On parle alors d'une architecture "sous-petite cellule cognitive"(CSCS - Cognitive Sub-small Cells for Sojourners). Nous considérons dans le chapitre 6 le cas d'utilisateurs classés en deux populations : les visiteurs et les habitants en miroir d'utilisateurs secondaires et primaires en radio cognitive. La petite cellule est divisée en deux sous-petites cellules : une sous-petite cellule sert les voyageurs et l'autre sert les habitants. La sous petite cellule qui sert les habitants possède une priorité plus élevée. Les habitants correspondent à des utilisateurs prioritaires (primaire) tandis que les visiteurs correspondent à des utilisateurs

secondaires dont l'accès et les allocations de ressources dépendent de leurs impacts sur les habitants.

Dans notre étude de CSCS pour servir conjointement des habitants et des visiteurs, nous cherchons i) à estimer le nombre idéal ou optimal d'antennes d'émission sur les points d'accès ; et ii) à contrôler les interférences entre sous-petite cellules. Un algorithme qui s'appuie sur la connaissance de la probabilité de distribution du nombre d'utilisateurs (sojourners) simultanés est proposé pour servir les deux populations. Un système de contrôle d'interférence est proposé pour résoudre le problème des interactions radio entre cellules. Il utilise le précodage (de type BD) s'appuyant sur des informations de l'état du canal et la synthèse de faisceau (Beamforming). La théorie des jeux pour gérer les interférences dans la petite cellule a fait l'objet de plusieurs travaux de recherche [22–25] dont nous nous inspirons dans la chapitre 7 (voir aussi [29]) pour répondre à l'utilisation simultanée du même spectre par des habitants et des visiteurs (qui ne doivent pas perturber des habitants prioritaires).

Nous analysons le cas de la liaison descendante impliquant plusieurs stations de base, des systèmes MIMO et des réseaux hétérogènes (HetNets). Plus particulièrement nous traitons le cas de MBS et FBS servant à partir du même spectre plusieurs utilisateurs dans leur zone commune de couverture. La théorie des jeux nous permet de décider dans quelles situations FBS agissent de manière coopérative via une approche CoMP (Coordinated Mutlipoint Transmission) ou de manière purement individuelle. Nous employons une approche unifiée qui combine des jeux coopératifs et non-coopératifs en nous appuyant sur un critère d'équilibre corrélé et de débit conjoint maximum (MESR-Maximum Expected Sum Rate). L'approche est comparée à la valeur de la coalition pour établir ou assurer la stabilité de la coalition.

Contributions

Nous résumons ci-dessous, les principales contributions de cette thèse :

- Nous proposons un nouveau système d'allocation des ressources avec l'objectif de maximiser la capacité de l'ensemble du réseau pour les réseaux cognitifs de type ad-hoc avec des technique de transmission et réception MIMO et modulations WPM. Le schéma d'allocation de ressource proposé prend en compte la priorité des utilisateurs primaires PU et la décomposition du cana MIMO.

- Une approche moins coûteuse que la transmission précise du CSIT qui est consommatrice de ressources en systèmes multicellulaires MIMO, est proposée. Elle s'appuie sur une information réduite du CSIT, le pré-codage et l'allocation de sous porteuse combinant une vue court et long terme de l'état du canal et le taux ergodique asymptotique directement fonction du gain de puissance et dues évanouissements.

- Un pré-codeur de type OSTBC qui prend en compte le niveau d'interférence acceptable par un lien primaire et le mode de polarisation du système d'antennes. Un modèle mathématique du pré-codeur utilisant une variable auxiliaire pour réduire la complexité via un mélange de contraintes linéaires et quadratiques.

- Le cas de macro et petites cellules pouvant s'appuyer sur la radio cognitive appliquée à des macro-cellules et petites cellules pour servir des habitants et des visiteurs correspondant respectivement à des utilisateurs primaires et des utilisateurs secondaires est abordé pour déterminer le nombre d'antennes d'émission optimal sur les points d'accès pour ce contexte. L'algorithme proposé s'appuie sur la distribution du nombre d'utilisateurs simultanément présents dans les cellules (sojourners). Un schéma de suppression de l'interférence, lorsque, générée par les utilisateurs secondaires pour protéger le primaire est présenté pour le cas où l'information de CSIT est incomplète ou réduite.
- Enfin la théorie des jeux est proposée pour traiter le cas de macro cellules et femto cellules (FBS ou Femto Base Stations) co-localisées et partageant le même spectre pour servir des utilisateurs communs. L'étude permet aux FBS de décider quand coopérer avec les macro-cellules et quand agir indépendamment ou individuellement. On montre qu'il existe une région de coopération non vide entre les deux types de stations.

Mots-clés

Réseaux radio cognitives, modulation multiporteuse, allocation des ressources, routage, ajustement de la puissance d'émission vers l'utilisateur (beamforming), réseau sans fil hétérogène, et la théorie des jeux.

Table of contents

Chapter 1

Introduction

Contents

1.1 Thesis Overview

The spectrum scarcity has passed into a crucial problem with the rapid development of wireless service. In allusion to this problem, Cognitive Radio (CR) networks have been proposed and caused great attention. Cognitive radio networks permit that unlicensed users access to the frequency spectrum in a manner that the Quality of Service (QoS) of the licensed users is not affected [1, 2]. CR technique has been suggested to be applied to the 4G standard [3,4]. For the above reasons, CR networks are of great importance for wireless communications. For the purpose of achieving CR networks with better performance, in this thesis we investigate general resource allocation problems, such as subcarrier allocation, power allocation, routing, and beamforming. Different multicarrier modulations, Multiple-Input and Multiple-Output (MIMO) technique and different network structures are taken into account in the proposed resource allocation schemes as the infrastructure of CR networks. Two types of multicarrier modulation: Wavelet-based Orthogonal Frequency Division Multiplexing (WOFDM) and Fourier-based OFDM are considered in this thesis. Three network structures are considered in this thesis: ad-hoc networks, multi-cell networks, and heterogeneous networks. Multiple-Input and Multiple-Output (MIMO) technology provides significant enhancement in the capacity of wireless networks without additional bandwidth or increased transmit power. Because of the above feature, MIMO

is a paramount technology in 4G standard. In this thesis, MIMO is integrated into each network structure to be investigated. Problems related to MIMO, such as beamforming, antenna allocation are also concerned in this work.

We first consider resource allocation problem in WPM CR ad-hoc networks. WOFDM adopts Wavelet Packet Modulation (WPM) [73]. Compared with fourier-based OFDM, wavelet-based OFDM achieves much lower side lobe in the transmitted signal. Wavelet-based OFDM excludes Cyclic Prefix (CP) which is used in fourier-based OFDM systems. Wavelet-based OFDM turns to exploit equalization to combat Inter-Symbol Interference (ISI) [66, 70, 71, 73, 74]. We evaluate the performance of WOFDM under different channel conditions. We compare the performance of fourier-based OFDM using equalization in the time domain to that of fourier-based OFDM with CP and the equalization in the frequency domain. Resource allocation problem in CR based ad-hoc networks attract extensive attention [5–10]. In [6,7], authors integrate such problem into multicarrier systems. In [8, 9], authors analyze such problem with considering MIMO technique. The resource allocation algorithms in ad-hoc networks can be categorized to be two types: distributed algorithms [5–8, 11] and centralized algorithms [12, 13]. The feature and technique of CR and MIMO have not been considered at same time in resource allocation problems. To this end, we propose subcarrier and power allocation scheme in MIMO WPM CR ad-hoc networks with the objective to maximize the capacity of the entire network in chapter 3 [26]. The feature of CR and technique of multi-user MIMO, such as the privilege of Primary User (PU) and MIMO channel decomposition [81] are considered in the above scheme. The subcarrier allocation scheme is designed as a distributed algorithm to be carried out at the active node. For the reason that the power of all the links with the same destination node is allocated simultaneously with some mutual restraint, the power allocation is a centralized algorithms which is implemented at a beacon node.

We go on to the multi-cell MIMO networks. The cancellation of inter-user interference in multi-cell MIMO networks using Block Diagonalization (BD) precoding is discussed in [14, 15]. BD precoding is dependent on Channel State Information at the Transmitter (CSIT). Subcarrier allocation scheme which is based on maximizing capacity also relies on CSIT. Therefore the accuracy of CSIT affects BD precoding and subcarrier allocation, and further impacts the throughput. On the other hand, the accuracy of CSIT requires intensive feedback that takes up too much resource for the information data when there is a large number of users. To this end, in chapter 4 [27], a design of subcarrier allocation and precoding using reduced feedback scheme is motivated to solve the above contradiction. Small scale fading has little influence on subcarrier allocation. However, the small scale fading is significant to precoding. On account of the above reason, a subcarrier allocation scheme is proposed to be based on the asymptotic ergodic rate that is a function of large

scale fading. Long-term feedback contains the power gain which captures pathloss and shadowing instead of accurate channel matrix. Long-term feedback is used to select users for serving together in one frame by the proposed subcarrier allocation scheme. Accurate CSIT is contained in the short-term feedback. Short-term feedback is used to determine the precoding matrix. In order to combat the effect of delay on the accuracy of CSIT, the predicted CSIT is contained in the short-term feedback. The simulation compares the throughput of system adopts subcarrier allocation and precoding using perfect CSIT with that of the proposed scheme, pursuantly verifies the practicability of the proposed scheme.

CR networks utilize Orthogonal Space Time Block Code (OSTBC) transmission is investigated in [16]. Authors in [16] provide a significant conclusion that the outage performance is dramatically enhanced when the number of antennas is large enough. Ground on this conclusion, we are motivated by the important application of OSTBC on CR networks to investigate the precoder design for OSTBC based CR networks in chapter 5 [28]. The proposed precoder design takes the tolerable interference caused by Secondary User (SU) and the orthogonality of OSTBC into account. The precoding matrix is designed at Secondary Transmitter (ST) using Minimum Variance (MV) approach to maximize the Signal to Noise Ratio (SNR) at Secondary Receiver (SR) on the premise that the orthogonality of OSTBC is kept, the interference introduced to Primary Link (PL) by Secondary Link (SL) is maintained under a tolerable level and the total transmitted power constraint at ST is satisfied. Moreover, the selection of polarization mode for SL is incorporated in the precoder design. The proposed precoder scheme can be described as an optimization problem with a mixture of linear and quadratic constraints. The solution of the proposed precoder scheme consists of the precoding matrix and polarization mode. In order to obtain an analytic solution, an auxiliary variable is introduced.

The architecture of heterogeneous networks is an evolution on network architecture. This architecture divides a macrocell into a number of small cells for the purpose of achieving higher capacity [17]. In such architecture, small cells use the same frequency spectrum as the macrocell. The interference between macro cell and small cell, as well as that among small cells is the main impediment of the development of heterogeneous networks. The CR inspired approach to coordinate the inter-cell interference in the heterogeneous networks attracts extensive attention [18–21]. Chapter 6 and 5 center on the resource allocation problem considering the constraint of inter-cell interference.

The architecture of heterogeneous network which splits small cell into several sub-small cells, where different sub-small cell possesses different priority according to the status of users inside is a novel architecture named Cognitive Sub-Small Cell for Sojourners (CSCS). CSCS can be a solution for many small cell scenarios. A broadly representative small cell scenario is considered in chapter 6, where users can be categorized into two groups:

sojourners and inhabitants. The small cell is divided into two sub-small cells, one sub-small cell serves sojourners and the other one serves inhabitants. According to the status of sojourner and inhabitant, the sub-small which serves inhabitants holds higher priority. Two design problems of CSCS for the above scenario is considered: i) determining the number of transmit antennas on sub-small cell APs; ii) controlling downlink inter-sub-small cell interference. An algorithm helped by the probability distribution of the number of concurrent sojourners is designed to solve the first problem. An interference control scheme is proposed to solve the second problem. This scheme uses BD precoding based on uncertain channel state information in conjunction with auxiliary optimal beamformer.

The application of game theory to cope with managing interference in small cell attracts extensive attention [22–25]. Inspired by the above work, in chapter 7 [29], we resort to game theory to investigate the problem of competition vs. cooperation in the downlink, between Base Stations (BSs), of a MIMO interference, heterogeneous wireless network (HetNet). Based on a scenario where a Macrocell Base Station (MBS) and a cochannel femtocell base station (FBS) each simultaneously serving their own user equipment (UE), the problem is defined as in which situation Femtocell Base Station (FBS) has to choose to act as individual systems and in which situation FBS has to cooperate in Coordinated Multipoint transmission (CoMP). We employ both the theories of non-cooperative and cooperative games in a unified procedure to analyze the decision making process. The BSs of the competing system are assumed to operate at the maximum expected sum rate (MESR) correlated equilibrium (CE), which we compare against the value of CoMP to establish the stability of the coalition. We prove that there exists a threshold geographical separation between the macrocell user equipment (MUE) and FBS, under which the region of coordination is non-empty.

1.2 Contributions

The key contributions of this thesis are:

1. We propose a new resource allocation scheme with the objective to maximize the capacity of the entire network for MIMO-WPM CR ad-hoc network. The proposed resource allocation takes the feature of CR and technique of multi-user MIMO into account, such as the privilege of PU and MIMO channel decomposition.

2. For the purpose of solving the contradiction between the impact of imperfect CSIT and the resource limitation for feeding CSIT back in multi-cell MIMO networks, a reduced CSIT feedback approach for subcarrier allocation and precoding is proposed. The proposed CSIT feedback scheme is classified into long term and short term. The

power gain and predicted CSIT are respectively fed back for subcarrier allocation and precoding. Moreover, we derive an asymptotic ergodic rate of multicell MIMO network in function of the power gain which captures pathloss and shadowing.

3. We put forward a new precoder design for OSTBC transmission based CR networks. The proposed precoder design takes the orthogonality of OSTBC, the tolerable interference of PU and polarization mode into account. In order to provide an analytic solution with low computational cost, we put forward an original precoder design algorithm which exploits an auxiliary variable to treat the optimization problem with a mixture of linear and quadratic constraints.

4. We propose a solution named CSCS in allusion to a broadly representative small cell scenario, where users can be categorized into two groups: sojourners and inhabitants. Inside the proposed solution, we design an algorithm for determining the number of transmit antennas on sub-small cell APs helped by the probability distribution of the number of concurrent sojourners. In addition, we proposed an interference control scheme for secondary systems which are hampered from imperfect secondary-to-primary Channel State Information (CSI).

5. Based on a scenario where a MBS and a cochannel FBS each simultaneously serving their own UE, we resort to game theory to investigate the problem that in which situation FBS has to choose to act as individual systems and in which situation FBS has to cooperate in CoMP. We prove that there exists a threshold geographical separation between the MUE and FBS, under which the region of coordination is non-empty.

Chapter 2

Background

Contents

In this chapter, we provide the relevant state of the art to summarize the key techniques and exhibit their development in the related work and our work. In this thesis, Cognitive Radio (CR) network is the storyline with all research issues connected. We conduct a study to achieve CR networks with better performance in different aspects. We investigate a general resource allocation problem in CR networks, such as subcarrier allocation, power allocation, and beamformer design. Moreover, different multicarrier modulations, Multiple-Input and Multiple-Output (MIMO) technique and different network structures are taken into account in the proposed resource allocation schemes as the infrastructure of CR networks.

CR networks are designed to increase the efficiency in spectrum use. In such networks, CR device is enabled to transmit in unlicensed spectrum on the premise that the licensed users can work in good order. CR device has two abilities: sensing and spectrum control. The former means that CR device can detect available spectrum on its own initiative. And the latter means that CR is able to adjust its transmit parameters for the efficient use of resources. Spectrum sensing and resource allocation are two principal research issues in CR

networks. The feature of CR networks leads new challenge to resource allocation problem: the interference caused by the unlicensed users should be alleviated to the degree such that licensed users can work properly. We focus on resource allocation in CR networks with different multicarrier modulations, different network structures and MIMO technique.

Multicarrier modulation modulates data symbol stream onto multiple orthogonal subchannels in order to eliminate Intersymbol Interference (ISI) by narrowband transmission. Two types of multicarrier modulation: Fourier-based Orthogonal Frequency Division Multiplexing (OFDM) and Wavelet-based Orthogonal Frequency-Division Multiplexing (WOFDM) are considered in this thesis. OFDM is considered as a excellent modulation scheme for CR networks [43] for the reason that it facilitates spectrum sensing and provides great flexibility. OFDM is considered in a proposed subcarrier allocation scheme in chapter 4 [27]. WOFDM adopts orthogonal wavelet bases to replace sine functions and excludes Cyclic Prefix (CP) in OFDM. As a multicarrier modulation, WOFDM inherits the features of OFDM which advantages the achievement of CR networks. WOFDM is taken into account in a proposed resource allocation scheme in chapter 3 [26]. The performance analysis of these two multicarrier modulations is provided in this chapter.

MIMO systems are the transceiver systems using multiple antennas at both the transmitter and receiver. MIMO systems aim at improving the performance of rate and reliability. In this thesis, two MIMO techniques: beamforming and Space-Time Coding (STC) are taken into consideration. Beamforming is the technique to produce directional transmission signal using antenna array. STC encodes data in the dimension of space and time for the purpose of maximizing the diversity of MIMO systems to combat channel fading and interference plus noise. Beamforming brings a new dimension–space to eliminate the interference caused by the unlicensed users in CR networks. However, this requires the premise that SU knows Channel State Information (CSI) perfectly. The design of beamforming with imperfect CSI considering the constraints issue from CR networks is investigated in chapter 6 and 7 [29]. Orthogonal Space-Time Block Coding (OSTBC) is a class of STC with advantage of low complexity for decoding and acquirement of full diversity. The orthogonality of OSTBC brings on a new constraint for the precoder design in CR networks and such problem is investigated in chapter 5 [28].

Ad-hoc networks, multi cell networks, and heterogeneous networks (HetNets) are three network structures considered in this thesis. Ad-hoc network is a structure of decentralized wireless network. The information in such networks is diffused by each distributed node not a centralized infrastructure, such as Base Station (BS), Access Point (AP). Ad-hoc networks are considered in the proposed resource allocation scheme in chapter 3. Multi cell network is the cellular network in which users are cooperatively served by multiple BSs. The Inter-Cell Interference (ICI) caused by frequency reuse is a challenge in multi

cell networks. This issue is taken into account in the proposed subcarrier allocation and beamforming scheme in chapter 4. HetNet is specifically referred to a macrocell into a number of small cells for the purpose of achieving higher capacity. Frequency reuse by small cells and macro cell causes interference between macro cell and small cell, as well as that among small cells. Beamformer design in chapter 6 and 7 takes the constraint of such interference into account.

The conception of CR networks is summarized in section 2.1.1. The state of the art of research issues in CR networks is provided in section 2.1.2. The brief introduction of multicarrier modulation and MIMO systems are given in section 2.2 and 2.3.

2.1 Cognitive Radio Networks

2.1.1 Basic Conception and Functions

The rapid rise in wireless device, coupled with the expansion of wireless service, radio spectrum is getting scarcer and more valuable. Most of available radio spectrum has been allocated to the important subscribers. However, in contradiction to the fierce competition for radio spectrum, most of the allocated spectrum is largely underutilized [30, 31]. This contradiction between spectrum regulation and usage gives rise to a tremendous waste of spectrum. To this end, CR networks were born to exploit the underused spectrum. CR networks enable Secondary Users (SUs) to get opportunistic access of unlicensed band so as to increase the efficiency in spectrum use.

CR device has two main functions: spectrum sensing and spectrum control. The former means that CR device can search available spectrum on its initiative. The latter means that CR device can adjust its transmission parameters according to the environment for two purposes: capturing the best available spectrum and avoiding inflicting interference on Primary User (PU)–licensed user.

Two roles are defined in CR networks: PU and SU. PU is the user who possesses the license to dominate the allocated spectrum bands. SU is the user who can transmit in the licensed bands on the premise that PU are ensured to work properly. There are three modes of spectrum sharing: underlay, overlay and hybrid [32–34]. In underlay cognitive systems, SU is allowed to transmit in licensed bands while PU is transmitting in the same bands under the premise that the interference inflicted by SU on PU is below a tolerable interference level. In overlay cognitive systems, the licensed spectrum bands can be utilized by SU only when PU is temporarily inoperative in these spectrum bands on the premise that SU inflicts no interference on other PUs who are transmitting on other spectrum bands. In hybrid cognitive systems, the above two modes coexist in cognitive radio networks, i.e. when SU finds some licensed spectrum bands which are not being used by PU, SU

immediately converts the mode of spectrum sharing from underlay into overlay for the purpose of gaining more capacity.

2.1.2 Research Issues in Cognitive Radio Networks

Spectrum sensing is significant to CR networks. The identification of available spectrum over a wide range of spectrum is a challenge for CR networks. Its process is complicated for the following reasons: i) In CR networks, various modulations, transmission power adopted by different PU, interference caused by SU, and noise increase the difficulty of the identification of PU [35]. ii) The process need to be completed fast to protect the validity of the spectrum sensing information from delay [36]. iii) The process is expensive for the reason that wideband spectrum sensing is supported by large data samples [37]. In order to cope with the above difficulties, the spectrum sensing has attracted extensive research attention. Energy detection and cyclostationary feature detection are two most common spectrum approaches [36,38]. Energy detection approach determines available spectrum by means of comparing the signal power with a threshold [37,39]. For the purpose of enhancing sensitivity, the threshold is set so much low, that bring about a very complicated problem that noise power and PU's transmission power cannot be distinguished. Cyclostationary feature detection utilizes the cyclostationarity of PU's transmission signal to detect the presence of PU [40–42].

In this thesis, the subject centers on another great research issue in CR networks– resource allocation. Since resource allocation is directly related to the interference introduced by SU to PU and the transmission rate, it plays a role as spectrum controller in CR networks. The research issues centering on resource allocation in CR networks can be greatly extended when different modulations, different network structures and MIMO technique are integrated into CR networks. A general resource allocation problem can include subcarrier allocation, power allocation, and beamformer design.

OFDM is recommended as ideal modulation for CR networks [43]. In [43], authors conclude several excellent features which meet the challenges in CR networks. The utilization of Fast Fourier Transform (FFT) in OFDM facilitates spectrum sensing. OFDM provides great flexibility due to the multicarrier feature, for example, the number of subcarrier, coding and transmit power of each subcarrier can be easily adjusted to adapt to the environment. Another multicarrier modulation–Wavelet based OFDM (WOFDM) is also proposed for CR networks [78]. As a multicarrier modulation, WOFDM inherits the features of OFDM which advantages the achievement of CR networks. Moreover, WOFDM adopts Wavelet Packet Modulation (WPM) which uses orthogonal wavelet bases to replace sine functions. WPM offers much lower magnitude side lobes [67]. WPM provides better performance in terms of sensitivity to nonlinear amplifiers [68], multipath channel distor-

tion, and synchronization error [69, 70]. In addition, WPM improves spectral efficiency due to the exclusion of Cyclic Prefix (CP) [71]. In [6, 44–48], authors consider resource allocation problem in OFDM based CR networks. In [44], authors take several kinds of resource into account, such as subcarrier, bit and power. In [45], the objective of resource allocation is to maximize the system energy-efficiency. In our thesis, resource allocation problem in multicarrier modulation based CR networks is considered in chapter 3 and 4. We propose a subcarrier and power allocation algorithm for WOFDM based systems in chapter 3. A scheduling algorithm using reduced feedback is proposed for OFDM based systems in chapter 4.

MIMO systems are transceiver systems which use multiple antennas at both transmitter and receiver. MIMO systems open up a new dimension–space to enhance the performance of rate and reliability. Beamforming, spatial diversity, and spatial multiplexing are three MIMO techniques to achieve spatial selectivity, diversity maximization, and date rate maximization. In this thesis, the first two techniques are concerned. Beamforming brings a new way that using directional signal transmission to solve the problem of frequency reuse. In MIMO CR networks, beamforming enable SU to transmit at the same frequency band and the same time as PU without any interference. However, this requires the premise that SU knows CSI perfectly. Since this premise is not practical, beamformer design using imperfect CSI has attracted extensive interests. In [49–52], beamforming optimization problems with imperfect CSI are analyzed. Such problems are investigated in chapter 6 and 7. MIMO systems enable combating channel fading and noise plus interference by spatial diversity. Spatial diversity is achieved by sending the replicas of original data through the dimension of space. STC is proposed to maximize spatial diversity. STC encodes data in the dimension of space and time. In [52, 63], the feature of STC is considered in the design of beamformer in CR networks. OSTBC is a principal class of STC. OSTBC has the prominent advantage of low complexity for decoding and acquirement of full diversity. In chapter 5, the orthogonality of OSTBC is considered as a constraint to the precoder design in CR networks.

Different network structures extend the area of research for CR networks. Ad-hoc networks, multi cell networks, and HetNets are three network structures considered in this thesis. Ad-hoc network is a decentralized structure of wireless network, where each node instead of a centralized infrastructure diffuses information. In [5–10, 54], authors analyze resource allocation problem in CR ad-hoc Networks. We propose a subcarrier and power allocation scheme in CR ad-hoc networks with the objective to maximize the capacity of the entire network in chapter 3. Multi cell network is the cellular network where users are cooperatively served by multiple BSs. In [55], the resource allocation problem in multi cell CR networks is considered. The ICI caused by frequency reuse in different cells is

a challenge in multi cell networks. Scheduling (subcarrier allocation) and Beamforming are two approaches to cope with this challenge. To this end, in chapter 4, scheduling and beamforming in multi cell networks is investigated. HetNet is specifically referred to a macrocell into a number of small cells for the purpose of achieving higher capacity. Frequency reuse by each small cell and macro cell causes interference between macro cell and small cell, as well as that among small cells. Managing interference in HetNet by resource allocation is a significant research issue. In [56, 57], resource allocation problem is investigated in heterogeneous CR Networks. The interference management schemes using game theory in HetNet are proposed in [22–25]. In chapter 7, beamformer design using game theory in HetNet is investigated.

2.2 Background Related to Identified Research Issues

2.2.1 Multicarrier Modulation

The essential thought of multicarrier modulation is to divide allocated spectrum band equally into multiple orthogonal subchannels. With a sufficiently large number of subchannels, the bandwidth of each subchannel is less than the coherence bandwidth. Therefore, each subchannel can be considered as a relatively flat fading channel. The ISI can be greatly suppressed [62]. Multicarrier modulation has passed into a main stream modulation scheme and adopted by 4G mobile communication standard.

OFDM is a practical discrete implementation of multicarrier modulation with the aid of FFT. OFDM adopts CP to combat frequency selective fading. ISI can be completely eliminated when CP is sufficiently long. OFDM is proposed to be applied to CR networks [43] for the following reasons: i) FFT helps to facilitates spectrum sensing. ii) OFDM provides great flexibility due to the multicarrier feature, such as the number of subcarrier, coding and transmit power of each subcarrier.

WOFDM is another discrete implementation of multicarrier modulation. WOFDM adopts Wavelet Packet Modulation (WPM) which uses orthogonal wavelet bases. WPM offers much lower magnitude side lobes. Moreover, WPM excludes CP in return for spectral efficiency. WPM requires equalization in time domain to cope with channel fading. As a multicarrier modulation, WOFDM inherits the features of OFDM which advantages the achievement of CR networks.

We give a brief introduction for these two multicarrier modulation techniques. We evaluate the performance of WOFDM and OFDM under different channel conditions. The Bit Error Rate (BER) analysis is carried out to compare the performance of these two modulations.

2.2.1.1 Fourier-based OFDM

OFDM is a typical case of multicarrier modulation. OFDM adopts Discrete Fourier transform (DFT) and CP. CP enables the original input sequence can be recovered from the received signal by means of equalization techniques in frequency domain. Moreover, from the view of matrix representation of OFDM [62], the utilization of DFT and CP converts the frequency selective fading into flat fading by the means of decomposing the channel coefficient matrix to a diagonal matrix. The discrete implementation of OFDM [62] is given below. The original data is first mapped to be complex symbol (typically via PSK or QAM). After the serial-to-parallel converter, these mapped symbols are distributed to N parallel subchannels. The set of N parallel mapped symbols $X[0], \ldots, X[N-1]$ are symbols transmitted by N subcarriers in each time slot. These N mapped symbols are the discrete frequency components of the transmitted signal $s(t)$. For the purpose of generating time domain signal, IFFT is performed on these symbols. The output of IFFT processor can be expressed as:

$$x[n] = \frac{1}{\sqrt{N}} \sum_{i=0}^{N-1} X[i] e^{j2\pi ni/N},\ 0 \le n \le N-1. \tag{2.1}$$

The cyclic prefix is added to $x[n] = x[0], \ldots,\ x[N-1]$ in order to generate digital OFDM signal $x'[n] = x[N-L], \ldots,\ x[N-1],\ x[0], \ldots,\ x[N-1]$. The digital OFDM signal then be converted into analog signal. Finally, the baseband transmitted signal is upconverted to be the passband signal.

In the receiver, the received signal is first converted into baseband signal. After A/D converter, the baseband analog signal is converted into digital signal which is $y(n) = x'[n] \otimes h[n] + v[n],\ -L \le n \le N-1$, where $h[n]$ is the equivalent lowpass impulse response of the channel. After removing the CP and passing through the serial-to-parallel converter, the set of N parallel received symbols $y[0], y[1], \ldots, y[N-1]$ is output. The output of IFFT processor can be expressed as:

$$Y[i] = \frac{1}{\sqrt{N}} \sum_{n=0}^{N-1} y[n] e^{-j2\pi ni/N},\ , 0 \le i \le N-1. \tag{2.2}$$

The OFDM modulated symbol sequence is $x[n] = x[0], \ldots,\ x[N-1]$. The cyclic prefix is designed as the last L values of $x[n]$, i.e. the sequence of $x[N-L], \ldots, x[N-1]$. L is calculated as T_m/T_s, where T_m is the channel delay spread, T_s is the sampling period and $L+1$ indicates the length of finite impulse response (FIR) of the channel. The sequence $x'[n] = x'[-L], \ldots, x'[N-1] = x[N-L], \ldots, x[N-1], x[0], \ldots, x[N-1]$. $x'[n] = x[n]_N$, where $[n]_N$ indicates n modulo N. Accordingly, $x'[n-k] = x[n-k]_N$ for $0 \le n-k \le N-1$.

By using the cyclic prefix, the received signal after removing the cyclic prefix can be finally expressed as the N-point circular convolution of the OFDM modulated symbol sequence $x[n]$ and the channel impulse response $h[n]$:

$$\begin{aligned} y[n] &= x'[n] \otimes h[n] + v[n] \\ &= x[n] \circledast h[n] + v[n],\ 0 \leq n \leq N-1, \end{aligned}$$

where $\otimes$ indicates linear convolution, $\circledast$ indicates circular convolution and $v[n]$ is the sample of Additive White Gaussian Noise (AWGN).

Due to the property of DFT, the circular convolution in time domain equals multiplication in frequency domain:

$$\mathrm{DFT}\{y[n]\} = Y[i] = X[i]H[i] + V[i],\ n \leq N-1,\ 0 \leq i \leq N-1. \tag{2.3}$$

The original input sequence $X[i]$ can be recovered from $Y[i]$ by means of equalization techniques in frequency domain.

2.2.1.2 Wavelet-based OFDM

As a classical multicarrier modulation, OFDM exploits sine functions to generate orthogonal subcarrier wave. The idea that designing other orthogonal wavelet bases instead of sine functions to gain better performance has been propounded recently.

As a novel alternative to Fourier-based OFDM, Wavelet-based OFDM adopts Wavelet Packet Modulation (WPM) which uses orthogonal wavelet bases to replace conventional Fourier bases. The principal benefit of this alternative multicarrier modulation is that WPM offers side lobes with much lower magnitude [64]. Fourier-based OFDM transmit pulses are sequences of signals which are limited in a rectangular window in time domain. The rectangular window corresponds to a sinc-type frequency response which has high side lobes. The high side lobes in transmitted signal enhances the sensitivity to inter-carrier interference (ICI) and narrowband interference (NBI) [65, 66]. Wavelet-OFDM allows the transmit pulses of consecutive symbols overlap, as these pulses can be separated by the receiver filter. This characteristic provides a spectral shape with higher suppression of side lobe than that of Fourier-based OFDM. In [64], authors drew the conclusion on numerical experiments that the side lobes of Fourier-based OFDM are only 13 dB below the main lobe, while Wavelet OFDM provides a side lobe attenuation of 35 dB. Moreover, WPM provides better performance in terms of sensitivity to non-linear amplifiers [68], multipath channel distortion, and synchronization error [69, 70]. In addition, OFDM employs CP to convert the channel matrix into a diagonal matrix. However, the CP reduces the spectral

efficiency. WPM improves spectral efficiency due to the exclusion of CP. Nevertheless, it requires the equalization of multipath fading channels [71].

The M-ary modulated data sequence $x(n) = x(1), x(2), \ldots$ is first converted to $\mathbf{x} = [\mathbf{u}_0, \ldots, \mathbf{u}_{\mathrm{N}-1}]^T$ by the serial to parallel converter, where

$$\begin{aligned} \mathbf{u}_{\mathrm{k}} &= [X(0+k), X(N+k), X(2N+k), \ldots] \\ &= [u_k(0), u_k(1), u_k(2), \ldots], k = 0, \ldots, N-1 \end{aligned} \tag{2.4}$$

denotes the kth row of $\mathbf{x}$.

The Inverse Discrete Wavelet Packet transform (IDWPT) is obtained by passing the N parallel subsequences $\mathbf{u}_{\mathrm{k}}, \mathrm{k} = 0, \ldots, \mathrm{N}-1$through N parallel N-fold interpolation filters and taking the sum. Each interpolation filter is composed of an N-fold expander and a corresponding synthesis filter $\psi_k^s(n)$. The input-output relation of an N-fold interpolation filter in the discrete time domain is given as [72]:

$$y_k(n) = \sum_{p=-\infty}^{\infty} u_k(p) \psi_k^s(n - pN). \tag{2.5}$$

The WPM baseband transmitted signal $s(n)$ is constructed as the sum of N individually amplitude modulated waveforms. It can be expressed as:

$$s(n) = \sum_{k=0}^{N-1} \sum_{p=0}^{S-1} u_k(p) \psi_k^s(n - pN), \tag{2.6}$$

where p denotes the WPM symbol index. We consider a WPM baseband transmitted signal which consists of successive WPM symbols in one frame.

An N-fold interpolation filter bank is equivalent to a $\log_2 N$ level tree structure filter bank. Since each interpolation filter can be built by successive iterations each consisting of up-sampling and filtering by the synthesis filter operations as expressed in the following recursive equations [73]:

$$\begin{cases} \psi_{j,2m}^s(n) = g_s(n) \otimes \left(\left(\psi_{j-1,m}^s(n) \right) \uparrow 2 \right) \\ \psi_{j,2m+1}^s(n) = h_s(n) \otimes \left(\left(\psi_{j-1,m}^s(n) \right) \uparrow 2 \right) \\ \psi_{0,m}^s(n) = \begin{cases} 1 & for\ n = 1 \\ 0 & otherwise \end{cases} \end{cases}, \tag{2.7}$$

where $\otimes$denotes convolution, j is the iteration index, $1 \leq j \leq \log_2 N$, and m is the 2^{j-1}-fold interpolation filter index in the $(j-1)$th level of the tree structure filter bank,$0 \leq m \leq (N-2)/2$. $(\bullet) \uparrow 2$ indicates 2-fold up-sampling. $g_s(n)$ and $h_s(n)$ are the synthesis

low-pass and high-pass filter impulse responses, respectively. They form a filter pair which can guarantee that the designed wavelet is valid [74].

2.2.2 Channel Model

In our thesis, the channel model which is treated of in the subsequent chapters will be specified. In this section, a general conception of channel fading is given concisely. In terms of Fourier-based OFDM and Wavelet-based OFDM over multipath channels, the basic equalizers which compensate for ISI is introduced briefly.

Fading channels can be classified as: small scale and large scale fading.

2.2.2.1 Small Scale Fading

In terms of small scale fading, two principal distinct effects are led to by multipath time delay spread and Doppler Spread respectively [75]. The former is able to quantify the propagation environment with two classifications: flat fading and frequency selective fading. The later enables to quantify how fast the wireless channels are changing with two classifications: fast fading and slow fading.

The principal parameters to measure and quantify fading effects owing to multipath time delay spread are: RMS delay spread σ_τ in time domain and coherence bandwidth $B_c \approx \frac{1}{50\sigma_\tau}$ in frequency domain.

For the purpose of channel simulation, two parameters are used to describe multipath channels: path Delays and average Path Gains. The first delay is the delay of the first arriving path. It is usually set to zero. The following path delay is between $1ns$ and $100ns$ for indoor environments, while that is between $100ns$ and $10\mu s$. The average path gains in the channel object indicate the average power gain of each fading path. In practice, an average path gain value is a large negative dB value. However, computer models typically use average path gains between -20 dB and 0 dB [77].

The channel with $B_S \ll B_c$ or $T_S \geqslant \sigma_\tau$ is categorized as flat fading, where B_S is the bandwidth and T_S is symbol period. The channel with $B_S \succ B_c$ or $T_S \prec \sigma_\tau$ is classified as frequency selective fading.

The principal parameters to measure and quantify fading effects owing to Doppler spread are: the maximum Doppler shift, Coherence time in time domain, and in frequency domain. Doppler spread is defined as $f_m = v_m/\lambda$, where v_m is the maximum speed of the mobile and λ is the wavelength of the signal. Coherence time is defined as $T_C \approx \frac{0.423}{f_m}$. Doppler spread is defined as $B_D = 2f_m$.

Since the maximum Doppler is expressed in terms of the speed of the mobile, the maximum Doppler values according to the mobile speed. The maximum Doppler for a

signal from a moving car might be about 80 Hz, while that for a signal from a moving pedestrian might be about 4 Hz [77].

The channel with $B_S \prec B_D$ or $T_S \succ T_C$ is categorized as fast fading. The channel with $B_S \gg B_D$ or $T_S \ll T_C$ is classified as slow fading.

Small scale fading is able to be modeled by a random variable with a certain probability distribution. For the circumstance that multipath environment with no direct line of sight, the amplitude of a small scale fading channel follows Rayleigh distribution. When a dominant nonfading signal component appears, the fading envelope follows Rice distribution.

2.2.2.2 Large Scale Fading

In this thesis, the large scale fading is considered with an analytical model in the subsequent chapters. This model defines P_r/P_t is characterized as a function of distance, where P_r is the received power and P_t is the transmitted power.

2.2.3 MIMO Systems

MIMO systems are transceiver systems which use multiple antennas at both transmitter and receiver. MIMO systems enhance the performance of rate and reliability through the use of MIMO techniques. MIMO techniques are developed towards three principal targets: date rate maximization, diversity maximization, and spatial selectivity [58, 59].

The first purpose is achieved by the approach of spatial multiplexing. In this fashion, independent data stream is sent in each subchannel, i.e. the number of data streams is equal to the number of antennas. In this way of using MIMO systems, the capacity can be increased. The capacity of such a MIMO system is proportional to the number of antennas [60]. In the circumstance that CSI is perfectly known at both transmitter and receiver, Singular Value Decomposition (SVD) precoding can make spatial multiplexing achieve the MIMO channel capacity [61]. SVD precoding makes each independent data stream to be transmitted without any interference. This is effectuated by using SVD to diagonalize the channel matrix and adding precoding matrix and postcoding matrix to remove the two unitary matrices. The capacity of MIMO systems using SVD precoding for spatial multiplexing is given in [60].

Spatial multiplexing helps MIMO systems to attain larger capacity. However, systems purchase capacity at the expenses of the error rate [59]. The second–and most important purpose is to combat channel fading and noise plus interference by spatial diversity. The spatial diversity is attained by sending the replicas of original data through every antenna. In this manner, the error rate caused by channel fading and noise plus interference is able to minimized. However, the price of error rate minimization is the data rate. The date rate of this manner is equivalent to a Single Input Single Output system. The maximum diversity

is equal to the product of the number of transmit antenna and that of receive antenna. In order to maximize the diversity of MIMO system, a coding approach named STC has been proposed and attracted extensive research interest. STC exploits diversity by means of encoding the data stream in the dimension of space and time [113]. OSTBC is a principal class of STC. OSTBC has the prominent advantage of low complexity for decoding and acquirement of full diversity. Alamouti STBC [113] is the first OSTBC. It can achieve full diversity of 2 without knowing CSI. In chapter 5, preserving the orthogonality of OSTBC is taken into account as a constraint to design precoder in CR networks.

The third purpose is achieved by beamforming technique which produces directional transmission signal using antenna array. The Signal-to-Interference-plus-Noise Ratio (SINR) at the target receiver is enhanced by this approach. Precoding for Multi-user MIMO systems can be considered as a typical beamforming technique. This beamforming technique enable multiple users simultaneously transmit on the same frequency without any interference. Dirty paper coding (DPC) [122, 123] and Block Diagonalization (BD) [88] are two widely adopted techniques. DPC is contrived to suit the capacity optimal requirement [124], however, it is hard to implement owing to its complexity. BD is a practical approach which adopts precoding to completely eliminate inter-user interference. However, this requires the premise that SU knows CSI perfectly. Since this premise is not practical, beamformer design using imperfect CSI has practical significance. Such problems are investigated in chapter 6 and 7.

Chapter 3

Resource Allocation in MIMO-WPM CR Ad-Hoc Networks

Contents

In this chapter, we consider the resource allocation and routing problem in MIMO-WPM CR ad-hoc networks. We comply with four principles to design our resource allocation scheme with the goal to maximize the capacity of entire network. First, PUs have higher priority to access to the subcarrier in private bands, while PUs and SUs have the equal opportunity in public bands. Second, the MIMO channel of each link on each subcarrier in each time slot is decomposed by Block Diagonal Geometric Mean Decomposition (BD-GMD) into multiple sub-channels with identical gain. In addition, the sub-channel gain of one link is determined by all other links sharing the same source node on the same subcarrier in the same time slot. Third, PUs have the privilege of higher SINR threshold for the successful decoding in private bands, but PUs and SUs have the same SINR threshold in public bands. Fourth, the interference caused by one link to all other links having the same destination node should be avoided, moreover, the power of all other links is not assumed to be known but also need to be allocated at the same time. Based on our proposed resource allocation scheme, we investigate a multicast routing strategy that aims to maximize network throughput. Numerical results demonstrate that our proposed resource allocation and routing scheme can noticeably improve network throughput.

In [80], authors incorporated WPM in MIMO and CR so as to endow the system with the excellent features of WPM. In order to eliminate the interference caused by links sharing the same source node, our network is based upon Block Diagonal Geometric Mean Decomposition (BD-GMD) based Dirty Paper Coding (DPC) scheme [81]. For the purpose of resisting fast time-varying fading to provide precise channel state information (CSI) for resource allocation and routing, we adopt Kalman filter to predict CSI.

Our proposed resource allocation and routing scheme is executed every time slot based on predicted CSI.

The MIMO channel of each link on each subcarrier in each time slot is decomposed by BD-GMD into multiple sub-channels with identical gains. In addition, the sub-channel gain of one link is determined by all other links sharing the same source node on the same subcarrier in the same time slot. The subcarrier allocation method selects the best combination of links to make the entire capacity be maximized. PUs have higher priority to access to the subcarrier in private bands. We set a threshold to balance the PUs' priority and the entire capacity. Our power allocation method pursues maximum capacity, on the premise that every active node has a sufficient signal to interference and noise ratio (SINR) to decode successfully. Moreover, the interference between every two links having the same destination node should be prevented. The power of all links is allocated simultaneously that creates the demand for global knowledge of SINR. Therefore we design a centralized power allocation algorithm. Throughput enhancement relies upon augmentation of capacity and back pressure. We design a multicast routing method which adopts Greedy Algorithm.

For each link, the subcarrier which achieves larger capacity is assigned to the segmentation of session which has higher back pressure.

3.1 Multi-hop MIMO-WPM CR ad-hoc network

We consider a multi-hop MIMO-WPM CR ad-hoc network in fast time-varying multipath fading environments, where every node can transmit and receive simultaneously in both private bands and public bands employing N_{SC}-subcarrier WPM with the bandwidth of each subcarrier B. A node in the network is designated as PU or SU. PUs have higher priority to access to the subcarrier and the privilege of higher SINR threshold for the successful decoding in private bands, while PUs and SUs have the equal opportunity and the same SINR threshold in public bands. In Table 3.1, we list the notations used. We assume $T_i \geq R_{i,n}^{NERA}$. In each time slot, node i is allowed to transmit to L_{RNSC} neighbor nodes on each subcarrier.

3.1.1 Block Diagonal Geometric Mean Decomposition

Single Value Decomposition is the most popular method to decompose single user MIMO channel. With perfect knowledge of CSI, the single user MIMO channel is decomposed into a set of Single Input Single Output (SISO) sub-channels [81]. Water-filling power allocation can be used in conjunction with SVD to maximize the channel capacity. However, SVD has its drawback that each sub-channel has disparate SNR value. This drawback can give rise to increasing the transceiver complexity as the different rate coding needs to be used in each sub-channel.

BD-GMD is proposed in [81] for Multi-User (MU) MIMO systems. The MIMO channel of each link is decomposed by BD-GMD into multiple sub-channels with identical gain. Therefore, the equal rate coding can be used for each link, that overcomes the SVD approach's drawback. BD-GMD based DPC scheme can effectively eliminate the inter-user interference for MU MIMO systems. The elimination of inter-user interference by DPC scheme is beyond the scope of our research for resource allocation and routing in this chapter.

Consider a MU MIMO system, where K users each has a channel matrix $\mathbf{H}_i \in \mathbb{C}^{\mathrm{N_{Ri}} \times \mathrm{N_T}}$, where $i = 1, \ldots, K$. Write $\mathbf{H} = \left[\mathbf{H}_1^T, \ldots, \mathbf{H}_\mathrm{K}^T\right]^T \in \mathbb{C}^{(\mathrm{N_{R1}}+\ldots\mathrm{N_{RK}}) \times \mathrm{N_t}}$, BD-GMD decomposes $\mathbf{H}$ as

$$\mathbf{H} = \mathbf{FLQ}^H, \tag{3.1}$$

where $\mathbf{Q} \in \mathbb{C}^{\mathrm{N_r} \times \mathrm{N_t}}$ is a unitary matrix, $\mathbf{F}$ is a block diagonal matrix, and $\mathbf{L}$ is a lower triangular matrix. $\mathbf{L} = \left[\mathbf{L}_1^T, \ldots, \mathbf{L}_\mathrm{K}^T\right]^T$ contains K blocks , where in each block has the

Table 3.1: Notations

$G(V,\ E)$: our network
V: the set of nodes
E: the set of links
$(i,\ j)$: a unidirectional link
V_n: the set of active nodes in time slot n with $\|V_n\| = N_n^{AVN}$
S_{PU}: the set of PUs
S_{SU}: the set of SUs
N_{SC}: the number of WPM subcarriers
B: the bandwidth of each subcarrier
S_{PRB}: the set of subcarriers in private bands
S_{PLB}: the set of subcarriers in public bands
S_B: the set of subcarriers employed
T_i: the number of transmit antennas at node i
R_i: the number of receive antennas at node i
$S_{i,n}^{NE} = \left\{\beta_1, \ldots, \beta_{L_{i,n}^{NE}}\right\}$: the set of neighbor nodes of node i in time slot n with $\left\|S_{i,n}^{NE}\right\| = L_{i,n}^{NE}$
$S_{i,k,n}^{RNSC} = \left\{\alpha_1^{i,k,n}, \ldots, \alpha_{L_{RNSC}}^{i,k,n}\right\}$: the set of neighbor nodes designated to receive data from node i on subcarrier k in time slot n with $\left\|S_{i,k,n}^{RNSC}\right\| = L_{RNSC}$
$S_{i,n}^{RN} = \left\{\delta_1^{i,n}, \ldots, \delta_{L_{i,n}^{RN}}^{i,n}\right\}$: the set of neighbor nodes designated to receive data from node i in time slot n with $\left\|S_{i,n}^{RN}\right\| = L_{i,n}^{RN}$
$S_{i,j,n}^{SC}$: the set of subcarriers which is allocated to node j by node i in time slot n
$L_{i,n}^{SE}$: the number of sessions waiting at node i in time slot n
$S_{s,i,n}^{POhop} = \left\{\rho_1^{s,i,n}, \ldots, \rho_{L_{s,i,n}^{POhop}}^{s,i,n}\right\}$: the set of possible next-hops for session s at node i in time slot n with $\left\|S_{s,i,n}^{POhop}\right\| = L_{s,i,n}^{POhop}$
$S_{s,i,n}^{HOP}$: the set of selected next-hops for session s at node i in time slot n
$W_{s,i,n}$: the number of packets of session s at node i in time slot n
$\triangle W_s\left(\alpha_g^{i,k,n}\right)$: the number of packets of session s transmitted from node i to node $\alpha_g^{i,k,n}$ on subcarrier k in time slot n

equal diagonal elements.

The diagonal element r_j is calculated as

$$r_j = \left[\frac{\det(\tilde{\mathbf{H}}_j \tilde{\mathbf{H}}_j^H)}{\det(\tilde{\mathbf{H}}_{j-1} \tilde{\mathbf{H}}_{j-1}^H)} \right]^{1/2N_{Rj}}, \tag{3.2}$$

where $\tilde{\mathbf{H}}_j = \left[\mathbf{H}_1^T, \ldots, \mathbf{H}_j^T \right]^T$.

Equation (3.2) indicates that the value of diagonal element varies as the order of sub-matrix changes. In the proposed subcarrier allocation algorithm, the order of channel matrix of individual link for BD-GMD is taken into account.

For the ad-hoc network that we investigate, the application of BD-GMD is introduced as follows. The MIMO channel in link $(i,\ j)$ on subcarrier k in time slot n can be characterized by channel matrix $\mathbf{H}_{i,j,k,n} \in \mathbb{C}^{R_j \times T_i}$, where $i \in V_n$, $j \in S_{i,k,n}^{RNSC}$ and $k \in S_B$. Write $\mathbf{H}_{i,k,n} = \left[\mathbf{H}^T_{i,\alpha_1^{\mathrm{i,k,n}},k,n}, \ldots, \mathbf{H}^T_{i,\alpha_{L_{RNSC}}^{i,k,n},k,n} \right]^T$. The BD-GMD decomposes $\mathbf{H}_{i,k,n}$ as : $\mathbf{H}_{i,k,n} = \mathbf{F}_{i,k,n} \mathbf{L}_{i,k,n} \mathbf{Q}_{i,k,n}^H$, where $\mathbf{L}_{i,k,n}$ is a lower triangular matrix with each block has identical diagonal elements which are calculated by:

$$\begin{aligned} r_{i,\alpha_g^{i,k,n},k,n} &= \left[\frac{\det(\tilde{\mathbf{H}}_{i,\alpha_g^{i,k,n},k,n} \tilde{\mathbf{H}}^H_{i,\alpha_g^{i,k,n},k,n})}{\det(\tilde{\mathbf{H}}_{i,\alpha_{g-1}^{i,k,n},k,n} \tilde{\mathbf{H}}^H_{i,\alpha_{g-1}^{i,k,n},k,n})} \right]^{1/2R_{\alpha_g^{i,k,n}}}, \\ 2 \le g \le L_{RNSC} & \end{aligned} \tag{3.3}$$

where $\tilde{\mathbf{H}}_{i,\alpha_g^{i,k,n},k,n}$ is the accumulated channel matrix from node $\alpha_1^{i,k,n}$ until node $\alpha_g^{i,k,n}$ and $r_{i,\alpha_1^{i,k,n},k,n} = \left[det(\tilde{\mathbf{H}}_{i,\alpha_1^{i,k,n},k,n} \tilde{\mathbf{H}}^H_{i,\alpha_1^{i,k,n},k,n}) \right]^{1/2R_{\alpha_1^{i,k,n}}}$.

3.1.2 Channel Estimation and Prediction for WPM-MIMO Systems

The Channel State Information (CSI) between antenna t and antenna r is estimated every time slot by a minimum mean square error (MMSE) estimator [82] by using training symbols, where $t \in S_i^{TA}$ and $r \in S_{i,n}^{NERA}$.

CSI is highly time dependent in fast time-varying fading environments. In order to reduce the deviation between the CSI used to determine the precoding matrix and the CSI during the transmission caused by the delay, we adopts Kalman filter to predict CSI.

Channel Estimation Consider a time varying multipath fading channel with the total number of pathes L between antenna t and antenna r, for the lth path in the nth time slot, the channel response $h_{t,r,l}(n)$ is a wide-sense stationary (WSS) narrow-band complex

Gaussian process, which is independent of l. From Jakes' model [84], the autocorrelation function (ACF) of $h_{t,r,l}(n)$ is

$$R_{h_{t,r,l}}(m) = E\{h_{t,r,l}(n)\, h_{t,r,l}(n+m)\} = \delta_l^2 J_0(2\pi m T_s f_d) \tag{3.4}$$

where δ_l^2 is the average power of the lth path and $J_0(\bullet)$ is the zeroth-order Bessel function of the first kind. T_s is the sampling period and f_d is the maximum Doppler frequency shift.

$\mathbf{h}_{t,r}(n) = [h_{t,r,1}(n), \ldots, h_{t,r,L}(n)]^T$denotes the CIR between antenna t and antenna r in the nth time slot. It is estimated in every time slot by a MMSE estimator exploiting the learning sequence. The channel is considered to be constant during each time slot.

Given a training sequence composed of $L \times Q$ WPM symbols $\mathbf{s}(m) = [s(m-1), \ldots, s(m-L)]^T$, where $m = 1, \ldots, Q$. The output from the channel can be expressed as:

$$d(m) = \mathbf{h}_{t,r}^T(m)\, \mathbf{s}(m) + e(m) \tag{3.5}$$

where $e(m)$is the additive white Gaussian noise (AWGN) with zero mean and variance σ^2.

Estimated CSI between of link $(t,\ r)$ is given as:

$$\hat{\mathbf{h}}_{t,r}(n) = \mathbf{R}^{-1}\mathbf{P} \tag{3.6}$$

where $\mathbf{R} = E\left[\mathbf{s}(m)\, \mathbf{s}^H(m)\right]$, and $\mathbf{P} = E[\mathbf{s}(m)\, \mathbf{d}^*(m)]$.

The MMSE channel estimation for Wavelet-OFDM systems is different from that for OFDM systems. OFDM systems adopts cyclic prefix to turn the linear convolution between transmitted signal and channel impulse response into a circular convolution, then DFT convert circular convolution in time domain to multiplication in frequency domain. The MMSE channel estimation for OFDM is to minimize the MSE between the desired signal and the channel output both in frequency domain [83], since multiplication in frequency domain can reduce the complexity of the frequency domain MMSE channel estimation. Wavelet-OFDM adopts DWPT which is unable to lead circular convolution in time domain to multiplication in frequency domain as DFT. Therefore, Wavelet-OFDM systems use the MMSE channel estimation in time domain which is performed before DWPT.

Channel Prediction

Auto-regressive Model Write $\hat{\mathbf{H}}_i(n) = \left[\hat{\mathbf{h}}_{1,1}^T(n), \ldots, \hat{\mathbf{h}}_{1,R_{i,n}^{NERA}}^T(n), \ldots, \hat{\mathbf{h}}_{T_i,R_{i,n}^{NERA}}^T(n)\right]^T$. The dynamics of $\hat{\mathbf{H}}_i(n)$ can be modeled by a complex auto-regressive (AR) process of order d:

$$\hat{\mathbf{H}}_i(n) = -\sum_{c=1}^{d} \mathbf{\Psi}_i(c)\,\hat{\mathbf{H}}_i(n-c) + \mathbf{z}_i(n), \tag{3.7}$$

where $\mathbf{\Psi}_i(c) = blkdiag\left[\boldsymbol{\gamma}_{1,i}(c), \ldots, \boldsymbol{\gamma}_{F,i}(c)\right]$ is a $FN_{SC} \times FN_{SC}$ matrix with $F = T_i R_{i,k,n}$ and $\mathbf{z}_i(n) = \left[\mathbf{z}_{1,i}^T(n), \ldots, \mathbf{z}_{F,i}^T(n)\right]^T$ is a $FN_{SC} \times 1$ complex Gaussian vector with covariance matrix $\mathbf{Z}_i$. The parameters $\mathbf{\Psi}_i(c)$, $c = 1, \ldots, d$ and $\mathbf{Z}_i = blkdiag\left[\mathbf{Z}_{1,i}, \ldots, \mathbf{Z}_{F,i}\right]$ can be determined by solving the set of Yule-Walker equations [85].

Kalman Filer The CSI space model is defined as

$$\mathbf{E}_i(n) = \left[\hat{\mathbf{H}}_i^T(n),\ \hat{\mathbf{H}}_i^T(n-1), \ldots,\ \hat{\mathbf{H}}_i^T(n-d+1)\right]^T$$

. We formulate the process model in Equation (3.8) using Equation (3.7) and the measurement model in Equation (3.9) using Equation (3.6):

$$\mathbf{E}_i(n) = \mathbf{S}_{1,i}\mathbf{E}_i(n-1) + \mathbf{S}_{2,i}\mathbf{z}_i(n), \tag{3.8}$$

$$\mathbf{J}_i(n) = \mathbf{S}_{3,i}\mathbf{E}_i(n) + \boldsymbol{e}_i(n), \tag{3.9}$$

where $\mathbf{S}_{1,i} = \begin{bmatrix} -\mathbf{\Psi}_i(1) & \cdots & -\mathbf{\Psi}_i(d) \\ \mathbf{I}_{(d-1)FN_{SC}} & & \mathbf{0}_{(d-1)FN_{SC},FN_{SC}} \end{bmatrix}$, $\mathbf{S}_{2,i} = \left[\mathbf{I}_{FN_{SC}}, \mathbf{0}_{FN_{SC},(d-1)FN_{SC}}\right]^T$, $\mathbf{S}_{3,i} = \left[blkdiag\left[\mathbf{x}_{1,1}(n), \ldots, \mathbf{x}_{T_i,R_{i,n}^{NERA}}(n)\right], \mathbf{0}_{FN_{SC},(d-1)FN_{SC}}\right]$ and $\boldsymbol{e}_i(n) = \left[u_1^T, \ldots, u_{T_i}^T\right]^T$ with $u_g = \left[\mathbf{w}_1^T(n), \ldots, \mathbf{w}_{R_{i,n}^{NERA}}^T(n)\right]^T$, $g = 1, \ldots, T_i$. Let $\hat{\mathbf{E}}_i(n)$ be the a priori state estimate in the nth time slot given knowledge of the process prior to the nth time slot and $\hat{\mathbf{E}}_i(n \mid n)$ be the a posteriori state estimate in the nth time slot given measurement $\mathbf{J}_i(n)$. $\mathbf{P}_i(n)$ and $\mathbf{P}_i(n \mid n)$ are the a priori and the a posteriori error estimate covariance matrices with the same size $dFN_{SC} \times dFN_{SC}$, respectively. The Kalman filter recursively updates $\hat{\mathbf{E}}_i(n)$ and $\mathbf{P}_i(n)$ by using Time Update Equations and Measurement Update Equations [86, 94].

3.2 Resource Allocation and Routing

Our proposed subcarrier allocation, power allocation and routing algorithms are performed in succession every time slot based on predicted CSI. The subcarrier allocation and routing algorithms can be carried out in a distributed fashion by each node. The power allocation algorithm is a centralized algorithm which is implemented at a beacon node, since the interference caused by one link to all other links having the same destination node is considered and the power of all other links is not assumed to be known but also need to be allocated at the same time.

3.2.1 Subcarrier Allocation

In the context of $\sum_{s=1}^{L_{i,n}^{SE}} W_{s,i}(n) \gg \sum_{k=1}^{N_{SC}} \sum_{g=1}^{L_{RNSC}} \triangle W_s\left(\alpha_g^{i,k,n}\right),\ i \in V_n$. This condition makes the total number of packets waiting for transmission far outweigh the capacity of the entire network. It intends to lead the network investigated to pursue maximizing capacity in the observed duration. Therefore, the subcarrier allocation problem can be modeled as: every time slot during the observed period, $S_{i,k,n}^{RNSC}$ selects L_{RNSC} nodes out of $L_{i,n}^{NE}$ nodes in $S_{i,n}^{NE}$ to maximize $\sum_{g=1}^{L_{RNSC}} r_{i,\alpha_g^{i,k,n},k,n}$ with respect to PUs' priority to access to the subcarrier in private bands. We propose a sub-optimal algorithm which adopts a threshold r_{SP}. In order to access the subcarrier in private bands, the sub-channel gain of SUs should be higher than that of PUs with the difference beyond the threshold r_{SP}. The proposed subcarrier allocation algorithm is described in detail by Algorithm 1.

Algorithm 1: *Subcarrier Allocation Algorithm*

1: *Initialize* r_{SP}, $S_{i,n}^{NE}$, $\hat{\mathbf{H}}_{i,j,k,n}$, $i \in V_n$, $j \in S_{i,n}^{NE}$, $k \in S_B$

2: for $i \in V_n$ *and* $k \in S_B$ ***do***

3: $S = S_{i,n}^{NE}$,

4: *Calculate* $r_1^{PU} = \max_{j \in S_{PU} \cap S}(\left[\det(\hat{\mathbf{H}}_{i,j,k,n}\hat{\mathbf{H}}_{i,j,k,n}^H)\right]^{1/2R_j})$
and $r_1^{SU} = \max_{j \in S_{SU} \cap S}(\left[\det(\hat{\mathbf{H}}_{i,j,k,n}\hat{\mathbf{H}}_{i,j,k,n}^H)\right]^{1/2R_j})$,

5: *Select the first user:*

$$\alpha_1^{i,k,n} = \begin{cases} \arg\max_{j \in S_{PU} \cap S} \det(\hat{\mathbf{H}}_{i,j,k,n}\hat{\mathbf{H}}_{i,j,k,n}^H), \\ \text{if } k \in S_{PRB},\ r_1^{SU} - r_1^{PU} \le r_{SP} \\ \text{or } k \in S_{PLB},\ r_1^{SU} - r_1^{PU} \le 0; \\ \arg\max_{j \in S_{SU} \cap S} \det(\hat{\mathbf{H}}_{i,j,k,n}\hat{\mathbf{H}}_{i,j,k,n}^H), \\ \text{if } k \in S_{PRB},\ r_1^{SU} - r_1^{PU} > r_{SP} \\ \text{or } k \in S_{PLB},\ r_1^{SU} - r_1^{PU} > 0 \end{cases},$$

6: $S = S - \left\{\alpha_1^{i,k,n}\right\}$, $\hat{\mathbf{H}}_1 = \hat{\mathbf{H}}_{i,\alpha_1^{i,k,n},k,n}$,

7: for $g = 2$ ***to*** L_{RNSC} ***do***

8: *Calculate* $r_g^{PU} = \max_{j \in S_{PU} \cap S}(\left[\frac{\det(\hat{\mathbf{H}}_{i,j,k,n}\hat{\mathbf{H}}_{i,j,k,n}^H)}{\det(\hat{\mathbf{H}}_{g-1}\hat{\mathbf{H}}_{g-1}^H)}\right]^{1/2R_j})$
and $r_g^{SU} = \max_{j \in S_{SU} \cap S}(\left[\frac{\det(\hat{\mathbf{H}}_{i,j,k,n}\hat{\mathbf{H}}_{i,j,k,n}^H)}{\det(\hat{\mathbf{H}}_{g-1}\hat{\mathbf{H}}_{g-1}^H)}\right]^{1/2R_j})$,
where $\hat{\mathbf{H}}_g = \left[\hat{\mathbf{H}}_{g-1}^T\ \hat{\mathbf{H}}_{i,j,k,n}^T\right]^T$

9: *Select the gth user:*

$$\alpha_g^{i,k,n} = \begin{cases} \arg\max_{j \in S_{PU} \cap S}(\left[\frac{\det(\hat{\mathbf{H}}_{i,j,k,n}\hat{\mathbf{H}}_{i,j,k,n}^H)}{\det(\hat{\mathbf{H}}_{g-1}\hat{\mathbf{H}}_{g-1}^H)}\right]^{1/2R_j}), \\ \text{if } k \in S_{PRB},\ r_g^{SU} - r_g^{PU} \le r_{SP} \\ \text{or } k \in S_{PLB},\ r_g^{SU} - r_g^{PU} \le 0; \\ \arg\max_{j \in S_{SU} \cap S}(\left[\frac{\det\hat{\mathbf{H}}_{i,j,k,n}\hat{\mathbf{H}}_{i,j,k,n}^H)}{\det(\hat{\mathbf{H}}_{g-1}\hat{\mathbf{H}}_{g-1}^H)}\right]^{1/2R_j}), \\ \text{if } k \in S_{PRB},\ r_g^{SU} - r_g^{PU} > r_{SP} \\ \text{or } k \in S_{PLB},\ r_g^{SU} - r_g^{PU} > 0 \end{cases},$$

10: $S = S - \left\{\alpha_g^{i,k,n}\right\}$, $\hat{\mathbf{H}}_g = \left[\hat{\mathbf{H}}_{g-1}^T\ \hat{\mathbf{H}}_{i,\alpha_g^{i,k,n},k,n}^T\right]^T$,

11: end for*,* ***end for***

3.2.2 Power Allocation

We investigate power allocation for active links and the power is presumed to be equally distributed among R_j sub-channels in link $(i,\ j)$.

The SINR of link $(i,\ j)$ on subcarrier k in time slot n is defined as:

$$\Upsilon_{i,j,k,n} = \frac{(P_{i,j,k,n}/R_j)\, r^2_{i,j,k,n}}{\sigma_j^2 + \sum_{p \in S^{RNSC}_{j,k,n},\, p \neq i} (P_{p,j,k,n}/R_j)\, r^2_{p,j,k,n}} \tag{3.10}$$

where $i \in V_n,\ j \in S^{RNSC}_{i,k,n},\ k \in S_B$, $P_{i,j,k,n}$ is the transmit power of link $(i,\ j)$ on subcarrier k in time slot n and $\mathbf{w}_j \sim N(0,\ \sigma_j^2 \mathbf{I}_{R_j})$ is AWGN at node j.

The capacity of the link $(i,\ j)$ on subcarrier k in time slot n can be calculated as:

$$C_{i,j,k,n} = BR_j \log_2 (1 + \Upsilon_{i,j,k,n}) \tag{3.11}$$

For each node, there is a SINR threshold which decides the highest bit error rate (BER) for the successful decoding of the received signal. In private bands, the SINR threshold for PUs is higher than that for SUs, thus we define the SINR threshold indicator function $\eta_{j,k}$ for node j on subcarrier k as: $\begin{cases} \eta_{j,k} = \eta_{PU}, & \text{if } j \in S_{PU},\ k \in S_{PRB} \\ \eta_{j,k} = \eta_{SU}, & \text{if } j \in V_n,\ k \in S_{PLB} \text{ or } j \in S_{SU},\ k \in S_{PRB} \end{cases}$.

For link $(i,\ j)$ on subcarrier k in time slot n, the successful decoding condition can be formulated as:

$$\Upsilon_{i,j,k,n} \geq \eta_{j,k},\ \forall i \in V_n,\ j \in S^{RNSC}_{i,k,n},\ k \in S_B \tag{3.12}$$

Based on the assupmtion that each node has the identical maximum transmit power, the total power of the network is fixed. The power budget constraint can be expressed as:

$$\sum_{k \in S_B} \sum_{i \in V_n} \sum_{j \in S^{RNSC}_{i,k,n}} P_{i,j,k,n} \leq P_{budget} \tag{3.13}$$

Our power allocation method aims to maximize the network capacity with respect to the above constraints. This can be expressed as:

P1: Given:$G(V,\ E)$, $S^{RNSC}_{i,k,n}$, $\hat{\mathbf{L}}_{i,k,n}$, $\eta_{i,j}$, $i \in V_n,\ j \in S^{RNSC}_{i,k,n},\ k \in S_B$, P_{budget}

Find: $P_{i,j,k,n}$ $i \in V_n,\ j \in S^{RNSC}_{i,k,n},\ k \in S_B$

Maximize: $\sum_{k \in S_B} \sum_{i \in V_n} \sum_{j \in S^{RNSC}_{i,k,n}} C_{i,j,k,n}$

Subject to: Equation (3.12) and (3.13)

The objective function (capacity in terms of power being assigned) is not concave in the joint variables. **P1** is a non-convex optimization. It is difficult to deal with computationally. The standard convex optimization methods can be used for this problem to provide a suboptimal solution.

For **P1**, we can write the Lagrangian function as:

$$\begin{aligned}\mathcal{L}(\mathbf{P}_n, \boldsymbol{\lambda}) &= \sum_{k\in S_B}\sum_{i\in V_n}\sum_{j\in S_{i,k,n}^{RNSC}} C_{i,j,k,n} \\ &+ \sum_{k\in S_B}\sum_{i\in V_n}\sum_{j\in S_{i,k,n}^{RNSC}} \left[\lambda_{i,j,k,n}\left(\eta_{j,k} - \Upsilon_{i,j,k,n}\right)\right] \\ &+ \theta\left(\sum_{k\in S_B}\sum_{i\in V_n}\sum_{j\in S_{i,k,n}^{RNSC}} P_{i,j,k,n} - P_{budget}\right)\end{aligned} \tag{3.14}$$

where $\boldsymbol{\lambda} = \left[\lambda_{i,j,k,n}\, i \in V_n,\ j \in S_{i,k,n}^{RNSC},\ k \in S_B,\ \theta\right]$ is a vector of Lagrange multipliers with $M = N_{SC}N_n^{AVN}L_{RNSC}$ and $\mathbf{P}_n = \left\{P_{i,j,k,n},\, i \in V_n, j \in S_{i,k,n}^{RNSC}, k \in S_B\right\}$.

From the Karush-Kuhn-Tucke condition:

$$\frac{\partial \mathcal{L}}{\partial P_{i,j,k,n}} = 0\ i \in V_n,\ j \in S_{i,k,n}^{RNSC},\ k \in S_B \tag{3.15}$$

$P_{i,j,k,n}$ can be expressed in terms of $\lambda_{i,j,k,n}$ and θ:

$$P_{i,j,k,n} = \left[\frac{BR_j}{(\lambda_{i,j,k,n} - \theta Q)\ln 2} - 1\right] Q \tag{3.16}$$

where $Q = \frac{\sigma_j^2 + \sum_{p\in S_{j,k,n}^{RNSC},\, p\neq i}\left(P_{p,j,k,n}/R_j\right) r_{p,j,k,n}^2}{r_{i,j,k,n}^2/R_j}$.

The multipliers are updated by subgradient method as:

$$\boldsymbol{\lambda}^{O+1} = \left[\boldsymbol{\lambda}^O - \xi^K \Phi \Psi\right]^+ \tag{3.17}$$

where $\Phi = \prod_{k\in S_B, i\in V_n, j\in S_{i,k,n}^{RNSC}}\left(\eta_{j,k} - \Upsilon_{i,j,k,n}\right)$, $\Psi = \sum_{k\in S_B}\sum_{i\in V_n}\sum_{j\in S_{i,k,n}^{RNSC}} P_{i,j,k,n} - P_{budget}$ and $\xi^K > 0$ is the Kth step size.

Our proposed power allocation algorithm is given by Algorithm 2.

Algorithm 2: Power Allocation Algorithm

1: Initialize $G(V,\ E), S_{i,k,n}^{RNSC}, \hat{\mathbf{L}}_{i,k,n}, \eta_{i,j}, i \in V_n, j \in S_{i,k,n}^{RNSC}, k \in S_B$, $P_{budget}, \boldsymbol{\lambda}, \xi^K, N_{step}$

2: for $K = 1$ to N_{step} **do**

3: Assign $P_{i,j,k,n}, i \in V_n,\ j \in S_{i,k,n}^{RNSC},\ k \in S_B$ as in Equation (3.16)

4: if $P_{i,j,k,n}$ satisfy Equation (3.12) and (3.13) **,** go to **7**, **else** return to **1**

5: end if

6: Update Lagrange Multipliers as in Equation (3.17)

7 : end for

Table 3.2: system parameters

N_{SC}	8	$T_{i,\, i\in V}$	2
B	150kHz	$R_{i,\, i\in V}$	2
$P_{budget/node}$	1W	SNR	25dB
$\|S_{PU}\|$	25	η_{SU}	15dB
$\|S_{SU}\|$	25	η_{PU}	19dB
AR model order	3	Average node speed	10km/h
Coverage area	5km × 5km	Wavelet type	db4

3.2.3 Routing

In our multi-hop ad-hoc network, we consider a multicast routing strategy which intends to maximize network throughput. We adopt Greedy Algorithm: For each active node, in each iteration, we choose a session which has the highest pressure [87], and then choose a subcarrier which has the largest capacity to convey a segmentation of the selected session until all the subcarriers are assigned. Our proposed routing algorithm is detailed by Algorithm 3.

Algorithm 3: Routing Algorithm

1: Initialize $G(V,\, E), S_{i,n}^{SE}, W_{s,i,n}, S_{i,n}^{RN}, S_{s,i,n}^{POhop}, S_{i,j,n}^{SC}, C_{i,j,k,n}$, $S_{s,i,n}^{HOP} = \emptyset$

2: for $i \in V_n$ **do, for** $s \in S_{i,n}^{SE}$ **do**

3: $s^* = \arg\max_{s\in S_{i,n}^{SE}} W_{s,i,n}$,

4: $\alpha(s^*, j^*, k^*, n) = \arg\max_{j\in S_{i,n}^{RN}\cap S_{s^*,i,n}^{POhop}, k\in S_{i,j,n}^{SC}} C_{i,j,k,n}$,

5: $S_{s^*,i,n}^{HOP} = S_{s^*,i,n}^{HOP} + \{\alpha(s^*, j^*, k^*, n)\}$,

6: $W_{s^*,i,n} = \left[W_{s^*,i,n} - \triangle W\left(\alpha(s^*, j^*, k^*, n)\right)\right]^+$,

7: If $W_{s^*,i,n} = 0$**, then** $S_{i,n}^{SE} = S_{i,n}^{SE} - s^*$

8: $S_{i,j,n}^{SC} = S_{i,j,n}^{SC} - \{k^*\}$,

9: end for, **end for**

3.3 Numerical Results

In order to validate our proposed scheme, we implement the proposed resource allocation and routing scheme using perfect CSI, estimated CSI and predicted CSI respectively. For the purpose of evaluating the contribution of each of the three methods in our proposed scheme to throughput enhancement, we design three test schemes using perfect CSI. These three schemes adopt different methods to replace Algorithm 1, 2 and 3 respectively. The first test scheme allocates the subcarriers randomly. The second scheme distributes the power equally among the active links. The third scheme, for each active node, chooses the session which has the shortest destination. The simulation parameters are summarized in Table 3.2.

Fig. 3.1 presents the effect of CSI precision on average throughput of entire network. As the number of sessions increases, throughput generated by the proposed scheme using three different types of CSI exhibits uptrend, where the scheme which adopts more precise CSI makes throughput grow faster and throughput generated by the proposed scheme using predicted CSI is very close to that of perfect CSI. It indicates that our proposed scheme based on correct CSI can effectively augment throughput. Additionally, channel prediction is indispensable in fast time-varying fading environments. We measure the performance of our proposed scheme and three test schemes by observing the variation of average throughput of entire network during 1 minute generated by each scheme as the number of session increases. Fig. 3.2 shows the variation tendencies of average throughput generated by four schemes. The test scheme 1 generates the lowest throughput which has the lowest increment. It implies that throughput is highly improved by our subcarrier allocation method compared to the other two methods. Test scheme 3 and 2 generate less throughput than our proposed scheme. The gap between the throughput generated by the test scheme 3 and that of the proposed scheme is extremely small in the region of the total number of sessions under 9, but then this gap is gradually enlarged by the increase of the total number of sessions. The gap between the throughput generated by the test scheme 2 and that of the proposed scheme appears and increases in the region of the total number of sessions between 4 and 7, but after it remains almost stable. We can conclude that the proposed subcarrier allocation method has the largest contribution to throughput enhancement, followed by the proposed routing method and the proposed power allocation method.

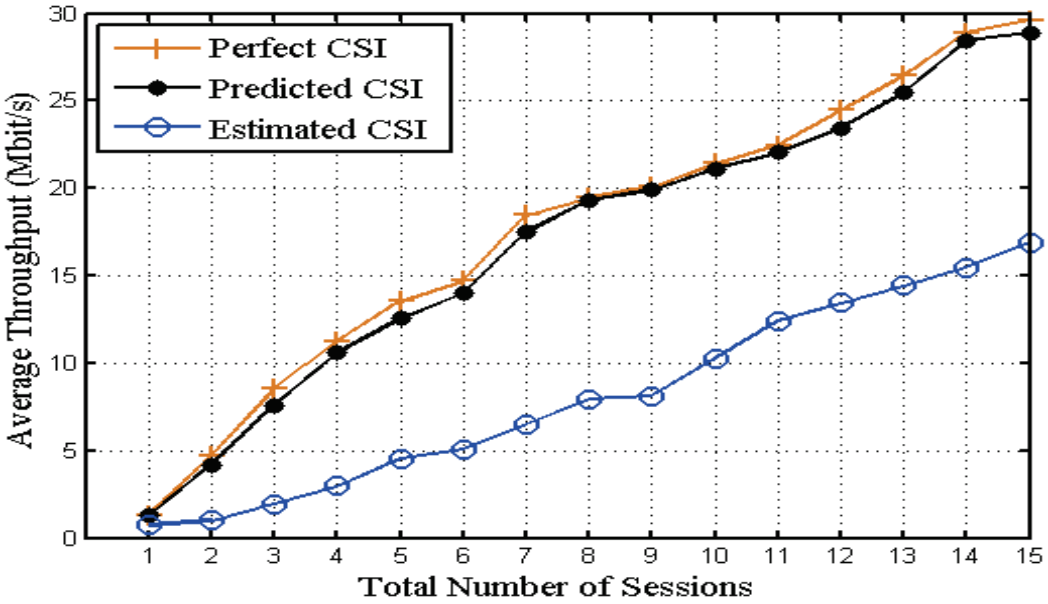

Figure 3.1: Average throughput for perfect CSI, predicted CSI and estimated CSI

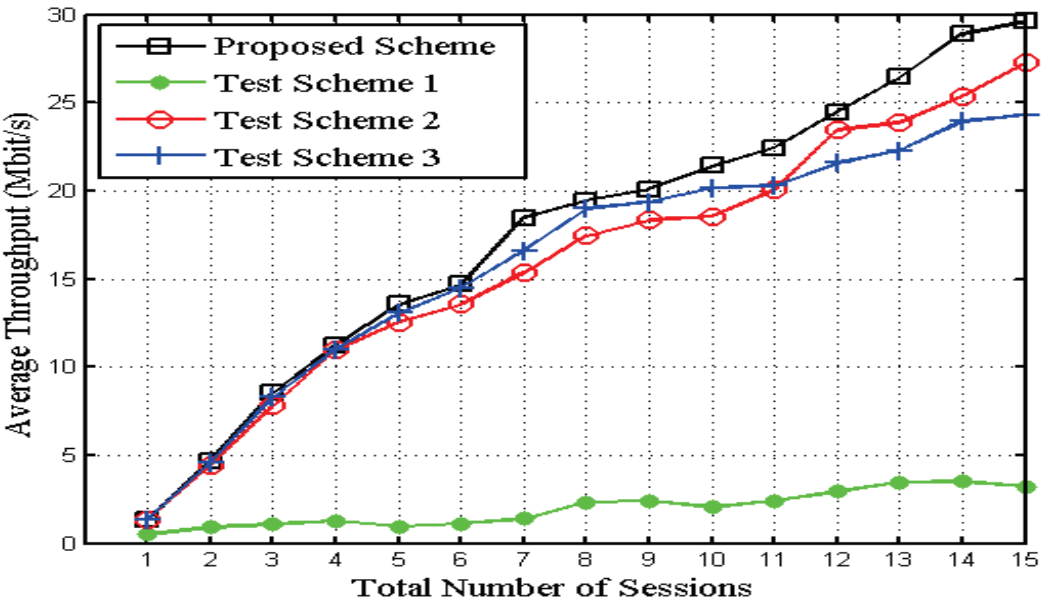

Figure 3.2: average throughput for proposed scheme, test scheme 1, 2, and 3

Chapter 4

Downlink Scheduling in Network MIMO

Contents

In this chapter, we propose a user scheduling scheme which is based merely on the ergodic rate. We derive the ergodic rate of each user for our network MIMO system from the average Signal-to-Noise Ratio (SNR) and the covariance of prediction error. Further more, we design a joint precoding for the selected users. The precoding matrices are contrived according to the predicted Channel State Information at Transmitter (CSIT) in the future time slot to reduce the deviation caused by delay. Such a network MIMO system is under consideration, where the users are cooperatively served by multiple Base Stations (BSs). User scheduling and joint precoding are executed by a central unit connected to all BSs. Both the above functions require the CSIT which is acquired by an uplink feedback overhead. Simulation results demonstrate a conspicuous improvement in user spectral efficiency with reduced feedback.

Frequency reuse among neighboring cells in conventional cellular networks can provoke Inter-Cell Interference (ICI) that leads to performance degradation. Base Station (BS) cooperation becomes a necessity to overcome the above problem. Multiple Input Multiple Output (MIMO) technique has been in a starring role to improve the throughput of broadband wireless networks. Assuming perfect back-haul connection, the network consisting of multiple cells can be viewed as a virtual MIMO system, and the users are jointly served by multiple BSs.

In each resource unit, the cooperating BSs in one cluster jointly select a set of active users. For the selected users, precoding is applied for the purpose that the received signal for the intended user is acquired with lowest interference. Linear precoding for Multi-User (MU) MIMO based on block diagonalization (BD) was proposed in [88], in which the signal for each user is projected onto the nullspace of the augmented channel matrix of other users. The authors in [89] considered precoding for clustered network MIMO with inter-cluster coordination. In [90], the authors proposed a greedy user selection algorithm for single-cell MU-MIMO networks based on BD precoding. Scheduling in network MIMO based on Successive Zero-Forcing (SZF) was discussed in [91], where the Multi-User Interference (MUI) is partially canceled.

The above works implicitly assumed that perfect Channel State Information at the Transmitter (CSIT) is available, which may not hold in practical systems. The ergodic capacity in single-cell MIMO system under delayed CSIT with BD precoding was analyzed in [92], where the authors pointed out that under certain conditions it is preferred to adopt Single-User (SU)-MIMO technique over MU-MIMO scenario. The authors in [93] addressed the scheduling problem considering different channel variation among users, and it classified the users into two categories: predictable and non-predictable. The users belong in the first category are served in MU mode, while the other users are served in SU mode.

The overhead introduced by CSIT feedback limits the performance of MIMO systems.

For multi-cell networks with large number of users, further feedback reduction is desired. In this paper, we propose a framework that performs scheduling based on the asymptotic ergodic rate which is a function of large-scale channel behavior and the maximum Doppler shift of users. Then channel prediction is applied at the transmitter side to provide a predicted CSIT for selected users, based on which the precoding matrix can be determined. Our main contributions are as follows. First, we analyze the asymptotic ergodic rate in network MIMO systems with imperfect predicted CSIT. We extend the work for single-cell MIMO systems by introducing the concept of equivalent Gaussian channels. It is shown that under low SNR or high channel variation, selecting less users may improve the throughput due to the reduced MUI. Second, we propose a user selection method based on a two-stage feedback mechanism. The *long-term* feedback contains the first and second order statistics of all users, and are used to select a set of users to be served together in one frame, while the *short-term* feedback is applied only to the selected users on each resource unit. In this way the CSIT required for precoding is available, while the amount of uplink overhead for feedback is reduced.

4.1 System Model

We consider a three-cell cluster layout depicted in Fig. 4.1. With sectoring, users in the dashed hexagonal area are jointly served by three BSs.

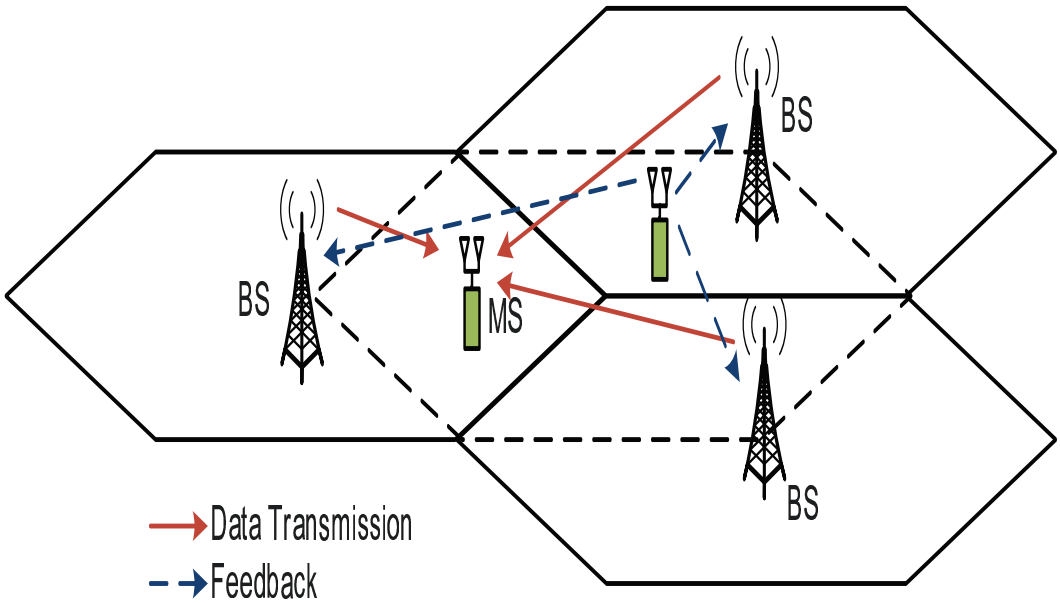

Figure 4.1: Three-cell Cluster

The aggregated channel coefficient matrix of user u from all the B cooperating BSs is written as

$$\mathbf{H}_u = [\rho_{u,1}\mathbf{H}_{u,1}, \cdots, \rho_{u,B}\mathbf{H}_{u,B}] \tag{4.1}$$

where $\mathbf{H}_{u,b} \in \mathbb{C}^{N_r \times N_t}$ represents the small-scale fading channel matrix associated with user u and BS b, where N_t and N_r are the number of antennas of one BS and one user, respectively. $\rho_{u,b}$ captures the large-scale fading behavior including pathloss and shadowing. The coefficients in $\mathbf{H}_{u,b}$ are modeled as wide-sense stationary (WSS), narrow-band complex Gaussian processes. The received signal of user u can be written as

$$\mathbf{y}_u = \mathbf{H}_u\mathbf{T}_u\mathbf{x}_u + \mathbf{H}_u \sum_{u' \neq u} \mathbf{T}_{u'}\mathbf{x}_{u'} + \mathbf{n}_u \tag{4.2}$$

where $\mathbf{T}_u = [\mathbf{T}_{u,1}, \cdots, \mathbf{T}_{u,B}]$ is the aggregated precoder matrix with orthonormal columns, $\mathbf{x}_u$ is the transmitted signal and $\mathbf{n}_u$ is a white complex Gaussian noise vector with covariance matrix $\sigma^2\mathbf{I}_{N_r}$. The second term in (4.2) represents the multi-user interference (MUI). With BD precoding and perfect CSIT, the MUI can be eliminated by transmitting the signal of one user on the nullspace of the augmented channel matrix of other simultaneously selected users. However, the MUI is not perfectly canceled in our system due to the inaccuracy of channel prediction.

To track the channel variation, here we adopt the same channel prediction method as introduced in Chapter 3. In which the channel coefficients in future slots are predicted based on previous channel feedback, by applying the auto-regressive (AR) model and Kalman filter.

4.2 Asymptotic Ergodic Rate Analysis

In this section, based on the approximated channel, we provide asymptotic ergodic capacity analysis for network MIMO systems for single-user (SU) and multi-user (MU) cases. For better tractability, total power constraint (TPC) in each cluster is applied instead of per BS power constraint (PBPC). Due to the utilization of multi-user interference cancellation pre-coding scheme (BD pre-coding), each user,Äôs MIMO channel is decomposed into N_r sub-channel. The power allocation scheme assigns power for each sub-channel. When m users are served simultaneously, with TPC and equal power allocation for each stream, the transmission power for one stream is given by $\gamma_m = P/(mN_r)$ for all users where P is the cluster power constraint, and assume N_r streams are assigned to each user. The asymptotic rates are given as functions of the large-scale fading behavior and the Doppler shift.

4.2.1 The Equivalent Channel Matrix

For single-cell MIMO systems with independent identically distributed (i.i.d.) Gaussian channel coefficients, the asymptotic ergodic rate is analyzed in [95]. To find the asymptotic ergodic rate for network MIMO systems where the elements of the aggregated channel matrix are not always i.i.d. Gaussian random variables, we propose a method to transform the network MIMO channel matrix into a virtual single cell MIMO channel. We first introduce the following definition [96]:

Definition 1 *Let $\mathbf{z}_i \in \mathbb{C}^{q\times 1}$, $i = 1, ..., l$ be multivariate normal distributed vectors with zero mean and covariance matrix $\mathbf{C}$, and $\mathbf{Z}$ denotes the $q \times l$ matrix composed of the column vectors $\mathbf{z}_i$, then the matrix $\mathbf{Z}\mathbf{Z}^H$ has a central Wishart distribution with covariance matrix $\mathbf{C}$ and l degrees of freedom, denoted as $\mathbf{Z}\mathbf{Z}^H \sim \mathcal{CW}_l(0, \mathbf{C})$.*

We observe that $\mathbf{H}_u\mathbf{H}_u^H = \sum_{b=1}^{B} \rho_{u,b}^2 \mathbf{H}_{u,b}\mathbf{H}_{u,b}^H$ is a linear combination of central Wishart matrices, and the row vectors of have identical covariance matrix. From [97], the distribution can be approximated $\mathbf{H}_u\mathbf{H}_u^H \sim \mathcal{CW}_{\hat{N}_{t,u}}(0, \rho_u \mathbf{I}_{N_r})$ where $\hat{N}_{t,u} = N_t \left(\frac{(\sum_b^B \rho_{u,b})^2}{\sum_b^B \rho_{u,b}^2} \right)$ and $\rho_u = \left(\frac{\sum_b^B \rho_{u,b}^2}{\sum_b^B \rho_{u,b}} \right)$.

The above approximation can be interpreted as if the user is communicating with a virtual BS with $\hat{N}_{t,u}$ transmitting antennas, and the channel is modeled as an equivalent $N_r \times \hat{N}_{t,u}$ channel matrix $\rho_u \hat{\mathbf{H}}_u$, where $\hat{\mathbf{H}}_u$ is the equivalent small-scale fading matrix and ρ_u is the equivalent large-scale fading parameter. Since ρ_u is determined by the large-scale fading gain from different BSs, it can be viewed that the user is actually served by the antennas from BSs with larger $\rho_{u,b}$'s.

4.2.2 Asymptotic Rate for SU Network MIMO

We first consider the case where only a single user is served in the multi-cell network.

Proposition 1 *Under single user network MIMO transmission, as $BN_t, N_r \to \infty$ with $BN_t/N_r = \beta$, the asymptotic ergodic rate per receive antenna with normalized thermal noise power can be approximated by*

$$\frac{C_{su}(\beta,\gamma)}{N_r} = \log\left[1 + \hat{\beta}\hat{\gamma} - F(\hat{\beta},\hat{\gamma})\right] + \hat{\beta}\log_2\left[1 + \hat{\gamma} - F(\hat{\beta},\hat{\gamma})\right] - \frac{\log_2(e)}{\hat{\gamma}} F(\hat{\beta},\hat{\gamma}) \tag{4.3}$$

where

$$F(x,y) = \frac{1}{4}\left[\sqrt{1+y(1+\sqrt{x})^2} - \sqrt{1+y(1-\sqrt{x})^2}\right]^2$$
$$\hat{\beta} = \hat{N}_{t,u}/N_r,\ \hat{\gamma} = \rho_u^2\gamma_m$$

Proof:
For SU-MIMO link using SVD, [92] provides an approximation of ergodic capacity per receive antenna with perfect CSIT:

$$C_{SVD} \approx \mathbb{E}\left[\log\det\left(\mathbf{I}_{N_r} + \frac{N_t}{N_r}\gamma\mathbf{H}\mathbf{H}^H\right)\right], \tag{4.4}$$

Where γ is the transmission power. For normalized noise, γ is the average SNR. The effective SNR of a SU-MIMO system using SVD with perfect CSIT is approximated as $\frac{N_t}{N_r}\gamma$ instead of γ which is the SNR of a point-to-point MIMO system.

For easily calculating, C_{SVD} can be further approximated based on C_{asypo}: the asymptotic capacity per receive antenna of a point-to-point MIMO system as $N_t,\ N_r \to \infty$ with $\frac{N_t}{N_r} \to \beta'$.

$$\begin{aligned} C_{SVD}/N_r &\approx C_{asypo}\left(\beta',\ \beta'\gamma\right)/N_r \\ &= \log_2\left[1+\beta'\gamma - F\left(\beta',\ \gamma\right)\right] + \\ \beta'\log_2\left[1+\gamma-F\left(\beta',\ \gamma\right)\right] &\quad -\frac{\log_2(e)}{\gamma}F\left(\beta',\ \gamma\right) \end{aligned} \tag{4.5}$$

In part. A, the channel matrix in network MIMO system is modeled as an equivalent channel matrix in a virtual single cell $\rho_u\hat{\mathbf{H}}_u \in \mathbb{C}^{N_r\times\hat{N}_{t,u}}$. Therefore, the asymptotic capacity per receive antenna of SU network MIMO system is $C_{su}/N_r = C_{SVD}\left(\hat{\beta},\ \hat{\beta}\hat{\gamma}\right)/N_r$. Then we can get result in 5.27.

4.2.3 Asymptotic Rate for MU Network MIMO

Denote the BD precoder for user u designed based on the predicted CSIT as $\mathbf{T}_u^{(P)}$, the received signal can be rewritten as

$$\mathbf{y}_u = \mathbf{H}_u\mathbf{T}_u^{(P)}\mathbf{x}_u + \mathbf{E}_u\sum_{u'\neq u}\mathbf{T}_{u'}^{(P)}\mathbf{x}_{u'} + \mathbf{n}_u \tag{4.6}$$

The achievable rate of user u is given by

$$\begin{aligned} R_u &= \mathbb{E}\left[\log_2\det\left(\hat{\mathbf{R}}_u + \gamma\beta_u^2\mathbf{H}_{eff,u}\mathbf{H}_{eff,u}^H\right)\right] \\ &- \mathbb{E}\left[\log_2\det\left(\hat{\mathbf{R}}_u\right)\right] \end{aligned} \tag{4.7}$$

where $\mathbf{R}_u^{-1}$ is the interference plus noise covariance matrix given by

$$\mathbf{R}_u = \mathbf{E}_u \left(\sum_{u' \neq u} \gamma_m \mathbf{T}_{u'}^{(P)} \mathbf{T}_{u'}^{(P)^H} \right) \mathbf{E}_u^H + \sigma^2 \mathbf{I}_{N_r} \tag{4.8}$$

Before deriving the asymptotic rate for the MU case, we need the following lemma.

Lemma 1 *Consider N complex random variables $x_i, i = 1, ..., N$ with $\sum_{i=1}^{N} \|x_i\|^2 = 1$. $x_k,\ k = 1, \ldots, N$ are K points randomly selected from the set of points $\mathbf{S} = \{x_i\}_{i=1}^{N}$. If $\|x_i\|^2$ are uniformly distributed, the mean of variable $\sum_{k=1}^{K} \|x_k\|^2$ is K/N.*

Proof:
Since the variable $\|x_i\|^2$ are uniformly distributed, and $\sum_{i=1}^{N} \|x_i\|^2 = 1$, The mean of variable $\|x_i\|^2$ is

$$E\left[\|x_i\|^2\right] = \frac{1}{N} \tag{4.9}$$

$x_k,\ k = 1, \ldots, N$ are K points randomly selected from the set of points $\mathbf{S} = \{x_i\}_{i=1}^{N}$, The mean of variable $\|x_k\|^2$ is

$$E\left[\|x_k\|^2\right] = E\left[\|x_i\|^2\right] = \frac{1}{N} \tag{4.10}$$

The mean of variable $\sum_{k=1}^{K} \|x_k\|^2$ is

$$E\left[\sum_{k=1}^{K} \|x_k\|^2\right] = \frac{K}{N} \tag{4.11}$$

The distribution can be found by a procedure similar to that in [98].

Proposition 2 *For a network MIMO system with imperfect CSIT, the asymptotic results for the achievable rate in MU mode with m simultaneously served users is approximated as*

$$\frac{R_u(m)}{N_r} \approx (m-1)\log_2\left(\frac{1 + N_r \rho_u^2 \gamma_m \kappa \epsilon_u^2 \eta_1}{1 + N_r \rho_u^2 \gamma_m \kappa \epsilon_u^2 \eta_2}\right) + \log_2(1 + N_r \gamma_m \rho_u^2 \kappa \eta_1) + \log_2 \frac{\eta_2}{\eta_1} + (\eta_2 - \eta_1)\log_2(e) \tag{4.12}$$

where κ, η_1 and η_2 are given in the proof.

Proof:
Using the Wishart matrix approximation, rewrite the received signal for user u as

$$\mathbf{y}_u = \hat{\mathbf{H}}_u \hat{\mathbf{T}}_u \mathbf{x}_u + \hat{\mathbf{E}}_u \sum_{u' \neq u} \mathbf{T}_{u'}^{(P)} \mathbf{x}_{u'} + \mathbf{n}_u \tag{4.13}$$

where $\hat{\mathbf{H}}_u$ is the equivalent channel matrix with size of $N_r \times \hat{N}_{t,u}$, $\hat{\mathbf{T}}_u$ is the $\hat{N}_{t,u} \times N_r$ equivalent precoding matrix. Let $\mathbf{g} = [g_1, \cdots, g_{\hat{N}_{t,u}}]$ be the column index of consisting of biggest large-scale fading coefficients, the equivalent precoding matrix is given by selecting the corresponding rows from the $N_r \times BN_t$ precoding matrix $\mathbf{T}_u^{(P)}$, that is, $\hat{\mathbf{T}}_u = [\mathbf{T}_u^{(P)}]_{(\mathbf{g},:)}$. With approximation method similar to that applied to channel matrix, the equivalent CSIT error matrix $\hat{\mathbf{E}}_u \in \mathbb{C}^{N_r \times \hat{N}_{t,u}}$ has zero mean Gaussian distributed elements with variance ϵ_u^2. The achievable rate of user u is rewritten as

$$\begin{aligned} R_u &= \mathbb{E}\left[\log_2 \det\left(\hat{\mathbf{R}}_u + \gamma\beta_u^2 \mathbf{H}_{eff,u}\mathbf{H}_{eff,u}^H\right)\right] \\ &- \mathbb{E}\left[\log_2 \det\left(\hat{\mathbf{R}}_u\right)\right] \end{aligned}$$

where $\mathbf{H}_{eff,u} = \hat{\mathbf{H}}_u\hat{\mathbf{T}}_u$ is the $N_r \times N_r$ effective small-scale channel matrix for user u, and $\hat{\mathbf{R}}_u$ is the equivalent interference-plus-noise covariance matrix:

$$\hat{\mathbf{R}}_u = \mathbf{I}_{N_r} + \hat{\mathbf{E}}_u \left[\sum_{u' \neq u} \gamma_m \rho_u^2 \hat{\mathbf{T}}_{u'}\hat{\mathbf{T}}_{u'}^H\right] \hat{\mathbf{E}}_u^H \tag{4.14}$$

Since $\hat{\mathbf{T}}_u$ is independent of $\hat{\mathbf{H}}_u$, the elements in $\mathbf{H}_{eff,u}$ are linear combinations of i.i.d. standard Gaussian random variables, which are zero mean Gaussian distributed with variance equal to the summation of the square of the coefficients in linear combination. Let $\mathbf{t}_i$ be the ith column of $\mathbf{T}_u^{(P)}$, since we have no knowledge of the small-scale fading behavior, a simple way is to assume the elements of $\mathbf{t}_i$ are independent uniformly distributed. Now pick the corresponding rows from $\mathbf{T}_u^{(P)}$ to form the equivalent precoder $\hat{\mathbf{T}}_u$. Let $\hat{\mathbf{t}}_i$ be the ith column of $\hat{\mathbf{T}}_u$, from *Lemma 1*, we have $\|\hat{\mathbf{t}}_i\|^2 = \hat{t}_{i,g_1}\hat{t}_{g_1,i}^H \cdots + \hat{t}_{g_{\hat{N}_{t,u}},i}\hat{t}_{g_{\hat{N}_{t,u}},i}^H \approx \hat{N}_{t,u}/(BN_t) = \kappa$, and thus $\mathbf{H}_{eff,u} \sim \mathcal{CN}(\mathbf{0}_{N_r}, \kappa\mathbf{I}_{N_r})$. Similarly, the effective channel error matrix $\mathbf{E}_{eff,u'} = \hat{\mathbf{E}}_u\hat{\mathbf{T}}_{u'}$ distributes as $\mathbf{E}_{eff,u'} \sim \mathcal{CN}(\mathbf{0}_{N_r}, \kappa\epsilon_u^2\mathbf{I}_{N_r})$.

Interpreting the system in (4.13) as a MIMO channel under interference, the achievable rate in (4.12) can be obtained using the approximation in [95], where η_1 and η_2 are solutions to

$$\eta_1 + \frac{N_r\gamma_m\rho_u^2\kappa\eta_1}{N_r\gamma_m\rho_u^2\kappa\eta_1 + 1} + (m-1)\frac{N_r\gamma_m\rho_u^2\kappa\epsilon_u^2\eta_1}{N_r\gamma_m\rho_u^2\kappa\epsilon_u^2\eta_1 + 1} = 1$$

$$\eta_2 + (m-1)\frac{N_r\gamma_m\rho_u^2\kappa\epsilon_u^2\eta_2}{N_r\gamma_m\rho_u^2\kappa\epsilon_u^2\eta_2 + 1} = 1$$

To verify the accuracy of the equivalent channel matrix, consider the system model in Fig. 4.1 with the number of antennas given as $N_t = 4$ and $N_r = 2$. Six users are randomly place in the area covered by the three sectors surrounding the cluster center. The users are moving at the speed of 10 km/h, and channel prediction with AR model

of order 2 is adopted. The cell edge signal-to-noise-ratio (SNR) is defined as the received SNR at the cell edge when one BS transmits at full power and other BSs are off. The asymptotic results compared with simulations are shown in Fig. 4.2. The largest difference between asymptotic and simulation results is around 20%. Fig. 4.2 also implies the SU/MU mode-switching for varying SNR.

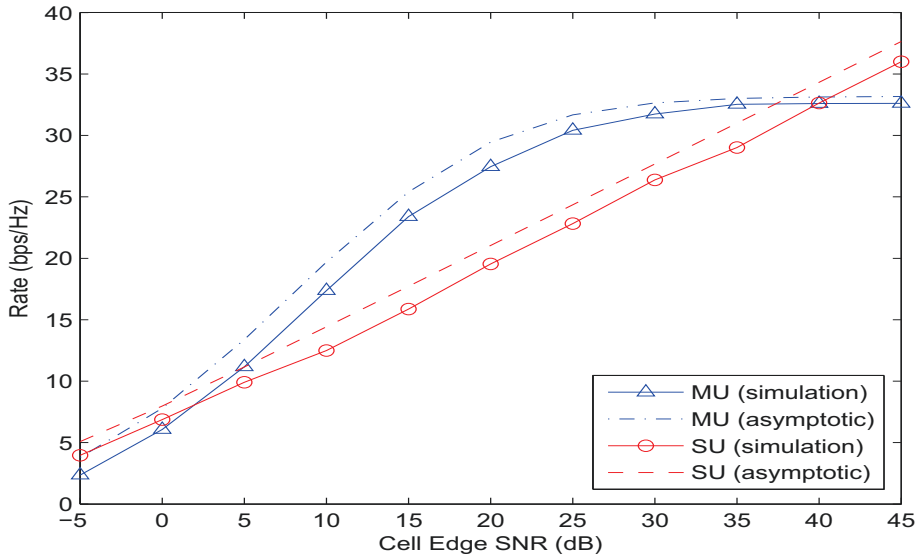

Figure 4.2: Sum rate vs. cell edge SNR ($N_t = 4$ and $N_r = 2$)

4.3 Two-stage Feedback and User Scheduling

The proposed two-stage feedback method is discussed in this section. At the beginning of each scheduling interval, each user reports its average SNR from all cooperating BSs and the maximum Doppler shift through the *long-term* feedback. Based on this information, the asymptotic ergodic rate is evaluated for each user, and a set of users are selected on each resource units. This allocation is repeated on every frames before the next long-term feedback. In each frame, the small-scale channel coefficients are periodically sent to the central unit through *short-term* feedback. Channel prediction is applied to generate hypothesized channel coefficients for future frames which are used to calculate the precoder. After receiving the downlink pilot symbol, the channel coefficients are updated based on the measurements. The feedback of channel coefficients occupies limited uplink bandwidth since the number of selected users is much smaller as compared to the total number of

users. Let U and G be the set of all users and RBs, respectively. On each resource unit

Algorithm 1 User Scheduling Algorithm

Initialization: $U_j \leftarrow \emptyset, \forall j \in G, \tilde{R}_u \leftarrow 0, \forall u \in U$
for each RB j **do**
  for each service mode m **do**
    for each user u **do**
      $v'_u \leftarrow v_u(\tilde{R}_u + R_u(m)) - v_u(\tilde{R}_u)$
    end for
    $S_m \leftarrow \arg\max_{S \subseteq U:|S|=m} \sum_{u \in S} v'_u$
    $r_m \leftarrow \sum_{u \in S_m} v'_u$
  end for
  $m^* = \arg\max_m r_m$, $U_j = S_{m^*}$.
  $\tilde{R}_u \leftarrow \tilde{R}_u + R_u(m^*), \forall u \in U_j$
end for

$j \in G$, a subset of users $U_j \subseteq U$ is selected, where the cardinality of U_j is less than or equal to $M = \lfloor BN_t/N_r \rfloor$ if the BD precoding is applied. Denote the achievable rate of user u on one resource unit as $R_u(n_j)$, where n_j is the number of simultaneously served users (service mode), the sum rate of user u is given by

$$\tilde{R}_u = \sum\nolimits_{j:u \in U_j} R_u(n_j) \tag{4.15}$$

For each user, the *utility* is defined as a function of its sum ergodic rate. The utility function affects the behavior of the scheduler. We consider two special cases of utility and scheduling. To perform maximum sum rate scheduling (MSRS), the utility equals to the ergodic rate,

$$v_u^{MSRS}(\tilde{R}_u) = \tilde{R}_u \tag{4.16}$$

To consider fairness among users, the proportional fair scheduling (PFS) is introduced with the utility given by

$$v_u^{PFS}(\tilde{R}_u) = \log(\tilde{R}_u) \tag{4.17}$$

In Orthogonal Frequency Division Multiple Access (OFDMA) systems, the radio resource in each frame is divided into units of a specific number of subcarriers (combined into a subchannel) for a predetermined amount of time (a slot), referred to as resource blocks (RBs). Then the goal of the scheduler is to assign the RBs to users so as to maximize the total utility based on the asymptotic ergodic rates for each user with different service mode, which can be calculated using the formulas given in Section III and stored in a lookup table. A simple user scheduling algorithm for each frame is presented in Algorithm 1. In brief, the algorithm assigns the RBs to a set of users sequentially. In each loop, for

different number of simultaneously served users, it selects the user set that provides the highest marginal utility. Then the service mode with largest utility improvement is chosen and corresponding set of users are scheduled on this RB.

4.4 Numerical Results

In this section, we present some numerical results to evaluate the performance of different scheduling methods. The assumptions for cell layout, pathloss, and number of antennas are the same as that in previous sections. According to the antenna number setting, at most $M = 6$ users are selected for each frame. We consider the frame structure of the 3GPP-LTE standard with bandwidth of 1.25 MHz partitioned into 6 subchannels each with 180 kHz bandwidth. In this work we assign the slots in one subchannel to the same set of users for simplicity. The users are initial generated at random location with equal number of users in each sector, and randomly move at speeds of 10 to 30 km/h.

We adopt a drop-based simulation method for performance evaluation. In this approach, each drop correspond to a realization of user location, and the large-scale fading parameter as well as the velocity of user movement are assumed to be constant during one drop. Thus, the only varying parameter is the small-scale fading experienced by users. For a given simulation setting (e.g., number of users), 100 drops are run and each drop consists of 1000 frames. In practice, one drop corresponds to one scheduling period, and user location and channel implementation are independent among drops. The final results are averaged over drops.

4.4.1 Cluster Throughput

In order to evaluate the effect of scheduling based on asymptotic rate, we also consider the traditional per-frame scheduling methods. Specifically, we simulate the MSRS with ideal CSI and predicted CSI, where the user set in each RB is selected in a greedy manner as in [90]. Fig. 4.3 depicts the cluster throughput of MSRS and PFS strategies versus different number of users. For all schedulers, as the number of user increases, the cluster throughput increases and then saturates due to the effect of multi-user diversity. The per-frame scheduler with ideal CSI outperforms the proposed algorithm by 17% to 30% with the cost of huge overhead. On the other hand, the scheduler based on predicted CSI brings limited improvement even the (predicted) CSI is fed back for all users. That is, with imperfect CSIT, it is efficient enough to schedule the users based only on the first and second order statistics. The effect of multi-user diversity is weaker for PFS as compared to that of MSRS, since it does not always choose users under best channel condition.

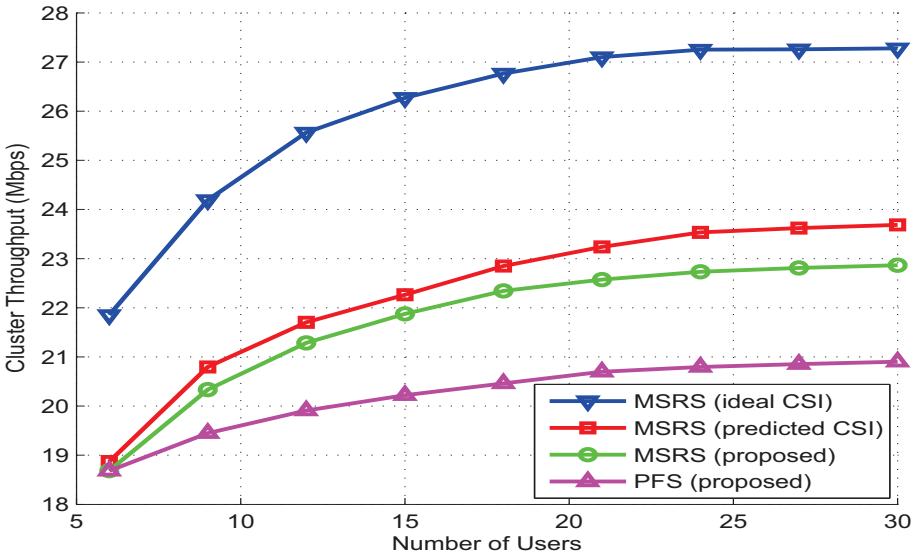

Figure 4.3: Cluster throughput versus number of users

4.4.2 Fairness

In addition to the throughput maximization, fairness among users is an important concern for scheduler design. The Jain's fairness index defined in [99] is adopted as the performance metric for the proposed asymptotic-rate-based PFS. Here we consider the average fairness index within an observation window consisting of several frames. For an arbitrary drop, the Jain's fairness index versus varying observation window size in frames is depicted in Fig. 4.4 with 15 users in total. We compare the actual fairness with the constant fairness index calculated using the asymptotic rate of users ($\tilde{R}_u$) after scheduling. It can be observed that the average fairness is relatively low for small window size, since some users may be scheduled on subchannels with poor channel condition. However, as the observation window grows, the fairness index approaches the value "promised" by the asymptotic-rate-based scheduler. That is, the proposed method achieves a good long-term fairness.

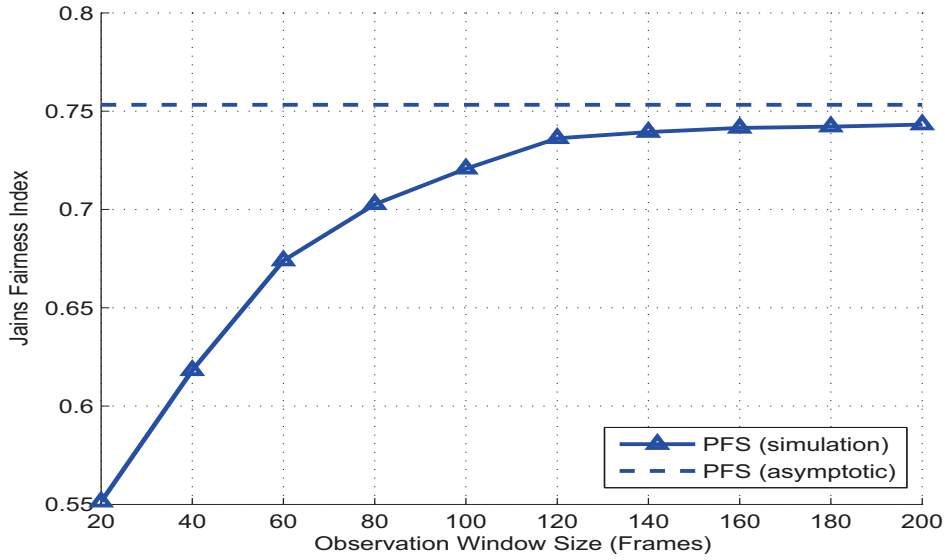

Figure 4.4: Jain's fairness index versus observation window size

Chapter 5

Precoder Design for OSTBC based Cognitive Radio

Contents

The spectrum sharing has recently passed into a mainstream CR strategy. We investigate the core issue in this strategy: interference mitigation at Primary Receiver (PR). We propose a linear precoder design which aims at alleviating the interference caused by Secondary User (SU) from the source for Orthogonal Space-Time Block Coding (OSTBC) based CR. We resort to Minimum Variance (MV) approach to contrive the precoding matrix at Secondary Transmitter (ST) in order to maximize the SNR at Secondary Receiver (SR) on the premise that the orthogonality of OSTBC is kept, the interference introduced to Primary Link (PL) by Secondary Link (SL) is maintained under a tolerable level and the total transmitted power constraint at ST is satisfied. Moreover, the selection of polarization mode for SL is incorporated in the precoder design. In order to provide an analytic solution with low computational cost, we put forward an original precoder design algorithm which exploits an auxiliary variable to treat the optimization problem with a mixture of linear and quadratic constraints. Numerical results demonstrate that our proposed precoder design enable SR to have an agreeable SNR on the prerequisite that the interference at PR is maintained below the threshold.

CR is an encouraging technology to combat the spectrum scarcity. In order to further enhance the spectrum utilization, the spectrum sharing strategy that PUs and SUs coexist in licensed bands as long as PUs are preserved from the interference caused by SUs attracts much research efforts. Such a strategy is tantamount to a multi-user system in which the inter-user interference mitigation is the core. Various inter-user interference mitigation techniques for spectrum sharing CR systems have been put forward. They can be roughly grouped into two categories: power allocation [100]- [102] and precoding in Multiple-Input Multiple-Output (MIMO) CR systems [103]- [106].

Space Time Block Coding (STBC) exploits time and space diversity in MIMO systems so as to heighten the reliability of the message signal. OSTBC are contrived in such a fashion that the vectors of coding matrix are orthogonal in both time and space dimensions. This feature yields a simple linear decoding at the receiver side so that no complex matrix manipulation—Singular Value Decomposition (SVD), for instance, is required for recovering the information bit from the gathered received symbols. Numerous precoding techniques have been mooted for unstructured codes. However, these techniques cannot be applied to OSTBC which should forcibly preserve a special space-time structure. The precoding design for OSTBC CR systems attracts less attention in previous work. Such previous work in [106] was based on the Maximum Likelihood (ML) space-time decoder, whereas the ML decoder is a nonlinear method. Inspired by Minimum Variance (MV) receiver applied for OSTBC multi-access systems [107] which used a weight matrix at the receiver side to quell the inter-user interference, we make use of MV approach to design a precoding matrix at Secondary Transmitter (ST).

The precoding matrix at ST is designed to comply with the needs in our CR system: maximizing the SNR at Secondary Receiver (SR) on the premise that the orthogonality of OSTBC is kept, the interference introduced to PL by SL is maintained under a tolerable level and the total transmitted power constraint at ST is satisfied.

The classic MV beamforming [108], [109] built an optimization problem which includes only one linear constraint, that cannot administer to the needs in our CR system. On the other hand, some precoder designs for CR systems [105] introduced a mixture of linear and quadratic constraints to the optimization problem which leads to iterative solutions with high computational complexity. For the purpose of contriving a precoder that applies to our CR system and provides an analytic solution with low computational cost, we moot an original precoder design algorithm: we first take advantage of an optimization problem which includes one linear constraint with the objective of preserving the orthogonality of OSTBC and making SL introduce minimal interference to PL for different combinations of the polarization mode at ST and SR. This optimization problem provides an analytic solution in terms of an auxiliary variable which is the system gain on SL. Then we regulate this auxiliary variable using the quadratic constraints evoked by the transmitted power budget at ST and the maximum tolerable interference at Primary Receiver (PR). The polarization mode at ST and SR are conclusively settled on based upon the maximization criteria of SNR at SR.

5.1 CR system exploiting OSTBC

We consider a CR system that consists of one SL which exploits OSTBC and one PL. ST and PT are only allowed to communicate with their peers. ST or PT is equipped with N_t antennas and SR or PR is equipped with N_r antennas. The antennas in the same array have identical polarization mode. On each link, the transmit antenna array or the receive antenna array is able to switch its polarization mode between vertical mode V and horizontal mode H. We denote by qt and qr, respectively, the transmit antenna array's polarization mode and the receive antenna array's polarization mode.

5.1.1 System Model

We exploit 3GPP Spatial Channel Model (SCM) [110]. The space channel impulse response between a pair of antennas u and s of path n can be expressed as a function in terms of the polarization channel response and the geometric configuration of the antennas at both sides of the link:

$$H_{u,s,n}\left(\chi_{BS}^{(v)}, \chi_{BS}^{(h)}, \chi_{MS}^{(v)}, \chi_{MS}^{(h)}, \theta_{n,m,AoD}, \theta_{n,m,AoA}\right) \tag{5.1}$$

where $\chi_{BS}^{(v)}$ is the BS antenna complex response for the V-pol component, $\chi_{BS}^{(h)}$ is the BS antenna complex response for the H-pol component, $\chi_{MS}^{(v)}$ is the MS antenna complex response for the V-pol component, $\chi_{MS}^{(h)}$ is the MS antenna complex response for the H-pol component, $\theta_{n,m,AoD}$ is the Angle of Departure (AOD) for the mth subpath of the nth path and $\theta_{n,m,AoA}$ is the Angle of Arrival (AOA) for the mth subpath of the nth path.

We assume that the system is operated over a frequency-flat channel with N_{path} paths and each path contains only one subpath. For a point to point communication link, the baseband input-output relationship at time-slot t is expressed as:

$$\mathbf{y}(t) = \sqrt{\frac{\rho}{N_t}}\mathbf{H}^{qt,qr}\mathbf{x}(t) + \mathbf{n}(t) \tag{5.2}$$

where ρ is the SNR at each receive antenna, $\mathbf{x}(t)$ is a $N_t \times 1$ size transmitted signal vector which satisfies $E\left\{\mathbf{x}(t)\,\mathbf{x}^H(t)\right\} = N_t$, $\mathbf{n}_j(t)$ is a $N_r \times 1$ size complex Gaussian noise vector at receiver with zero-mean and unit-variance and $\mathbf{H}^{qt,qr}$ is the $N_r \times N_t$ channel matrix for the specified qt and qr with the entry

$$H_{u,s}^{qt,qr} = \sum_{n=1}^{N_{path}} H_{u,s,n}\left(\chi_{BS}^{(x\neq qt)} = 0,\, \chi_{MS}^{(y\neq qr)} = 0\right) \tag{5.3}$$

where $x, y \in \{V, H\}$. $\mathbf{H}^{qt,qr}$ has unit variance and satisfies $E\left\{\mathrm{tr}\left(\mathbf{H}^{qt,qr}\mathbf{H}^{qt,qr\,H}\right)\right\} = N_t N_r$.

Assuming that the channel is constant from $t = 1$ to $t = T$, then Equation (5.2) can be extended into:

$$\mathbf{Y} = \sqrt{\frac{\rho}{N_t}}\mathbf{H}^{qt,qr}\mathbf{X} + \mathbf{N} \tag{5.4}$$

where $\mathbf{Y} = [\mathbf{y}(1), \ldots, \mathbf{y}(T)]$, $\mathbf{X} = [\mathbf{x}(1), \ldots, \mathbf{x}(T)]$ and $\mathbf{N} = [\mathbf{n}(1), \ldots, \mathbf{n}(T)]$.

5.1.2 Orthogonal Space-Time Block Coding

If $\mathbf{X}$ is OSTBC matrix, then $\mathbf{X}$ has a linear representation in terms of complex information symbols prior to space-time encoding s_k, $k = 1, \ldots, K$ [111]:

$$\mathbf{X} = \sum_{k=1}^{K}\left(\mathbf{C}_k \mathrm{Re}\{s_k\} + \mathbf{D}_k \mathrm{Im}\{s_k\}\right) \tag{5.5}$$

where $\mathbf{C}_k$ and $\mathbf{D}_k$ are $N_t \times T$ code matrices [112].

OSTBC matrix has the following unitary property:

$$\mathbf{X}\mathbf{X}^H = \left(\sum_{k=1}^{K}|s_k|^2\right)\mathbf{I}_{N_t \times N_t} \tag{5.6}$$

In order to represent the relationship between the original symbols and the received signal by multiplication of matrices, we introduce the "underline" operator [112] to rewrite Equation (5.2) as:

$$\underline{\mathbf{Y}} = \mathcal{H}^{qt,qr}\mathbf{A}\underline{\mathbf{s}} + \underline{\mathbf{N}} \tag{5.7}$$

where $\mathbf{s} = [s_1, \ldots, s_K]$ is the data stream which is QPSK modulated,

$$\mathcal{H}^{qt,qr} = \begin{bmatrix} \mathrm{Re}\left\{\mathbf{I}_T \otimes \mathbf{H}^{qt,qr}\right\} & -\mathrm{Im}\left\{\mathbf{I}_T \otimes \mathbf{H}^{qt,qr}\right\} \\ \mathrm{Im}\left\{\mathbf{I}_T \otimes \mathbf{H}^{qt,qr}\right\} & \mathrm{Re}\left\{\mathbf{I}_T \otimes \mathbf{H}^{qt,qr}\right\} \end{bmatrix}$$

is the equivalent channel matrix with the specified polarization mode, $\mathbf{A} = \left[\underline{\mathbf{C}_1}, \ldots, \underline{\mathbf{C}_k}, \underline{\mathbf{D}_1}, \ldots, \underline{\mathbf{D}_k}\right]$ is the OSTBC compact dispersion matrix and the "underline" operator for any matrix $\mathbf{P}$ is defined as:

$$\underline{\mathbf{P}} \triangleq \begin{bmatrix} \mathrm{vec}\left\{\mathrm{Re}\left(\mathbf{P}\right)\right\} \\ \mathrm{vec}\left\{\mathrm{Im}\left(\mathbf{P}\right)\right\} \end{bmatrix} \tag{5.8}$$

where $\mathrm{vec}\{\bullet\}$ is the vectorization operator stacking all columns of a matrix on top of each other.

The earliest OSTBC scheme which is well known as Alamouti's code was proposed in [113]. Alamouti's code gives full diversity in the spatial dimension without data rate loss. The transmission matrix of Alamouti's code C_2 is given as:

$$C_2 = \begin{bmatrix} s_1 & s_2 \\ -s_2^* & s_1^* \end{bmatrix} \tag{5.9}$$

In [114], Alamouti's code was extended for more antennas. For instance, four antennas, the transmission matrix of the half rate code C_4 is given as:

$$C_4 = \begin{bmatrix} s_1 & s_2 & s_3 & s_4 \\ -s_2 & s_1 & -s_4 & s_3 \\ -s_3 & s_4 & s_1 & -s_2 \\ -s_4 & -s_3 & s_2 & s_1 \\ s_1^* & s_2^* & s_3^* & s_4^* \\ -s_2^* & s_1^* & -s_4^* & s_3^* \\ -s_3^* & s_4^* & s_1^* & -s_2^* \\ -s_4^* & -s_3^* & s_2^* & s_1^* \end{bmatrix} \tag{5.10}$$

5.2 Precoder for OSTBC based CR with Polarized Antennas

We design a precoding matrix at ST which acts on the entry of the OSTBC compact dispersion matrix and has no influence on the codes' structure. Our precoder design relies

on the equivalent transmit correlation matrix on the link between ST and PR (SPL). This matrix can be estimated easily by SU in the sensing step and enables our precoder design to regulate the interference introduced by SL to PL.

5.2.1 Constraints from SL

With the precoding operation, the received signal at SR for the specified polarization mode at ST and SR can be expressed as:

$$\underline{\mathbf{Y}_{ST,SR}^{qt,qr}} = \sqrt{\frac{\rho_{SR}}{N_t}}\mathcal{H}_{ST,SR}^{qt,qr}\mathbf{W}^{qt,qr}\mathbf{A}\underline{\mathbf{s}} + \underline{\mathbf{N}} \tag{5.11}$$

where ρ_{SR} is the SNR at each receive antenna of SR, $\mathcal{H}_{ST,SR}^{qt,qr}$ is the SL equivalent channel matrix with the specified polarization mode at ST and SR, $\mathbf{W}^{qt,qr}$ is the precoding matrix for the specified polarization mode at ST and SR.

A straightforward approach to estimate the transmitted signal from ST is using the following soft output detector:

$$\begin{aligned} \hat{\underline{\mathbf{s}}} &= \mathbf{A}^T\mathcal{H}_{ST,SR}^{qt,qr^T}\underline{\mathbf{Y}_{ST,SR}^{qt,qr}} \\ &= \sqrt{\frac{\rho_{SR}}{N_t}}\mathbf{A}^T\mathcal{H}_{ST,SR}^{qt,qr^T}\mathcal{H}_{ST,SR}^{qt,qr}\mathbf{W}^{qt,qr}\mathbf{A}\underline{\mathbf{s}} + \mathbf{A}^T\mathcal{H}_{ST,SR}^{qt,qr^T}\underline{\mathbf{N}} \end{aligned} \tag{5.12}$$

The OSTBC structure conservation puts forward the following constraint:

$$\mathbf{A}^T\mathcal{H}_{ST,SR}^{qt,qr^T}\mathcal{H}_{ST,SR}^{qt,qr}\mathbf{W}^{qt,qr}\mathbf{A} = \alpha^{qt,qr}\mathbf{I}_{2K} \tag{5.13}$$

where $\alpha^{qt,qr}$ is the system gain on SL for the specified polarization mode at ST and SR which will be adjusted to satisfy the other constraints.

Additionally, the transmitted power budget at ST induces another constraint:

$$P_t^{qt,qr} \leq P_{tmax} \tag{5.14}$$

where $P_t^{qt,qr} = \frac{\rho_{SR}}{N_t}\mathrm{tr}\left(\mathbf{W}^{qt,qr^T}\mathbf{W}^{qt,qr}\right)$ and P_{tmax} are, respectively, the transmitted power for the specified polarization mode at ST and SR and the maximum transmitted power at ST.

5.2.2 Constraints from PL

The received signal at PR from ST is deemed as baleful signal by PL and can be expressed as:

$$\underline{\mathbf{Y}_{ST,PR}^{qt,qr'}} = \sqrt{\frac{\rho_{PR}}{N_t}}\mathcal{H}_{ST,PR}^{qt,qr'}\mathbf{W}^{qt,qr}\mathbf{A}\underline{\mathbf{s}} + \underline{\mathbf{N}} \tag{5.15}$$

where ρ_{PR} is the SNR at each receive antenna of PR and $\mathcal{H}_{ST,PR}^{qt,qr'}$ is the equivalent channel matrix for the specified polarization mode at ST and PR.

The interference power introduced by SL to PL for the specified polarization mode at ST and PR can be calculated as:

$$\begin{aligned} P_{ST,PR}^{qt,qr'} &= \mathrm{tr}\left[E\left(\underline{\mathbf{Y}_{ST,PR}^{qt,qr'}}\,\underline{\mathbf{Y}_{ST,PR}^{qt,qr'}}^{H}\right)\right] \\ &= \frac{\rho_{SR}}{N_t}\mathrm{tr}\left(\mathbf{W}^{qt,qr^T}R_{PR,ST}^{qt,qr'}\mathbf{W}^{qt,qr}\right) \end{aligned} \tag{5.16}$$

where $\mathcal{R}_{PR,ST}^{qt,qr'} = E\left(\mathcal{H}_{PR,ST}^{qt,qr'^T}\mathcal{H}_{PR,ST}^{qt,qr'*}\right)$ is the equivalent transmit correlation matrix on SPL for the specified polarization mode at ST and PR. The maximum tolerable interference power η at PR evokes the following constraint:

$$P_{ST,PR}^{qt,qr'} \leq \eta \tag{5.17}$$

5.2.3 Minimum Variance Algorithm

SU can dominate the configuration of the precoding matrix and the polarization mode on SL, while SU has no eligibility to select the polarization mode on PL. Our algorithm is based on an optimization problem which includes one linear constraint with the objective of preserving the orthogonality of OSTBC and making SL introduce minimal interference to PL for different combinations of the polarization mode at ST and SR. This optimization problem provides an analytic solution in terms of an auxiliary variable which is the system gain on SL. Then this auxiliary variable is regulated by using the quadratic constraints evoked by the transmitted power budget at ST and the maximum tolerable interference at PR. The polarization mode at ST and SR are conclusively settled on based upon the maximization criteria of SNR at SR.

Such an optimization problem that includes one linear constraint is described as follow:

$$\left(\widehat{\mathbf{W}^{qt,qr}},\, \widehat{qt},\, \widehat{qr}\right) = \arg\min_{\mathbf{W}^{qt,qr},\, qt,\, qr} \frac{\rho_{SR}}{N_t}\mathrm{tr}\left(\mathbf{W}^{qt,qr^T}\mathcal{R}_{PR,ST}^{qt,qr'}\mathbf{W}^{qt,qr}\right) \tag{5.18}$$

$$\text{subject to}: \ \mathrm{tr}\left(\mathbf{A}^T\mathcal{H}_{ST,SR}^{qt,qr^T}\mathcal{H}_{ST,SR}^{qt,qr}\mathbf{W}^{qt,qr}\mathbf{A} - \alpha^{qt,qr}\mathbf{I}_{2K}\right) = 0 \tag{5.19}$$

We exploit the method of Lagrange multipliers to find $\widehat{\mathbf{W}^{qt,qr}}$ for each combination of the polarization mode at ST and SR. The Lagrangian function can be written as:

$$L\left(\mathbf{W}^{qt,qr},\,\mathbf{\Lambda}\right) = \frac{\rho_{SR}}{N_t}\mathrm{tr}\left(\mathbf{W}^{qt,qr^T}\mathcal{R}_{PR,ST}^{qt,qr'}\mathbf{W}^{qt,qr}\right) - \mathrm{tr}\left(\mathbf{\Lambda}^T\left(\mathbf{A}^T\mathcal{R}_{ST,SR}^{qt,qr}\mathbf{W}^{qt,qr}\mathbf{A} - \alpha^{qt,qr}\mathbf{I}_{2K}\right)\right) \tag{5.20}$$

where $\mathcal{R}_{ST,SR}^{qt,qr} = \mathcal{H}_{ST,SR}^{qt,qr^T}\mathcal{H}_{ST,SR}^{qt,qr}$ and $\mathbf{\Lambda}$ is a $2K \times 2K$ size matrix of Lagrange multipliers.

By differentiating the Lagrange function with respect to $\mathbf{W}^{qt,qr}$ and equating it to zero, we obtain an analytic solution in terms of $\alpha^{qt,qr}$ which is expressed as:

$$\widehat{\mathbf{W}^{qt,qr}} = \alpha^{qt,qr}\mathcal{R}_{PR,ST}^{qt,qr'\ -1}\mathcal{R}_{ST,SR}^{qt,qr}\mathbf{A}\mathbf{Q}^{qt,qr}\mathbf{A}^T \tag{5.21}$$

where $\mathbf{Q}^{qt,qr} = \left(\mathbf{A}^T\mathcal{R}_{ST,SR}^{qt,qr}\left(R_{PR,ST}^{qt,qr'}\right)^{-1}\mathbf{A}\right)^{-1}$.

The estimated interference power at PR can be expressed in terms of $\alpha^{qt,qr}$ as:

$$\widehat{P_{ST,PR}^{qt,qr}} = \frac{\rho_{SR}\left(\alpha^{qt,qr}\right)^2\mathrm{tr}\left(\mathbf{Q}^{qt,qr}\right)}{N_t} \tag{5.22}$$

The estimated SNR at SR can be written in terms of $\alpha^{qt,qr}$ as:

$$\widehat{SNR_{ST,PR}^{qt,qr}} = \frac{\rho_{SR}\left(\alpha^{qt,qr}\right)^2\gamma^{qt,qr}}{N_t} \tag{5.23}$$

where

$$\gamma^{qt,qr} = \mathrm{tr}\left(\mathbf{Q}^{qt,qr}\mathbf{A}^T\left(\mathcal{R}_{ST,SR}^{qt,qr}R_{PR,ST}^{qt,qr'\ -1}\right)^2\mathcal{R}_{ST,SR}^{qt,qr}\mathbf{A}\mathbf{Q}^{qt,qr}\right) \tag{5.24}$$

.

The estimated transmit power at ST in terms of $\alpha^{qt,qr}$ is given by:

$$\widehat{P_t^{qt,qr}} = \frac{\rho_{SR}\left(\alpha^{qt,qr}\right)^2\delta^{qt,qr}}{N_t} \tag{5.25}$$

where

$$\delta^{qt,qr} = \mathrm{tr}\left(\mathbf{Q}^{qt,qr}\mathbf{A}^T\mathcal{R}_{ST,SR}^{qt,qr}\left(R_{PR,ST}^{qt,qr'}\right)^{-2}\mathcal{R}_{ST,SR}^{qt,qr}\mathbf{A}\mathbf{Q}^{qt,qr}\right) \tag{5.26}$$

We derive $\alpha^{qt,qr}$ by substituting $\widehat{P_t^{qt,qr}}$ and $\widehat{P_{ST,PR}^{qt,qr}}$ into Equation (5.14) and Equation (5.17) which indicate the transmitted power budget constraint and the maximum tolerable interference constraint:

$$\alpha^{qt,qr} = \min\left(\sqrt{\frac{N_t}{\delta^{qt,qr}}}, \sqrt{\frac{N_t\eta}{\rho_{SR}\mathrm{tr}\left(\mathbf{Q}^{qt,qr}\right)}}\right) \tag{5.27}$$

Therefore the estimated SNR at SR can be determined as:

$$\widehat{SNR}^{qt,qr}_{ST,PR} = \min\left(\frac{\rho_{SR}}{\delta^{qt,qr}}, \frac{\eta}{\mathrm{tr}\left(\mathbf{Q}^{qt,qr}\right)}\right)\gamma^{qt,qr} \tag{5.28}$$

Based upon the maximization criteria of SNR at SR, Finally, we destine the estimated polarization mode of ST and SR as:

$$\left(\widehat{qt}, \widehat{qr}\right) = \arg\max_{qt,qr}\left[\min\left(\frac{\rho_{SR}}{\delta^{qt,qr}}, \frac{\eta}{\mathrm{tr}\left(\mathbf{Q}^{qt,qr}\right)}\right)\gamma^{qt,qr}\right] \tag{5.29}$$

5.3 Numerical Results

For the purpose of validating our proposed precoding design algorithm, we simulated our CR system using the proposed precoder design algorithm and measure the SNR at SR by using varying maximum transmitted power at ST and a reasonable interference threshold at PR.

We firstly carried out our simulation with Alamouti's code at ST for different combinations of qt and qr on SL under different multipath scenarios. Then, we executed our simulation with different codes for different number of transmit antennas at ST based upon a determinate combination of qt and qr on SL and multipath scenario. In both simulation scenarios, the Signal to Interference plus Noise Ratio (SINR) threshold to perceive the received signal at PR was chosen equal to 0dB and the Cross-polar Discrimination (XPD) was set to 8dB. The channel matrix on each link was modeled according to 3GPP SCM. Since the status of polarization at PR qr' is normally unidentified for SU, the equivalent transmit correlation matrix on SPL becomes random. This thereby results in a random SNR at SR. The noise at secondary receiver is considered as normalized AWGN with zero mean and unit variance. Therefore, P_{maxSU}/P_{noise} has the same variation tendency as P_{maxSU}. In our simulation, we calculated the SNR at SR in terms of the polarization tilt angle at PR by introducing a rotation matrix to the equivalent transmit correlation matrix on SPL. We assumed that the polarization tilt angle at PR follows a continuous uniform distribution between 0 and $\frac{\pi}{2}$. Then we sampled uniformly over the range of the polarization tilt angle at PR and calculated the SNR at SR for each sample of tilt angle. Finally, we worked out an average the SNR at SR to evaluate the system performance.

5.3.1 Performance Analysis of Polarization Diversity

We simulated a CR system, where ST is equipped with 2 antennas, SR is equipped with 1 antenna and PR is equipped with 2 antennas. We observe the variation of the average SNR at SR for different combinations of qt and qr on SL as the transmit power at ST increases. First, we set SL channel as a 2-path frequency flat fading channel and SPL channel as a single path frequency flat fading channel. The variation tendencies in this scenario were depicted in Fig.5.1. Then we reset SPL channel as a 4-path frequency flat fading channel and the corresponding variation tendencies were shown in Fig.5.2. The average SNR at SR for a large number of samples leads to the smooth curves. As the transmit power at ST increases, the average SNR at SR of all different combinations of qt and qr on SL exhibit uptrend in both scenarios and linear increase is obtained when P_{maxSU}/P_{noise} are below 15dB in both scenarios, where P_{noise} denotes the noise power at SR. The mismatch of qt and qr on SL induces a 15dB gap between the matched modes and the mismatched modes when the average SNR at SR has linear increase in the first scenario. When we enhanced the number of paths in SPL channel, the average SNR at SR for the mismatched modes was declined by 6dB and the gap was enlarged in the second scenario.

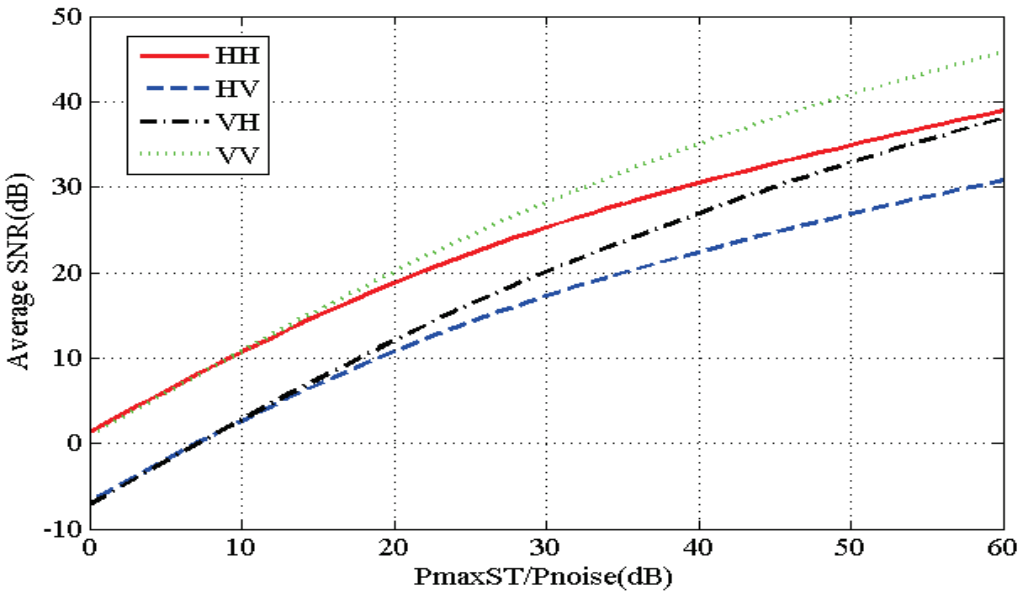

Figure 5.1: Average SNR at SR vs. P_{maxST}/P_{noise} with SL:2-path, SPL:1-path, ST:2

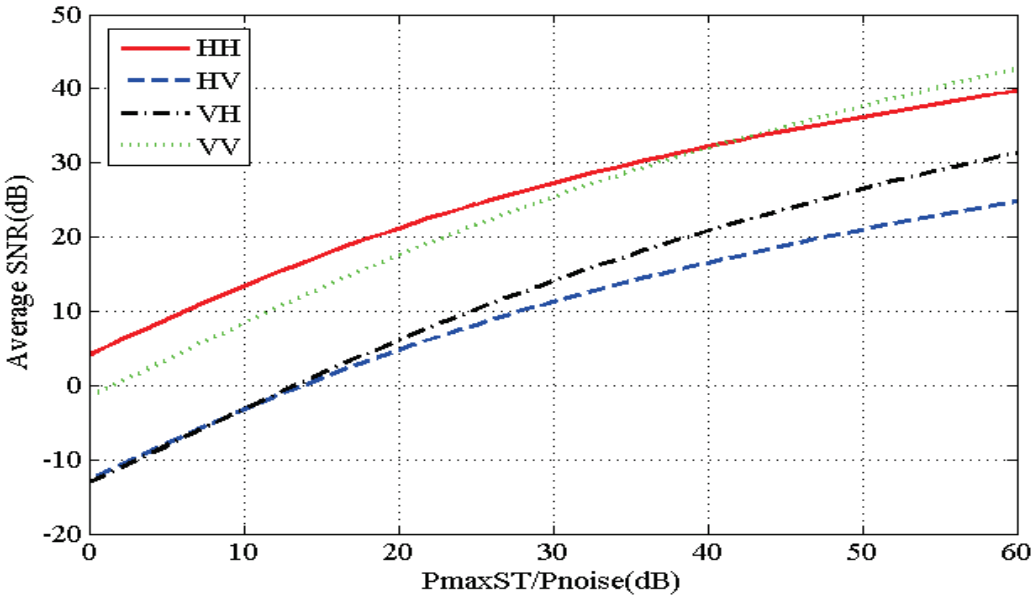

Figure 5.2: Average SNR at SR versus P_{maxST}/P_{noise} with SL:2-path, SPL:4-path, ST:2

5.3.2 Performance Analysis of Transmit Antennas Diversity

In the second simulation, we aimed to observe the average SNR at SR by using different number of transmit antennas. In the first circumstance, 2 transmit antennas and Alamouti's code C_2 were utilized at ST. In the second circumstance, 4 transmit antennas and the half rate code C_4 were utilized at ST. In both circumstances, we set $qt = V$ and $qr = V$. SR is equipped with 1 antenna and PR is equipped with 4 antennas. The number of paths is chosen equal to 2 on SL and 6 on SPL.

For the case of 2 transmit antennas at ST, the SNR at SR reaches the saturation point at 20dB when P_{maxSU}/P_{noise} achieves 40dB. Compare to the previous results in Fig. 5.1 and 5.2, the SNR at SR reaches the saturation point faster due to the increase in number of paths on the SPL. However, the increase in number of antennas will significantly delay the arrival of the saturation point even the number of paths on the SPL is also increased. For the case of 4 transmit antennas at ST, the SNR at SR reaches the saturation point at 65dB when P_{maxSU}/P_{noise} achieves 100dB.

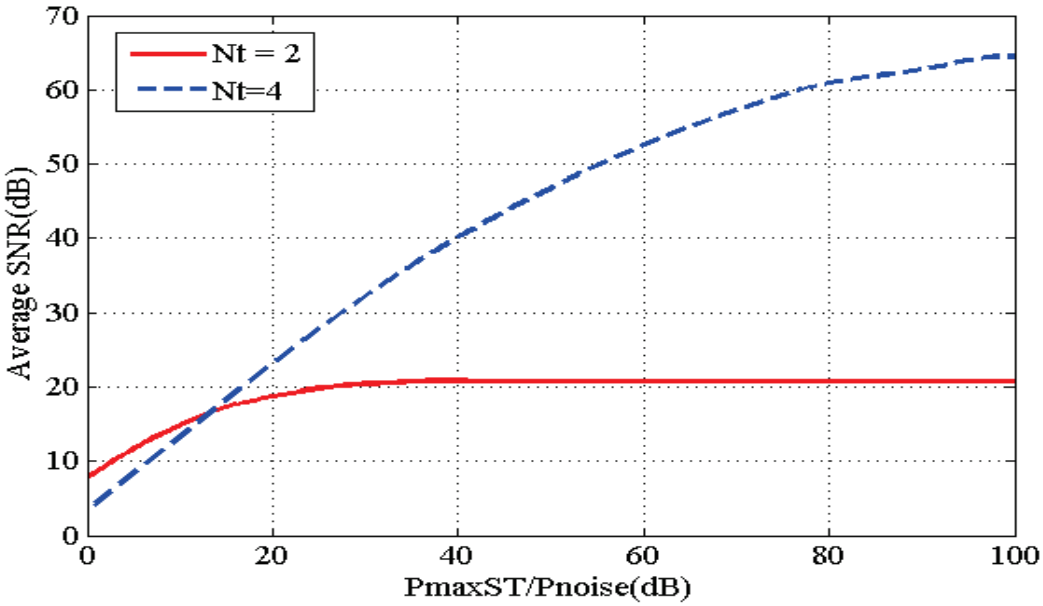

Figure 5.3: Average SNR at SR versus P_{maxST}/P_{noise} with SL:2-path, SPL:6-path, ST:2, 4

Chapter 6

Cognitive Sub-Small Cell for Sojourners

Contents

Small cells such as femto, pico, and microcells have been aroused general interest lately due to their consequential effect on enhancing network capacity, stretching service coverage and cutting back network energy consumption [115, 116].

In many residential and enterprise small cells, according to the duration of stay, users can be grouped into two categories: sojourners and inhabitants. Besides the duration of stay, other features can be pinpointed: the status in the network, the Quality of Service (QoS) requirements, the geographical location, the regularity or predictability of the entry and exit time.

Motivated example: A concrete instance in real life can well elaborate the above concept. An office area is covered by a small cell. The staffs and visitors can be classified as inhabitants and sojourners, respectively. Staffs have fixed entry and exit time, while visitors enter and depart randomly. Staffs have higher status, settled and specific QoS requirements, while visitors do not. The staffs and visitors have their own area to stay in, such as the working area for staffs and the reception area for visitors. They also have the common area to stay like the meeting room.

Existing approaches and their limitations: Multiple-Input Multiple-Output (MIMO) technologies are essential components in 3GPP Long Term Evolution (LTE)-Advanced [117,118]. Among them, multiuser MIMO technology is markedly advantageous to enhance the cell capacity especially in highly spatial correlated channels [119–121], since multiuser MIMO technology can serve multiple users simultaneously on the same frequency. Dirty paper coding (DPC) [122,123] and Block Diagonalization (BD) [88] are two widely adopted techniques for multiuser MIMO. DPC is contrived to suit the capacity optimal requirement [124], however, it is hard to implement owing to its complexity. BD is a practical approach which adopts precoding to completely eliminate inter-user interference. The deficiency of this technique is that BD precoding and full rank transmission requires that the number of transmit antennas is not less than the total number of receive antennas. Therefore, the number of concurrently supportable users is restricted by the number of transmit antennas.

Cognitive Sub-Small Cell for Sojourners (CSCS) solution: The above example and the limitations of existing techniques inspire us to put forward a solution named CSCS in allusion to the following small cell scenario. i) Users can be categorized into two groups: sojourners and inhabitants. ii) Inhabitants have fixed entry and exit time, while visitors enter and depart randomly. iii) Inhabitants have higher status, settled and specific QoS requirements. iv) The small cell coverage area is relatively large. v) The number of users is relatively large. vi) The overlapping area between the inhabitants' activity area and the sojourners' activity area is relatively small. CSCS divides one small cell into two customized sub-small cells for inhabitants and sojourners respectively for the following reasons.

1) CSCS is a design in line with the trend of green communications [115, 125], which

plays a significant role of saving energy:

- Each of two sub-small cells is served by its own sub-small cell Access Point (AP). In the case of a small overlap between the two groups' activity areas, utilizing two sub-small cell APs instead of one single small cell AP shortens the average distance between User Equipment (UE) and AP. Accordingly, it reduces the total transmit power.

- Considering that inhabitants and sojourners may have two different active timetables, CSCS can turn the sub-small cell AP off outside the active period of the group which it serves. However, AP of a collective small cell can only turn itself off when both groups are inactive.

2) CSCS enhances the number of concurrently supportable users. We consider this in the context of BD precoding and full rank transmission. The number of transmit antennas on AP restricts the number of concurrently supportable users. The number of transmit antennas on a single AP is limited by many factors, such as the processing speed of AP and the size of AP. By utilizing two different sub-small cell APs, CSCS enables more transmit antennas to be installed in the whole small cell, thereby enhancing the number of concurrently supportable users.

3) CSCS enshields inhabitants according to the priority. The QoS requirements and higher status for the inhabitants are ensured by a primary sub-small cell. The sojourners are served by a secondary sub-small cell. The primary sub-small cell and the secondary sub-small cell utilize the same spectrum on condition that the level of interference caused by the secondary sub-small cell to the primary sub-small cell is kept tolerable [126].

Design challenges:

(1) Determining the number of transmit antennas: BD precoding and full rank transmission requires that the number of transmit antennas is not less than the total number of receive antennas. Therefore, the number of concurrently supportable users is limited by the number of transmit antennas. When the number of users is greater than the number of concurrently supportable users, AP will select users to simultaneously serve using some kind of user selection algorithm.

QoS requirements and the number of users who simultaneously present make demands on the number of concurrently supportable users. On the other hand, configuring overmany transmit antennas results in a waste of resources.

The number of antennas is fixed after network launch. The determination of the number of antennas is a pre-launch parameter design task.

(2) Inter-sub-small cell interference: Due to BD precoding, ISSC and SSSC will not cause downlink inter-sub-small cell interference when perfect IAP-to-sojourner CSI and

SAP-to-inhabitant CSI are acquired by IAP and SAP respectively.

In practice, the perfect acquisition of SAP-to-inhabitant CSI is hampered by the lack of explicit coordination and full cooperation between ISSC and SSSC, since inhabitants are scant of willingness to feedback SAP-to-inhabitant CSI by using their own bandwidth and power. SAP has to turn to blind CSI estimate or other inexact CSI estimates which will furnish imperfect SAP-to-inhabitant CSI [131,132]. Therefore, the root cause of interference inflicted by SSSC on ISSC is uncertain SAP-to-inhabitant CSI.

In this thesis, the interference inflicted by ISSC on SSSC is not a key focus of our study. We make the assumption that either sojourners are willing to feedback IAP-to-sojourner CSI by using their own bandwidth and power to avoid interference owing to perfect IAP-to-sojourner CSI, or sojourners will not access the spectrum which is heavily used by the inhabitants.

Main contributions:

(1) Algorithm for determining the number of transmit antennas: We propose an algorithm for determining the number of transmit antennas on sub-small cell APs helped by the probability distribution of the number of concurrent sojourners. The number of antennas is fixed after network launch. The determination of the number of antennas is a pre-launch parameter design task or guideline for network planning (parameter optimization).

(2) BDBF: We proposed an interference control scheme named BDBF for secondary systems which are hampered from perfect secondary-to-primary Channel State Information (CSI). We prove and verify that BDBF can gain more capacity than the interference controller using optimal Beamformer (BF) alone within a bearably large radius of uncertainty region.

(3) Performance Analysis: i) From simulation and numerical results, we find how the factors, such as the standard deviation of the duration of stay, the mean of the duration of stay, the distribution of arrival rate, and the total number of sojourners during the observation time interval, influence the number of concurrent sojourners and further impact the number of transmit antennas on sub-small cell APs. ii) We show the benefit of BDBF.

6.1 Cognitive Sub-Small Cell for Sojourners

We consider downlink transmission in a small cell served by a single AP. The AP is equipped with N_T transmit antennas and every UE is equipped with N_R receive antennas (We listed some notations used in Table 6.1.). The AP adopts N_C-subcarrier Orthogonal Frequency Division Multiplexing (OFDM), BD precoding and full rank transmission. Based on BD precoding and full rank transmission, the number of concurrently supportable users is determined by $\lceil N_T/N_R \rceil$ [88, 127]. When the number of users in the small cell is greater

Table 6.1: Notations

Symbol	Definition
$\ulcorner \bullet \urcorner$	the ceiling operator
N_T	the number of transmit antennas on the AP
N_R	the number of receive antennas at each UE
N_1	the total number of inhabitants
$N_2(t)$	the total number of sojourners at time t
$N_1^{'}$	the number of inhabitants who stay in the overlap of ISSC and SSSC
$N_2^{'}(t)$	the number of sojourners who stay in the overlap of ISSC and SSSC at time t
Q	the minimum QoS requirements of sojourners
Q'	the QoS requirements of inhabitants
N_U	the number of concurrently supportable sojourners
N_{ST}	the possible number of transmit antennas on SAP
N_{ST}^*	the selected number of transmit antennas on SAP
N_{IT}	the number of transmit antennas on IAP
$U_I^{'} = \left\{ I_1, \ldots, I_{N_1^{'}} \right\}$	the set of inhabitants who stay in the overlap of ISSC and SSSC
$U_{S(t)}^{'} = \left\{ S_1, \ldots, S_{N_2^{'}(t)} \right\}$	the set of sojourners who stay in the overlap of ISSC and SSSC at time t
U_S	the set of sojourners
$\mathbf{I}_N$	the identity matrix of size $N \times N$
$\mathrm{Tr}(\bullet)$	the trace operator
$(\bullet)^{\mathcal{H}}$	Hermitian transpose
$\mathrm{vec}(\mathbf{X})$	the vector is made up of the columns of matrix $\mathbf{X}$
$\otimes$	the Kronecker product

than the number of concurrently supportable users, some kind of user selection algorithm [127, 128] is implemented.

We assume for simplicity that

- N_1 inhabitants always stay in the small cell.
- $N_2(t)$ sojourners stay in the small cell at time t.
- Sojourners arrive the small cell according to a time-varing Poisson process with arrival rate $\lambda(t)$ and $N_2(t=0)=0$.
- The inhabitants' activity area A_1 is a disk of radius R_1. The sojourners' activity area A_2 is a disk of radius R_2. The small cell coverage area A_3 is a disk of radius R_3. A_1 and A_2 partially overlap. A_3 accommodates A_1 and A_2 with $R_3 = \frac{R_1 \cos w_1 + R_2 \cos w_2 + R_1 + R_2}{2}$, where w_1, w_2 and the positional relationship of A_1, A_2, and A_3 are illustrated in Figure 1.

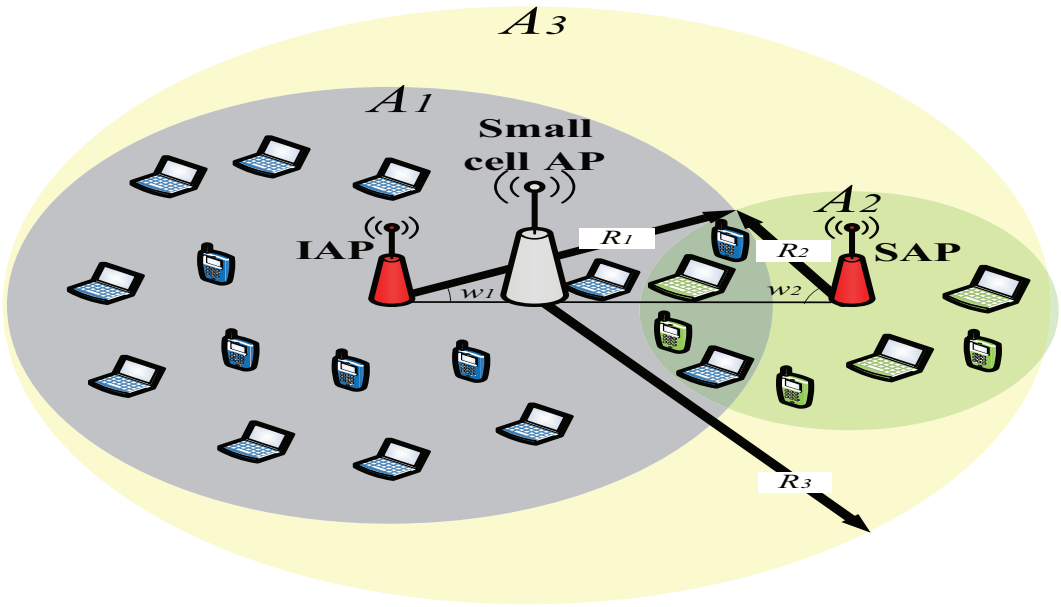

Figure 6.1: The system model for CSCS

- The area of A_1, A_2, and A_3 are, respectively, S_{A_1}, S_{A_2}, and S_{A_3}. The area of overlap between A_1 and A_2 is $S_{A_1 \cap A_2}$.
- S_{A_3} is relatively large. $S_{A_1 \cap A_2}$ is relatively small.
- N_1' inhabitants always stay in the overlapping area between A_1 and A_2.

- $N_2^{'}(t)$ sojourners stay in the overlapping area between A_1 and A_2 at time t.
- Inhabitants and sojourners are uniformly distributed in their respective activity areas. The number of users is relatively large.
- The inhabitants have higher status.

The coverage area of IAP and SAP is not required to cover the coverage area of small cell AP. The mandatory condition is that the inhabitants' activity area is covered by IAP, the sojourners' activity area is covered by SAP, and small cell AP covers both the inhabitants' activity area and the sojourners' activity area. For the purpose of simplifying the problem, a specifical model is considered in this thesis where the coverage area of small cell AP accommodates the coverage area of IAP and SAP. In order to meet the mandatory condition, the coverage of IAP and SAP can be beyond the boundary of the coverage area of small cell AP.

6.1.1 Cognitive Sub-Small Cell for Sojourners

CSCS turns the single small cell into two sub-small cells: Inhabitant Sub-Small Cell (ISSC) and Sojourner Sub-Small Cell (SSSC), each of which is served by its own AP. ISSC serves the inhabitants by Inhabitant Access Point (IAP). SSSC serves the sojourners by Sojourner Access Point (SAP). Both IAP and SAP exploit BD precoding and full rank transmission. The sub-small cells use the same number of subcarriers and the same spectrum as that are used by the small cell AP. We assume that both sub-small cell APs take inhabitants and sojourners in their respective coverage area into account to design BD precoding.

6.1.2 Number of Concurrent Sojourners

Our analysis for SSSC is based on the following assumptions:

- Sojourners arrive SSSC according to a time-varing Poisson process with arrival rate $\lambda(t)$ and $N_2(t=0)=0$.
- The duration of stay of one sojourner is modeled as duration of a continuous time Markov process with $m+1$ states from its starting until its ending in the absorbing state, where $m \geq 1$. The probability of this process starting in the state i is α_i, where $i = 1, \ldots, m+1$. The state $m+1$ is the absorbing state and the others are transient states. We assume that this process will never start in the absorbing state, i.e. $\alpha_{m+1} = 0$.

The duration of stay of one sojourner has a phase-type distribution [129,130]. We denote by $\mathbf{R}$ the matrix which contains the transition rates among the transient states. $\mathbf{R}$ is a matrix

of size $m \times m$. The duration of stay of one sojourner is denoted by X. The Cumulative Distribution Function (CDF) of X is given by

$$F_X(x) = 1 - \boldsymbol{\alpha} \exp(\mathbf{R}x)\,\mathbf{1},\ x \geq 0, \tag{6.1}$$

where $\boldsymbol{\alpha} = [\alpha_1, \ldots, \alpha_m]$, $\exp(\bullet)$ is the matrix exponential and $\mathbf{1}$ is an $m \times 1$ vector with all elements equal to 1.

Remark

Under the above assumptions, SSSC can be modeled as an $M_t/G/\infty$ queue with service time follows a phase type distribution, arrival rate $\lambda(t)$ and $N_2(t=0) = 0$. Authors in [130] have given the probability distribution of the number of concurrent users in such queueing system. Accordingly, $N_2(t)$ has a Poisson distribution with parameter

$$v(t) = \int_0^t \lambda(\tau)\left[1 - F_X(t-\tau)\right] d\tau,\ t \geq 0. \tag{6.2}$$

The Probability Mass Function (PMF) of $N_2(t)$ is

$$f_{N_2(t)}(n) = \mathbb{P}(N_2(t) = n) = \frac{[v(t)]^n}{n!} \exp(-v(t)), \tag{6.3}$$

where $n \in \mathbb{Z}_0^+$.

The CDF of $N_2(t)$ is

$$F_{N_2(t)}(n') = \sum_{n=0}^{n'} f_{N_2(t)}(n), \tag{6.4}$$

where $n' \in \mathbb{Z}_0^+$.

6.1.3 Downlink inter-sub-small cell interference

Due to BD precoding, ISSC and SSSC will not cause downlink inter-sub-small cell interference when perfect IAP-to-sojourner CSI and SAP-to-inhabitant CSI are acquired by IAP and SAP respectively.

Remark In practice, the perfect acquisition of SAP-to-inhabitant CSI is hampered by the lack of explicit coordination and full cooperation between ISSC and SSSC, since inhabitants are scant of willingness to feedback SAP-to-inhabitant CSI by using their own bandwidth and power. SAP has to turn to blind CSI estimate or other inexact CSI estimates which will furnish imperfect SAP-to-inhabitant CSI [131,132]. Therefore, the root cause of interference inflicted by SSSC on ISSC is that BD precoding utilizes uncertain CSI.

We consider that IAP-to-sojourner CSI is perfect. We suppose the coverage areas of ISSC and SSSC are respectively consistent with the inhabitants' activity area A_1 and the

sojourners' activity area A_2. It is also assumed that the inter-sub-small cell interference only exists in the overlapping area between A_1 and A_2.

Since the IAP-to-inhabitant CSI and SAP-to-sojourner CSI are perspicuous for IAP and SAP, there is no interference inside ISSC or SSSC in our system. In some relevant papers about underlay multicarrier cognitive radio systems with uncertain CSI, the subcarrier scheduling is the way for steering clear of the interference inside the secondary systems [133, 134].

6.2 Determining Number of Transmit Antennas on Sub-small Cell AP

BD precoding and full rank transmission requires that the number of transmit antennas is not less than the total number of receive antennas. Therefore, the number of concurrently supportable users is limited by the number of transmit antennas. When the number of users is greater than the number of concurrently supportable users, AP will select users to simultaneously serve using some kind of user selection algorithm.

QoS requirements and the number of users who simultaneously present make demands on the number of concurrently supportable users.

In our system, we express the required number of concurrently supportable sojourners as $N_2(t)\,Q$, where Q indicates the minimum QoS requirements of sojourners, $Q \leq 1$, and $N_2(t)\,Q \in \mathbb{Z}^+$.

We investigate the issue of determining the number of transmit antennas under the premise that AP can support the installation of selected number of transmit antennas.

We put forward a criterion to determine an appropriate number of transmit antennas on Sub-small Cell Access Points:

- It pursues the minimum number of transmit antennas which ensures BD and full rank transmission to be validated.
- It ensures that the average value of the probability of the number of concurrently supportable sojourners being adequate during an applicable period is no less than the predetermined probability or the growth of this average value of probability led by adding one more supportable sojourner is less than a threshold.

We denote by N_U the number of concurrently supportable sojourners. For our system, the probability of the number of concurrently supportable sojourners being adequate at time t is

$$P(N_U,\ t) = F_{N_2(t)}(N_U/Q)\,. \tag{6.5}$$

The average value of the probability of the number of concurrently supportable sojourners being adequate during the time interval $[0,\ T]$ as

$$E\left[P\left(N_U,\ t\right)\right] = \frac{1}{T}\int_{t=0}^{T} P\left(N_U,\ t\right) dt. \tag{6.6}$$

According to the first item of our criterion, we have

$$N_U = N_{ST}/N_R - N_1^{'}, \tag{6.7}$$

where N_{ST} is the possible number of transmit antennas on SAP and $N_U \in \mathbb{Z}^+$.

Proposition 1.

The number of transmit antennas on sub-small cell APs can be determined as follows: as N_R and $N_1^{'}$ are supposed to be known in our system model, the selected number of transmit antennas on SAP N_{ST}^* is determined by (6.8) or (6.9):

$$N_{ST}^* = \min_{N_{ST}} \left\{E\left[P\left(N_U,\ t\right)\right] \geq \eta\right\}, \tag{6.8}$$

$$N_{ST}^* = \min_{N_{ST}} \left\{E\left[P\left(N_U+1,\ t\right)\right] - E\left[P\left(N_U,\ t\right)\right] \leq \gamma\right\}, \tag{6.9}$$

where η is a predetermined probability and γ is a threshold.

We denote by N_{IT} the selected number of transmit antennas on IAP. N_{IT} is determined by

$$N_{IT} = N_R Q' \left(N_1 + \frac{N_U^* S_{A_1 \cap A_2}}{S_{A_2}}\right). \tag{6.10}$$

where $N_U^* = N_{ST}^*/N_R - N_1^{'}$ and Q' indicates the QoS requirements of inhabitants.

6.3 Downlink Inter-sub-small Interference Control

As discussed above, for our system, due to the use of BD, no inter-sub-small cell interference is caused by downlink transmission under the situation that IAP and SAP acquire perfect IAP-to-sojourner CSI and SAP-to-inhabitant CSI respectively. However, the interference inflicted by SSSC on ISSC has its origins in BD precoding exploiting CSI with inevitable uncertainty. We proposed an interference control scheme named *BDBF* for secondary systems which are hampered from perfect secondary-to-primary CSI. *BDBF* utilizes BD Precoding based on uncertain CSI in conjunction with auxiliary optimal BF. In view of the adoption of OFDM, we turn the design of auxiliary optimal BF of *BDBF* into a multi-user multi-subcarrier optimal BF design under channel uncertainties. For such optimization problems that contain the uncertainty region constraint, S-Procedure is an efficacious tool to transform semi-infinite programs into equivalent semi-definite programs [132, 133]. We

prove and verify that *BDBF* performs better than the interference controller using optimal BF alone for gaining more capacity within a bearably large radius of uncertainty region.

6.3.1 Block Diagonalization

For each user u_i, BD algorithm [88] constructs a precoding matrix $\mathbf{W}_{t,u_i,s}$ which achieves the zero-interference constraint, i.e.

$$\mathbf{H}_{t,u_j,s}\mathbf{W}_{t,u_i,s} = 0,\ \forall j \neq i, \tag{6.11}$$

where $\mathbf{H}_{t,u_j,s} \in N_r \times N_t$ denotes the channel matrix from transmitter t to user u_j at subcarrier s, N_r denotes the number of receive antennas at every UE and N_t denotes the number of transmit antennas at transmitter t.

Suppose that N_u users are within the coverage area of transmitter t and we define

$$\tilde{\mathbf{H}}_{t,u_i,s} = \left[\mathbf{H}^T_{t,u_1,s} \dots \mathbf{H}^T_{t,u_{i-1},s}\ \mathbf{H}^T_{t,u_{i+1},s} \dots \mathbf{H}^T_{t,u_{N_u},s}\right]^T. \tag{6.12}$$

Hereupon, Equation (6.11) has another equivalent form

$$\tilde{\mathbf{H}}_{t,u_i,s}\mathbf{W}_{t,u_i,s} = 0. \tag{6.13}$$

From Equation (6.13), it is deduced that $\mathbf{W}_{t,u_i,s}$ is a basis set in the null space of $\tilde{\mathbf{H}}_{t,u_i,s}$. The Singular Value Decomposition (SVD) of $\tilde{\mathbf{H}}_{t,u_i,s}$ is expressed as

$$\tilde{\mathbf{H}}_{t,u_i,s} = \tilde{\mathbf{U}}_{t,u_i,s}\left[\tilde{\mathbf{\Lambda}}_{t,u_i,s}\mathbf{0}\right]\left[\tilde{\mathbf{V}}^{(1)}_{t,u_i,s}\tilde{\mathbf{V}}^{(0)}_{t,u_i,s}\right]^{\mathcal{H}}, \tag{6.14}$$

where $\tilde{\mathbf{V}}^{(0)}_{t,u_i,s} \in \mathbb{C}^{\mathrm{N_t}\times\left(\mathrm{N_t}-\mathrm{rank}\left(\tilde{\mathbf{H}}_{t,u_i,s}\right)\right)}$ contains the right-singular vectors corresponding to the zero singular values of $\tilde{\mathbf{H}}_{t,u_i,s}$, i.e. $\tilde{\mathbf{V}}^{(0)}_{t,u_i,s}$ forms a null space basis of $\tilde{\mathbf{H}}_{t,u_i,s}$. Therefore $\mathbf{W}_{t,u_i,s}$ can be constructed by any linear combinations of the columns in $\tilde{\mathbf{V}}^{(0)}_{t,u_i,s}$. Correspondingly, $\mathbf{H}_{t,u_i,s}\tilde{\mathbf{V}}^{(0)}_{t,u_i,s}$ forms the equivalent channel.

The SVD precoding can be performed using the equivalent channel:

$$\mathbf{H}_{t,u_i,s}\tilde{\mathbf{V}}^{(0)}_{t,u_i,s} = \mathbf{U}_{t,u_i,s}\begin{bmatrix}\mathbf{\Lambda}_{t,u_i,s} & \mathbf{0}\\ \mathbf{0} & \mathbf{0}\end{bmatrix}\left[\mathbf{V}^{(1)}_{t,u_i,s}\mathbf{V}^{(0)}_{t,u_i,s}\right]^{\mathcal{H}}, \tag{6.15}$$

where $\mathbf{V}^{(1)}_{t,u_i,s} \in \mathbb{C}^{\left(\mathrm{N_t}-\mathrm{rank}\left(\tilde{\mathbf{H}}_{t,u_i,s}\right)\right)\times\mathrm{rank}\left(\mathbf{H}_{\mathrm{t,u_i,s}}\tilde{\mathbf{V}}^{(0)}_{\mathrm{t,u_i,s}}\right)}$ contains the right-singular vectors corresponding to the non-zero singular values of $\mathbf{H}_{t,u_i,s}\tilde{\mathbf{V}}^{(0)}_{t,u_i,s}$. $\mathbf{V}^{(1)}_{t,u_i,s}$ is used as SVD precoder and $\mathbf{U}^{\mathcal{H}}_{t,u_i,s}$ is used as SVD decoder. Consequently, the precoding matrix $\mathbf{W}_{t,u_i,s}$ can be chosen as $\tilde{\mathbf{V}}^{(0)}_{t,u_i,s}\mathbf{V}^{(1)}_{t,u_i,s}$.

For the full rank transmission, i.e. the number of streams sent to a UE is no less than the number of receive antennas, it is needed that $N_t - \mathrm{rank}\left(\tilde{\mathbf{H}}_{t,u_i,s}\right) \geq N_r$, i.e. $N_t \geq N_r N_u$.

In this paper, we consider the situation that the number of streams sent to a UE equals the number of receive antennas, i.e $N_t = N_r N_u$. Accordingly, $\mathbf{W}_{t,u_i,s}$ is a matrix of size $N_t \times N_r$.

6.3.2 *BDBF*

As explained in Remark 1, SAP-to-inhabitant CSI is unable to be perfect. The SAP-to-inhabitant channel matrix at subcarrier s can be expressed as

$$\mathbf{H}_{SAP,I_i,s} = \hat{\mathbf{H}}_{SAP,I_i,s} + \triangle\mathbf{H}_{SAP,I_i,s}, \tag{6.16}$$

where $\hat{\mathbf{H}}_{SAP,I_i,s}$ is the estimated channel matrix from transmitter SAP to user $I_i \in U_I^{'}$ at subcarrier s and $\triangle\mathbf{H}_{SAP,I_i,s}$ is the channel uncertainty matrix from transmitter SAP to user $I_i \in U_I^{'}$ at subcarrier s. In this paper, we adopt a channel uncertainty model [135] which defines the uncertainty region as

$$\triangle(\epsilon) = \left\{\triangle\mathbf{H}_{SAP,I_i,s} \mid \mathrm{Tr}\left\{\mathbf{E}\right\} \leq \epsilon^2\right\}, \tag{6.17}$$

where $\mathbf{E} = \triangle\mathbf{H}_{SAP,I_i,s}\triangle\mathbf{H}^{\mathcal{H}}_{SAP,I_i,s}$.

Based on the assumption that the inter-sub-small cell interference only exists in the overlapping area between A_1 and A_2, SAP only need to take the inhabitants in the overlap between A_1 and A_2 into account for restraining interference.

Proposition 2.

For secondary systems which are hampered from perfect secondary-to-primary CSI, secondary systems can exploit BDBF: BD precoding based on uncertain CSI in conjunction with auxiliary optimal BF to control interference to primary systems.

After BDBF, the transmitted signal from SAP to sojourner S_i can be expressed as

$$\mathbf{S}_{SAP,S_i,s} = \mathbf{W}_{SAP,S_i,s}\mathbf{P}_{SAP,S_i,s}\mathbf{x}_{SAP,S_i,s} \tag{6.18}$$

where

$\mathbf{x}_{SAP,I_i,s} \in \mathbb{C}^{N^*_{ST}\times 1}$ *is the information symbol vector transmitted from SAP to* I_i *at subcarrier* s *with covariance matrix* $\mathbb{E}\left\{\mathbf{x}_{SAP,I_i,s}\mathbf{x}^{\mathcal{H}}_{SAP,I_i,s}\right\} = \mathbf{I}_{N^*_{ST}}$,

$\mathbf{P}_{SAP,I_i,s} \in \mathbb{C}^{N_R\times N^*_{ST}}$ *is the auxiliary optimal BF,*

and $\mathbf{W}_{SAP,S_i,s}$ *is the BD precoding matrix of size* $N^*_{ST} \times N_R$.

$\mathbf{W}_{SAP,S_i,s}$ *is generated by* $\tilde{\mathbf{H}}_{SAP,S_i,s} = \left[\breve{\mathbf{H}}_{SAP,S_i,s}\ \mathbf{H}^T_{SAP,I_1,s}\ldots\mathbf{H}^T_{SAP,I_{N_1^{'}},s}\right]^T$ *and* $\breve{\mathbf{H}}_{SAP,S_i,s} = \left[\mathbf{H}^T_{SAP,S_1,s}\ldots\mathbf{H}^T_{SAP,S_{i-1},s}\ \mathbf{H}^T_{SAP,S_{i+1},s}\ldots\mathbf{H}^T_{SAP,S_{N_2(t)},s}\right]$.

For inhabitant $I_i \in U_I^{'}$, the received signal at subcarrier s is given by

$$\begin{aligned}\mathbf{y}_{I_i,s} &= \mathbf{U}^{\mathcal{H}}_{IAP,I_i,s}\mathbf{H}_{IAP,I_i,s}\mathbf{W}_{IAP,I_i,s}\mathbf{x}_{IAP,I_i,s} \\ &+ \sum_{S_i\in U_S}\mathbf{H}_{SAP,I_i,s}\mathbf{W}_{SAP,S_i,s}\mathbf{P}_{SAP,S_i,s}\mathbf{x}_{SAP,S_i,s} \\ &+ \mathbf{n}_{I_i,s}, \end{aligned} \tag{6.19}$$

where

$\mathbf{x}_{IAP,I_i,s} \in \mathbb{C}^{N_{IT}\times 1}$ is the information symbol vector transmitted from IAP to I_i at subcarrier s with covariance matrix $\mathbb{E}\left\{\mathbf{x}_{IAP,I_i,s}\mathbf{x}^{\mathcal{H}}_{IAP,I_i,s}\right\} = \mathbf{I}_{N_{IT}}$,

$\mathbf{n}_{I_i,s} \in \mathbb{C}^{N_R\times 1}$ is the i.i.d. circularly symmetric white Gaussian noise at subcarrier s at reciever I_i with covariance matrix $\mathbb{E}\left\{\mathbf{n}_{I_i,s}\mathbf{n}^{\mathcal{H}}_{I_i,s}\right\} = \mathbf{I}_{N_R}$,

$\mathbf{W}_{IAP,I_i,s}$ is the BD precoding matrix of size $N_{IT}\times N_R$,

and $\mathbf{U}^{\mathcal{H}}_{IAP,I_i,s}$ is the SVD decoding matrix of size $N_R\times N_R$.

$\mathbf{W}_{IAP,I_i,s}$ and $\mathbf{U}^{\mathcal{H}}_{IAP,I_i,s}$ are generated by $\tilde{\mathbf{H}}_{IAP,I_i,s} = \left[\overline{\mathbf{H}}_{IAP,I_i,s}\ \mathbf{H}^T_{IAP,S_1,s}\cdots\mathbf{H}^T_{t,S_{N'_2(t)},s}\right]^T$ and $\overline{\mathbf{H}}_{IAP,I_i,s} = \left[\mathbf{H}^T_{IAP,I_1,s}\cdots\mathbf{H}^T_{IAP,I_{i-1},s}\ \mathbf{H}^T_{IAP,I_{i+1},s}\cdots\mathbf{H}^T_{IAP,I_{N_1},s}\right]$.

Theorem 1. *The auxiliary optimal BF of BDBF can be formulated as the following multi-user multi-subcarrier optimal BF design under channel uncertainties: trying for the maximum capacity of secondary system under the precondition that the interference inflicted to the primary system is kept below the threshold.*

$$(\mathbf{P1})\ \max_{\boldsymbol{Q}_{SAP,S_i,s}}\sum_{s=1}^{N_C}\sum_{S_i\in U_S}\log\det\left(\mathbf{I}_{N_R}+\frac{SNR}{N^*_{ST}}\mathbf{A}\right) \tag{6.20a}$$

$$\text{s.t. } \boldsymbol{Q}_{SAP,S_i,s}\succcurlyeq 0,\ \forall S_i\in U_S,\ \forall s, \tag{6.20b}$$

$$\sum_{S_i\in U_S}\mathrm{Tr}\left(\breve{\boldsymbol{Q}}_{SAP,S_i,s}\right)\le P_{SAP},\ \forall S_i\in U_S,\ \forall s, \tag{6.20c}$$

$$\mathrm{Tr}\left(\mathbf{B}\right)\le\zeta,\ \forall\triangle\mathbf{H}_{SAP,I_i,s}\in\triangle\left(\epsilon\right),\ \forall S_i\in U_S,\ \forall I_i\in U_I^{'},\ \forall s, \tag{6.20d}$$

where

$\boldsymbol{Q}_{SAP,S_i,s} = \mathbb{E}\left\{\mathbf{P}_{SAP,S_i,s}\mathbf{P}^{\mathcal{H}}_{SAP,S_i,s}\right\}$,

$\breve{\boldsymbol{Q}}_{SAP,S_i,s} = \mathbf{W}_{SAP,S_i,s}\boldsymbol{Q}_{SAP,S_i,s}\mathbf{W}^{\mathcal{H}}_{SAP,S_i,s}$,

$\mathbf{A} = \boldsymbol{\Lambda}_{SAP,S_i,s}\boldsymbol{Q}_{SAP,S_i,s}\boldsymbol{\Lambda}^{\mathcal{H}}_{SAP,S_i,s}$,

$\mathbf{B} = \mathbf{H}_{SAP,I_i,s}\breve{\boldsymbol{Q}}_{SAP,S_i,s}\mathbf{H}^{\mathcal{H}}_{SAP,I_i,s}$,

P_{SAP} is the maximum downlink transmit power of SAP,

and ζ is the inter-sub-small interference tolerable threshold on each subcarrier for inhabitant $I_i\in U_I^{'}$.

$\boldsymbol{Q}_{SAP,S_i,s}$ *is a positive semidefinite matrix to render certain that the elements on the main diagonal of* $\mathbf{A}$ *and* $\mathbf{B}$ *are real and non-negative. Additionally,* $\boldsymbol{Q}_{SAP,S_i,s}$ *is a symmetric matrix to ensure that linear matrix inequality (LMI) holds.*

$\triangle(\epsilon)$ is a set of infinite cardinality and accordingly the inequality (6.20d) imposes infinite constraints. This means that (P1) is a semi-infinite program. (P1) can be transformed into an equivalent semi-definite program (P2) with the constraint (6.21d) which contains finite constraints instead of the constraint (6.20d):

$$(\mathbf{P2}) \max_{\boldsymbol{Q}_{SAP,S_i,s}} \sum_{s=1}^{N_C} \sum_{S_i \in U_S} \log\det\left(\mathbf{I}_{N_R} + \frac{SNR}{N_{ST}^*}\mathbf{A}\right) \tag{6.21a}$$

$$\text{s.t. } \boldsymbol{Q}_{SAP,S_i,s} \succcurlyeq 0,\ \forall S_i \in U_S,\ \forall s, \tag{6.21b}$$

$$\sum_{S_i \in U_S} \mathrm{Tr}\left(\breve{\boldsymbol{Q}}_{SAP,S_i,s}\right) \leq P_{SAP},\ \forall S_i \in U_S,\ \forall s, \tag{6.21c}$$

$$\begin{aligned} &\begin{bmatrix} \alpha\mathbf{I}_{N_T \times N_R} + \mathbf{G} & \mathbf{J}^{\mathcal{H}} \\ \mathbf{J} & k - \alpha\epsilon^2 \end{bmatrix} \ \succeq\ 0, \\ &\forall \alpha \geq 0,\ \forall I_i \in U_I^{'},\ \forall S_i \in U_S,\ \forall s \end{aligned} \tag{6.21d}$$

Proof:
The inequality (6.20d) contains infinite contraints which makes (P1) to be a semi-infinite program. For the purpose of converting (P1) into semi-definite program, the S-lemma [136, 137] is used to provide an equivalent constraint in Linear Matrix Inequality (LMI) form.

*Lemma 1 (S-Procedure):*For $\mathbf{E}, \mathbf{F} \in \mathbb{C}^{n\times n}$, $\mathbf{c} \in \mathbb{C}^n$, $c,\ e \in \mathbb{R}$, the inequality

$$\mathbf{x}^{\mathcal{H}}\mathbf{E}\mathbf{x} + 2\Re\left(\mathbf{c}^{\mathcal{H}}\mathbf{x}\right) + c \geq 0,\ \forall \mathbf{x}^{\mathcal{H}}\mathbf{F}\mathbf{x} \leq e \tag{6.22}$$

holds if and only if there exists $\gamma \geq 0$ such that

$$\begin{bmatrix} \gamma\mathbf{F}+\mathbf{E} & \mathbf{c} \\ \mathbf{c}^{\mathcal{H}} & c - e\gamma \end{bmatrix} \succeq \mathbf{0}. \tag{6.23}$$

According to the relationship between the trace operator and the vec operator $\mathrm{Tr}\left(\mathbf{C}^{\mathcal{H}}\mathbf{D}\mathbf{C}\right) = \mathrm{vec}\left(\mathbf{C}\right)^{\mathcal{H}}\left(\mathbf{I}\otimes\mathbf{D}\right)\mathrm{vec}\left(\mathbf{C}\right)$ and $\mathrm{Tr}\left(\mathbf{C}^{\mathcal{H}}\mathbf{D}\right) = \mathrm{vec}\left(\mathbf{C}\right)^{\mathcal{H}}\mathrm{vec}\left(\mathbf{D}\right)$, the inequality (6.20d) can be converted to an equivalent form:

$$
\begin{aligned}
-vec\left(\triangle\mathbf{H}_{SAP,I_i,s}^{\mathcal{H}}\right)^{\mathcal{H}}\left(\mathbf{I}_{N_R}\otimes\breve{\boldsymbol{Q}}_{SAP,S_i,s}\right)vec\left(\triangle\mathbf{H}_{SAP,I_i,s}^{\mathcal{H}}\right)\\
-2\Re\left(\mathrm{vec}\left(\breve{\boldsymbol{Q}}_{SAP,S_i,s}{}^{\mathcal{H}}\hat{\mathbf{H}}_{SAP,I_i,s}^{\mathcal{H}}\right)^{\mathcal{H}}\mathrm{vec}\left(\triangle\mathbf{H}_{SAP,I_i,s}^{\mathcal{H}}\right)\right)\\
-\mathrm{Tr}\left(\hat{\mathbf{H}}_{SAP,I_i,s}\breve{\boldsymbol{Q}}_{SAP,S_i,s}\hat{\mathbf{H}}_{SAP,I_i,s}^{\mathcal{H}}\right)\\
+\zeta\geq 0,\\
\forall vec\left(\triangle\mathbf{H}_{SAP,I_i,s}^{\mathcal{H}}\right)^{\mathcal{H}}\mathbf{I}_{N_T\times N_R}vec\left(\triangle\mathbf{H}_{SAP,I_i,s}^{\mathcal{H}}\right)\leq\epsilon^2,\\
\forall I_i\in U_I^{'},\ \forall S_i\in U_S,\ \forall s
\end{aligned}
\tag{6.24}
$$

Applying Lemma 1 to the inequality (6.24), a single constraint is obtained to replace the infinite constraints: if and only if there exists $\alpha\geqslant 0$ such that the inequality (6.25) is ture.

$$
\left[\begin{array}{cc}\alpha\mathbf{I}_{N_T\times N_R}+\mathbf{G} & \mathbf{J}^{\mathcal{H}}\\ \mathbf{J} & k-\alpha\epsilon^2\end{array}\right]\geq 0,\ \forall I_i\in U_I^{'},\ \forall S_i\in U_S,\ \forall s \tag{6.25}
$$

where

$\mathbf{G}=-\mathbf{I}_{N_R}\otimes\breve{\boldsymbol{Q}}_{SAP,S_i,s}$,

$\mathbf{J}=-\mathrm{vec}\left(\breve{\boldsymbol{Q}}_{SAP,S_i,s}^{\mathcal{H}}\hat{\mathbf{H}}_{SAP,I_i,s}^{\mathcal{H}}\right)$,

and

$k=\zeta-\mathrm{Tr}\left(\hat{\mathbf{H}}_{SAP,I_i,s}\breve{\boldsymbol{Q}}_{SAP,S_i,s}\hat{\mathbf{H}}_{SAP,I_i,s}^{\mathcal{H}}\right)$.

The semi-definite program (P2) can be solved by interior point methods [137, 138].

Theorem 2. *BDBF* can gain more capacity than the interference controller that using optimal BF alone within a bearably large radius of uncertainty region.

Proof:

We denote by $\mathbf{W}_{SAP,S_i,s}^{a}$ and $\mathbf{W}_{SAP,S_i,s}^{b}$ the BD precoding matrix which is generated by $\tilde{\mathbf{H}}_{SAP,S_i,s}^{a}=\left[\breve{\mathbf{H}}_{SAP,S_i,s}\ \hat{\mathbf{H}}_{IAP,I_1,s}^{T}\dots\hat{\mathbf{H}}_{t,I_{N_1^{'}},s}^{T}\right]^{T}$ and the BD precoding matrix which is generated by $\tilde{\mathbf{H}}_{SAP,S_i,s}^{b}=\left[\breve{\mathbf{H}}_{SAP,S_i,s}\right]^{T}$, respectively. Since $\mathbf{W}_{SAP,S_i,s}^{a}$ is a basis set in the null space of $\tilde{\mathbf{H}}_{SAP,S_i,s}^{a}$, then for $\epsilon^2\leq\iota$, we have $\mathrm{Tr}\left(\mathbf{H}_{SAP,I_i,s}\mathbf{W}_{SAP,S_i,s}^{a}\mathbf{W}_{SAP,S_i,s}^{a\mathcal{H}}\mathbf{H}_{SAP,I_i,s}^{\mathcal{H}}\right)<\mathrm{Tr}\left(\mathbf{H}_{SAP,I_i,s}\mathbf{W}_{SAP,S_i,s}^{b}\mathbf{W}_{SAP,S_i,s}^{b\mathcal{H}}\mathbf{H}_{SAP,I_i,s}^{\mathcal{H}}\right)$, where ι is a constant. Accordingly, for $\epsilon^2\leq\iota$, when $\mathrm{Tr}\left(\mathbf{B}^{a}\right)=\mathrm{Tr}\left(\mathbf{B}^{b}\right)=\zeta$, we have $\mathrm{Tr}\left(\boldsymbol{Q}_{SAP,S_i,s}^{a}\right)>\mathrm{Tr}\left(\boldsymbol{Q}_{SAP,S_i,s}^{b}\right)$,

where

$\mathbf{B}^{a}=\mathbf{H}_{SAP,I_i,s}\mathbf{W}_{SAP,S_i,s}^{a}\boldsymbol{Q}_{SAP,S_i,s}^{a}\mathbf{W}_{SAP,S_i,s}^{a\mathcal{H}}\mathbf{H}_{SAP,I_i,s}^{\mathcal{H}}$,

and

$\mathbf{B}^b = \mathbf{H}_{SAP,I_i,s}\mathbf{W}^b_{SAP,S_i,s}\boldsymbol{Q}^b_{SAP,S_i,s}\mathbf{W}^{b\mathcal{H}}_{SAP,S_i,s}\mathbf{H}^{\mathcal{H}}_{SAP,I_i,s}$.

Therefore, for $\epsilon^2 \leq \iota$, based upon Theorem 1., the capacity of SSSC using $\mathbf{W}^a_{SAP,S_i,s}$ is larger than that of SSSC using $\mathbf{W}^b_{SAP,S_i,s}$. We simulate the SSSC using $\mathbf{W}^a_{SAP,S_i,s}$ and $\mathbf{W}^b_{SAP,S_i,s}$ for different ϵ^2 in Section IV. We find that ι can be much larger than the normally acceptable radius of uncertainty region.

6.4 Simulation

6.4.1 Number of Transmit Antennas on Sub-small Cell Access Points

Since the number of transmit antennas on SAP and that on IAP are in direct relation with the number of concurrent sojourners, we design 8 data sets to observe and analyze the number of concurrent sojourners in 8 representative circumstances.

We consult a medium-sized software enterprise in Paris to help us to design data sets to approximate the actual situation. We receive the following information on visitors in this enterprise:

- There are more than fifty visitors daily at an average.
- In view of long term observation, there is no such a working day when the number of visitors is particularly large or small within five working days.
- After the holidays, the number of visitors is inclined to peak.

First, we exclude those days when the number of visitors is inclined to peak after holidays. Based on the second item above, we consider that the observations of the number of arrivals at the reference time on different working days are independent and identically distributed (i.i.d.). We observe the average value of the cumulative probability of the number of concurrent sojourners during one entire working day based on the first six data sets. Here, we set $Q = 1$. We adopt $E[P(N_U,\, t)]$ which is defined in Equation (6.6) to indicate the average value of the cumulative probability of the number of concurrent sojourners during the observation time interval. We interpret $P(N_U,\, t)$ as the probability of the number of concurrent sojourners being less than N_U at time t.

Then we consider separately those days after holidays. We also consider that the observations of the number of arrivals at the reference time on different working days during those days are i.i.d.. We observe the average value of the cumulative probability of the number of concurrent sojourners during one entire working day based on the last two data sets.

We list the attributes of these 8 test data sets in Table (6.2).

Table 6.2: Attributes of test data sets

Data set index			
Observation time interval (9 am to 5 pm)			
Total number of sojourners during the observation time interval			
Sample mean of the duration of stay of one sojourner (minute)			
Standard deviation of the duration of stay of one sojourner			
Arrival rate (arrivals per time slot)			
Data set 1	Data set 2	Data set 3	Data set 4
-	-	-	-
60	60	60	60
60	60	90	90
3.7947	148.0447	3.7947	148.0447
60/48	60/48	60/48	60/48
Data set 5	Data set 6	Data set 7	Data set 8
-	-	-	-
60	60	90	90
60	60	60	60
3.7947	148.0447	2.7809	134.5144
5(10-11 am), 30/42(else)	5(10-11 am), 30/42(else)	60/48	60/48

The staffs' working hours are from 9 am to 5 pm. The visitors arrive randomly during working hours. The observation time interval is set to be consistent with the working hours for all data sets. We divide the observation time interval into 48 time slots, each 10 minutes in length. Data set 1 and data set 2 have the same attributes except the standard deviation of the duration of stay. These two data sets are considered as the benchmark for comparison and designing the other data sets. Data set 3 and data set 4 are designed by adding 30 minutes to every sample of the duration of stay in data set 1 and set 2. Data set 5 and data set 6 are designed by changing the immutable arrival rate of data set 1 and data set 2 to 5 arrivals per time slot during 10-11 am and 30/42 arrivals per time slot during the other working hours. Date set 7 and set 8 are designed by adding 30 to the total number of sojourners during the observation time interval of data set 1 and data set 2 and make the the standard deviation of the duration of stay of data set 7 and data set 8 to be close to that of data set 1 and data set 2 respectively.

We exploit EMPHT algorithm [139, 140] to fit the phase type distribution to the data of duration of stay in each data set. The EMPHT is an iterative maximum likelihood estimation algorithm which outputs the $m \times 1$ vector $\boldsymbol{\alpha}$ and $m \times m$ matrix $\mathbf{R}$. We chose the number of phases as 4, i.e. $m = 4$. We acquire these two parameters based on each data set after sufficient iterations when the likelihood function reaches zero growth and accordingly obtain the CDF of the duration of stay for each data set.

We further calculate the average value of the cumulative probability of the number of concurrent sojourners during the observation time interval base on each of these 8 data sets and showed them in Figure 6.2. From them, we can observe how the following factors influence the number of concurrent sojourners and further impact the number of transmit antennas on sub-small cell APs:

- the standard deviation of the duration of stay
- the mean of the duration of stay
- the distribution of arrival rate
- the total number of sojourners during the observation time interval

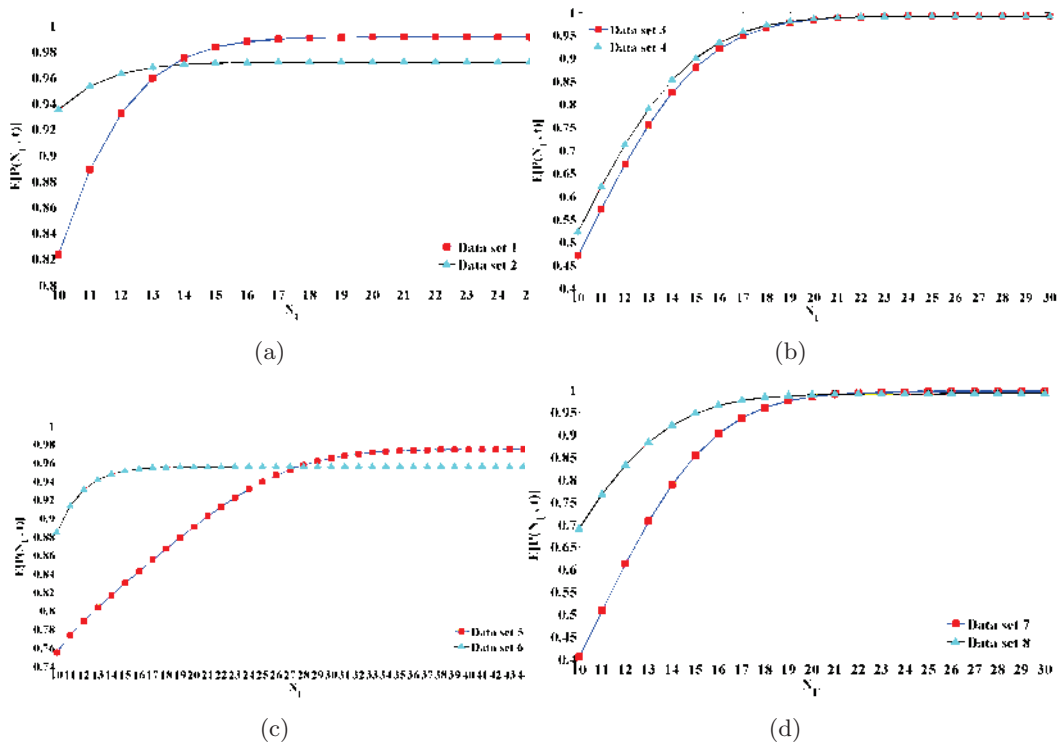

(a) (b)

(c) (d)

Figure 6.2: The average value of the CDF of the number of concurrent sojourners during the observation time interval base on each data set

From Figure 6.2, we observe that as N_U increases, its average value of the cumulative probability of the number of concurrent sojourners during the observation time interval based on 8 data sets all exhibit uptrend and the rate of growth declines gradually. The values of $E\left[P\left(N_U = 10,\ t\right)\right]$ based on data set 1 until data set 8 are: 0.8237, 0.9354, 0.4711,

0.5223, 0.7550, 0.8849, 0.4048 and 0.6905. The values of $E\left[P\left(N_U = 20,\ t\right)\right]$ based on data set 1 until data set 8 are: 0.9911, 0.9719, 0.9841, 0.9857, 0.8908, 0.9554, 0.9852 and 0.9895. The pair of $n = \min_{N_U}\left\{E\left[P\left(N_U + 1,\ t\right)\right] - E\left[P\left(N_U,\ t\right)\right] \leq 0.001\right\}$ and $E\left[P\left(n,\ t\right)\right]$ based on data set 1 until data set 8 are: (19, 0.991), (15, 0.9712), (24, 0.9912), (24, 0.9911), (38, 0.9741), (19, 0.9553), (26, 0.9961) and (22, 0.9912).

We can observe that: for data set 1, 2, 3, 4, 7 and 8, the number of concurrent sojourners during the observation time interval being more than 20 has a very small probability ($<$ 0.03). For data set 5 and 6, that has a small probability (< 0.11). This number being no more than 10 has a large probability (> 0.8) for data set 1 and 2, followed by data set 5 and 6 (> 0.75). For data set 3, 4, 7 and 8, This number being no more than 10 and between 10 and 20 have almost the same probability (≈ 0.4).

Referring to Figure 6.2, we can find that the increasement of the mean of the duration of stay, non-uniform arrival rate or the increase of the total number of sojourners during the observation time interval improves the probability of the number of concurrent sojourners being a relatively large number. The increasement of standard deviation of the duration of stay brings down this probability. However, when the mean of the duration of stay is relatively large, the standard deviation of the duration of stay has minimal impact on this probability as shown in Figure 2 (b). Accordingly, the number of transmit antennas on sub-small cell access points are chosen to be relatively large when the mean of the duration of stay or the total number of sojourners is relatively large, the arrival rate is non-uniform or the standard deviation of the duration of stay is relatively small.

From the third set of experimental result, we can see that the augmentation of standard deviation of the duration of stay causes that the convergence of the average value of the cumulative probability of the number of concurrent sojourners during the observation time interval to be more slowly and the low growth rate emergences earlier. But when the mean of the duration of stay is relatively large, this phenomenon is not obvious. So we need to choose a relatively small value for η in Equation (6.8) or γ in Equation (6.9) when the standard deviation of the duration of stay is relatively large and the mean of the duration of stay is relatively small.

6.4.2 BD precoding based on uncertain CSI in conjunction with auxiliary optimal BF

We consider that 2 sojourners and 2 inhabitants stay in the overlap of ISSC and SSSC, where all the sojourners and inhabitants have the same distance from the SAP. The path loss component is normalized to one. $\mathbf{H}_{SAP,S_i,s}$ and $\mathbf{H}_{SAP,I_i,s}$ are both modeled as a matrix with coefficients which are i.i.d. circularly symmetric, complex Gaussian random variables, with zero mean and unit variance. $\triangle\mathbf{H}_{SAP,I_i,s}$ is modeled as a matrix with coefficients

which are i.i.d. circularly symmetric, complex Gaussian random variables, with zero mean and variance σ^2. We set that ϵ^2 in Equation (6.17) equals to σ^2. The number of receive antennas at every UE is set to be 2 and the maximum Signal-to-Noise Ratio (SNR) at every UE is set to be 20 dB. The maximum downlink transmit power of SAP is 10W. The SAP exploits 4 subcarriers for downlink transmission. Each subcarrier occupies a normalized bandwidth of 1 Hz.

For the purpose of comparing the performance of *BDBF* with the interference controller that uses optimal BF alone, we design two test systems: 1. downlink BD precoding for the secondary sub-small cell takes both sojourners and inhabitants who stay in the coverage area into consideration, i.e. the SSSC using $\mathbf{W}^a_{SAP,S_i,s}$; 2. downlink BD precoding for the secondary sub-small cell takes only sojourners into consideration, i.e. the SSSC using $\mathbf{W}^b_{SAP,S_i,s}$. We simulate the above systems which exploit BD precoding based on SAP-to-inhabitant CSI with different radius of uncertainty region (ϵ^2=0, 0.1, 1, 5 and 10) and fed perfect SAP-to-inhabitant CSI to the optimal BF. We plot the average capacity of SSSC and the average interference to inhabitants on each subcarrier which are obtained by using 2000 Monte-Carlo realizations in Figure 6.3 and Figure 6.4 respectively.

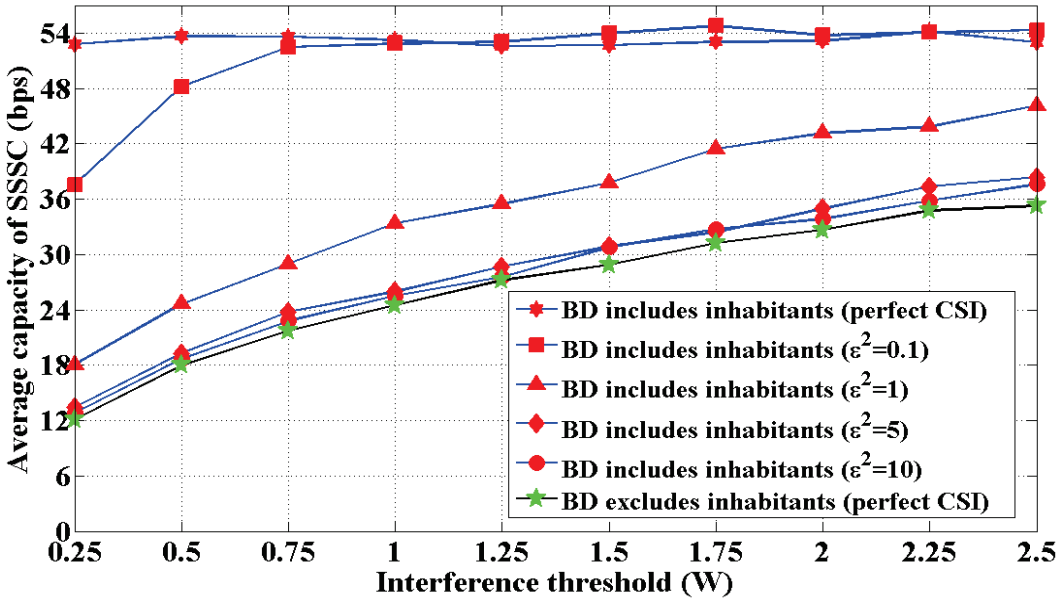

Figure 6.3: Average capacity of SSSC vs. interference threshold

Figure 6.3 reveals the following information. 1. For the system adopts BD precoding including inhabitants, the average capacity of SSSC shakes off the shackles of interference threshold within the small radius of uncertainty region. For $\epsilon^2 = 0.1$, the average capacity of

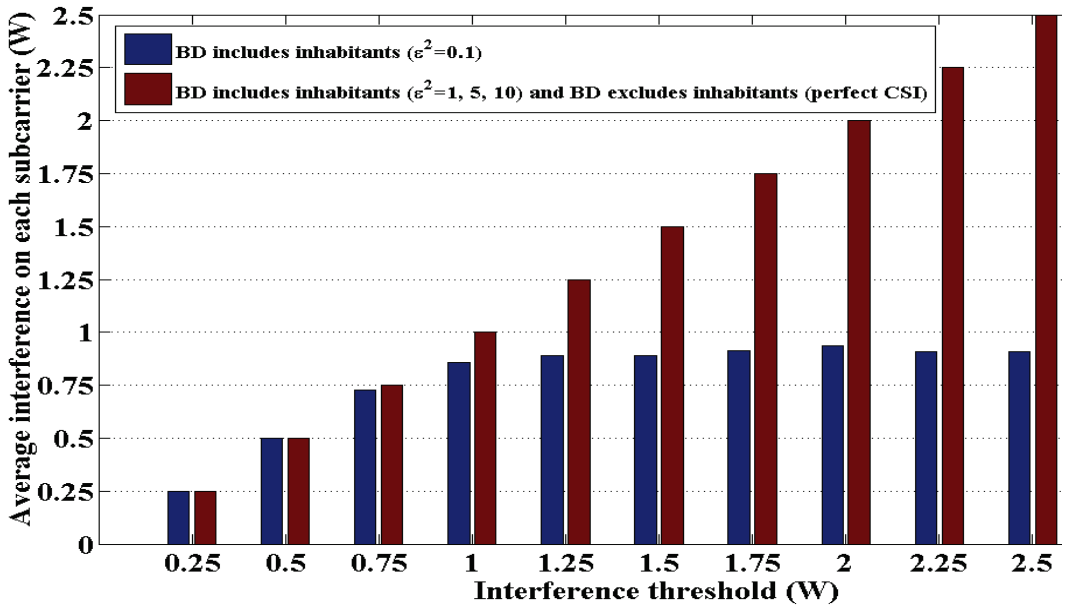

Figure 6.4: Average interference on each subcarrier vs. interference threshold

SSSC achieves 54.7651 bps when the interference threshold is 1.75W. After that it oscillates on small scale and no longer increases with the enhancement of threshold. This is because BD precoding based on uncertain CSI can inhibit the interference below the interference threshold within the small radius of uncertainty region. Figure 6.4 exhibits that the average interference to inhabitants on each subcarrier for $\epsilon^2 = 0.1$ is maintained below the threshold when the threshold is no less than 0.25W. For $\epsilon^2 = 0$, since BD precoding based on perfect CSI, the interference is completely eliminated and accordingly the average capacity of SSSC has no relationship with the interference threshold. It fluctuates slightly with the fluctuation of channel between SAP and sojourners. For $\epsilon^2 = 1,\ 5,$ and 10, the auxiliary optimal BF plays the leading role in inhibiting the interference. The actual interference is always equal to the threshold. The average capacity of SSSC exhibits uptrend as the threshold is enhanced. 2. System adopts BD precoding including inhabitants achieves higher capacity compared with that exploits BD precoding excluding inhabitants within a considerably large radius of uncertainty region. The average capacity of SSSC of the first system declines as the radius of uncertainty region increases. It should be noted that until ϵ^2 increases to 10, the average capacity of SSSC of the first system is still higher than that of the second system with $\epsilon^2 = 0$. This verifies Theorem 2.

Chapter 7

Game-Theoretic Decision Mechanism for HetNets

Contents

This chapter addresses the issue of competition vs. cooperation in the downlink, between base stations (BSs), of a multiple input multiple output (MIMO) interference, heterogeneous wireless network (HetNet). We present a scenario where a macrocell base station (MBS) and a cochannel femtocell base station (FBS) each simultaneously serving their own user equipment (UE), has to choose to act as individual systems or to cooperate in *coordinated multipoint transmission* (CoMP). We employ both the theories of non-cooperative and cooperative games in a unified procedure to analyze the decision making process. The BSs, of the competing uncoordinated system, are assumed to operate at the *maximum expected sum rate* (MESR) *correlated equilibrium* (CE) which we compare against the coalition value to establish the stability of the *core* of the coordinated system. We prove that there exists a threshold geographical separation, d_{th}, between the macrocell user equipment (MUE) and FBS, under which the region of coordination is non-empty. Theoretical results are verified through simulation.

Small cells are an attractive easily deployable solution to the increasing demand for capacity [141]. Underlay small cells improve the capacity of the network through frequency reuse and higher link gains due to shorter distances to the user equipment (UE). On the downside the unplanned deployment of small cells in the larger cell structure creates unforeseen interference conditions for both the macro and small cell networks. Such dynamic interference situations require novel solutions [142].

Coordinated multipoint transmission (CoMP) introduces dynamic interaction between multiple cells to increase network performance and reduce interference. In our research we consider the CoMP scheme of joint transmission (JT) [143]. We begin with the hypotheses that JT must be a rational decision which is profitable for both macro- and femto-systems, since these systems may belong to independent operators/users. In human interactions, cooperation among a group is justifiable if all the members are better off in that group than if they were in any other group structure among themselves. This rational behavior is embedded in the solution concept of *core* in coalition formation games.

Past research of heterogeneous networks (HetNets) of macro- femtocells, has used both non-cooperative and cooperative games. In [144] a Stackelberg game is formulated where pricing is employed to move the equilibria towards a tolerable interference level for the *macrocell base station* (MBS). In [145] a potential game based analysis of *Nash equilibrium* (NE) of power and subcarrier allocation, for a multicell interference environment is presented. In [146] power distribution over resource blocks of cognitive *femtocell base stations* (FBSs) is analyzed for their *correlated equilibrium* (CE). In [147, 148] ϵ-correlated equilibrium solution is presented for underlayed femtocells to minimize interference to the macro-system. CE is the form of equilibrium used in this chapter as well.

In [149,150] coalition formation games with externalities are used to group the femtocells

to mitigate collisions and reduce interference. In [151] a coalition game together with the solution concept of *recursive core* is used to model the cooperative interaction between *macrocell user equipment* (MUE) and *femtocell user equipment* (FUE). They conclude that forming of disjoint coalitions increases the rates of both MUE and FUE. In [152] a coalition formation game is employed to partition a dense network of femtocells to minimize interference where they introduce a polynomial time algorithm for group formation. In [153] both *transferable utility* (TU) and *non-transferable utility* (NTU) coalition formation games are used for cooperation of receivers and transmitters in an interference environment.

Our work is set apart from the above related research, since we bring together both the theories of non-cooperative and coalition formation games to model the femto-maro interaction in JT. To the best of our knowledge this is the first such attempt in this domain. We use the terms non-cooperative and cooperative according to their use in the game theory literature whereas the terms coordination, CoMP, and JT are used synonymously.

7.1 System Model

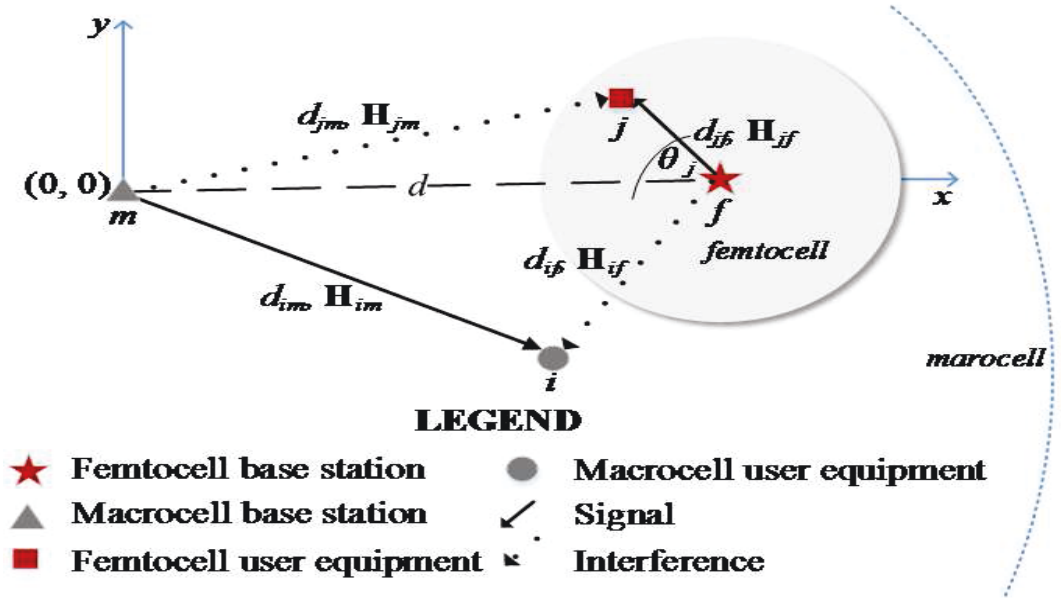

Figure 7.1: System model.
The attributes on arrows indicate the distance between elements and their respective channel matrices.

We consider the downlink transmission of a HetNet which consists of a single MBS m and a single FBS f, separated by a distance $d > 0$. Each *base station* (BS) has an

active *user equipment* (UE). It is possible that the BSs serve more than one user but the assumption is that at any given instant each BS transmits to only one selected user. The two BSs each possesses T number of transmit antennas while each UE possesses R number of receive antennas. Fig. 7.1 depicts the system model. The origin of the plane is at MBS. We define two modes of operation in the two tier HetNet, namely uncoordinated and coordinated. In uncoordinated mode of operation the two BSs act as separate transmitters where MBS serves MUE while FBS serves FUE. On the contrary if the two cells conform to the coordinated mode, then the two BSs cooperate through CoMP.

We adopt a channel model with provision for signal attenuation by distance [154]. The complex channel gain matrix is multiplied by a magnitude which is a path loss function of distance between the BS and the UE. We assume that the distances of separation between antennas are smaller compared to the separation between BSs and UE, hence consider a single distance parameter for a transmitter-receiver pair. The received baseband equivalent signal y_i at MUE i and the received signal y_j at FUE j for uncoordinated transmission are

$$\mathbf{y}_i \triangleq d_{im}^{-\alpha}\mathbf{H}_{im}\mathbf{V}_m\mathbf{s}_i + d_{if}^{-\alpha}\mathbf{H}_{if}\mathbf{V}_f\mathbf{s}_j + \mathbf{n}_i, \tag{7.1}$$

$$\mathbf{y}_j \triangleq d_{jf}^{-\alpha}\mathbf{H}_{jf}\mathbf{V}_f\mathbf{s}_j + d_{jm}^{-\alpha}\mathbf{H}_{jm}\mathbf{V}_m\mathbf{s}_i + \mathbf{n}_j, \tag{7.2}$$

where d_{im}, d_{if}, d_{jf}, $d_{jm} \geq 0$ are the absolute distances between the respective indexed elements, $\mathbf{H}_{im}$ is the $R \times T$ complex valued channel gain matrix from MBS m to MUE i and $\mathbf{H}_{if}$, $\mathbf{H}_{jf}$, $\mathbf{H}_{jm}$ are interpreted analogously. The matrix $\mathbf{V}_m$ (resp. $\mathbf{V}_f$) is the precoder at MBS (resp. FBS). The transmit symbol vector of unit power at MBS m (resp. at FBS m) to MUE i (resp. to FUE j) is denoted by $\mathbf{s}_i$ (resp. $\mathbf{s}_j$). The exponent $(-\alpha)$, where α is a positive real valued scalar, accounts for path loss, and $\mathbf{n}_i$, $\mathbf{n}_j$ are circular symmetric, uncorrelated additive withe Gaussian noise vectors (AWGN).

The channel capacity, R_{uc}^m, of the macro system in uncoordinated transmission is given by (7.3).

$$R_{\text{uc}}^m \triangleq \log\det\left(\mathbf{I}_R + \frac{d_{im}^{-2\alpha}\mathbf{H}_{im}\mathbf{V}_m\mathbf{V}_m^H\mathbf{H}_{im}^H}{d_{if}^{-2\alpha}\mathbf{H}_{if}\mathbf{V}_f\mathbf{V}_f^H\mathbf{H}_{if}^H + \sigma^2\mathbf{I}_R}\right), \tag{7.3}$$

$$R_{\text{uc}}^f \triangleq \log\det\left(\mathbf{I}_R + \frac{d_{jf}^{-2\alpha}\mathbf{H}_{jf}\mathbf{V}_f\mathbf{V}_f^H\mathbf{H}_{jf}^H}{d_{jm}^{-2\alpha}\mathbf{H}_{jm}\mathbf{V}_m\mathbf{V}_m^H\mathbf{H}_{jm}^H + \sigma^2\mathbf{I}_R}\right). \tag{7.4}$$

Above σ^2 is the variance of the circular symmetric noise and $\mathbf{I}_R$ is the $R \times R$ identity matrix [155]. For a matrix $\mathbf{X}$ in the complex field, $\mathbf{X}^H$ denotes the conjugate (Hermitian) transpose. Analogously we define the capacity, R_{uc}^f, of the femto-system (7.4).

Now suppose that the two BSs coordinate through JT. The coordination is such that, FBS must transmit to both UE their respective symbols. It is possible to extend this model

to include the case where both BSs transmit to both UE. However, we only consider MUE receiving JT since a fat chance MBS serves FU for the following reasons. i)FUE are mostly home/office users who are less mobile and they have higher downlink gains; ii)FU normally possess lower priority compare to MU. On the other hand, MUE may be highly mobile and operate under high signal fading and interference. The received signals at MUE and FUE in coordinated transmission are then given by (7.5) and (7.6) respectively.

$$y_i \triangleq d_{im}^{-\alpha}\mathbf{H}_{im}\mathbf{V}_m\mathbf{s}_{im} + d_{if}^{-\alpha}\mathbf{H}_{if}\mathbf{V}_{if}\mathbf{s}_{if} + \mathbf{n}_i, \tag{7.5}$$

$$y_j \triangleq d_{jf}^{-\alpha}\mathbf{H}_{jf}\mathbf{V}_{jf}\mathbf{s}_j + d_{jm}^{-\alpha}\mathbf{H}_{jm}\mathbf{V}_m\mathbf{s}_i + \mathbf{n}_j. \tag{7.6}$$

$$R_{\mathrm{c}}^{f} \triangleq \log\det\left(\mathbf{I}_R + \frac{d_{jf}^{-2\alpha}\mathbf{H}_{jf}\mathbf{V}_{jf}\mathbf{V}_{jf}^H\mathbf{H}_{jf}^H}{d_{jm}^{-2\alpha}\mathbf{H}_{jm}\mathbf{v}_m\mathbf{v}_m^H\mathbf{H}_{jm}^H + \sigma^2\mathbf{I}_R}\right). \tag{7.7}$$

$$R_{\mathrm{c}}^{m} \triangleq \log\det\left(\mathbf{I}_R + \frac{d_{im}^{-2\alpha}}{\sigma^2}\mathbf{H}_{im}\mathbf{V}_m\mathbf{V}_m^H\mathbf{H}_{im}^H + \frac{d_{if}^{-2\alpha}}{\sigma^2}\mathbf{H}_{if}\mathbf{V}_{if}\mathbf{V}_{if}^H\mathbf{H}_{if}^H\right), \tag{7.8}$$

Above $\mathbf{V}_{if}$ (resp. $\mathbf{V}_{jf}$) is the precoder matrix at FBS for MUE (resp. FUE), $\mathbf{V}_m$ is the MBS precoder. The above signal model assumes that the precoders $\mathbf{V}_{if}$ and $\mathbf{V}_{jf}$ are such that there is no interuser interference from FBS to the two UE. To that end methods such as block diagonalization or frequency domain techniques can be employed at FBS. Then the channel capacity of FUE and MUE for the coordinated transmission scheme is given by (7.7) and (7.8) respectively. In what follows we consider the precoders to be defined in a finite set. The finite model not only affords us a finite action space game, but also reflects the digital systems in practical implementations which can only provide finite discrete levels.

7.2 Core Solution

Now we construct two non-cooperative games one for the uncoordinated system, $\mathtt{G}_1$ and one for the coordinated system, $\mathtt{G}_2$. We establish the relation between $\mathtt{G}_1$ and $\mathtt{G}_2$ in the ensuing development. Both games have identical set of players $\mathcal{N} \triangleq \{\text{MBS, FBS}\}$, i.e., the two BSs. The action spaces of the players are their discrete precoders. In the uncoordinated case, the sets of precoders of MBS and FBS are denoted by $\mathcal{A}_{\mathrm{muc}}$ and $\mathcal{A}_{fuc}$. In the coordinated case, the sets of precoders of MBS and FBS are denoted by $\mathcal{A}_{mc}$ and $\mathcal{A}_{f\mathrm{c}}$. For the uncoordinated case, we define the product sets of the action spaces as $\mathcal{A}_{\mathrm{uc}} \triangleq \mathcal{A}_{m\mathrm{uc}} \times \mathcal{A}_{f\mathrm{uc}}$. For the coordinated case, we define the product sets of the action spaces as $\mathcal{A}_{\mathrm{c}} \triangleq \mathcal{A}_{mc} \times \mathcal{A}_{f\mathrm{c}}$. The utility functions of the two players in the uncoordinated case are R_{uc}^{m} and R_{uc}^{f}. The utility

functions of the two players in the coordinated case are R_{c}^{m} and R_{c}^{f}. The joint action of $\mathtt{G}_1$ is $\mathbf{V} \triangleq (\mathbf{V}_m, \mathbf{V}_f) \in \mathcal{A}_{\mathrm{uc}}$ where $\mathbf{V}_m \in \mathcal{A}_{m\mathrm{uc}}$ and $\mathbf{V}_f \in \mathcal{A}_{f\mathrm{uc}}$. The joint action of $\mathtt{G}_2$ is $\mathbf{V} \in \mathcal{A}_{\mathrm{c}}$ such that $\mathbf{V} \triangleq (\mathbf{V}_m, \mathbf{V}_f)$ where $\mathbf{V}_m \in \mathcal{A}_{m\mathrm{c}}$ and $\mathbf{V}_f \in \mathcal{A}_{f\mathrm{c}}$. Note that FBS's action $\mathbf{V}_f \in \mathcal{A}_{f\mathrm{c}}$, consists of two precoders $\mathbf{V}_f \triangleq (\mathbf{V}_{if}, \mathbf{V}_{jf})$. The MBS (resp. FBS) has identical maximum transmit power in both uncoordinated and coordinated cases, i.e.,

$$\max_{\mathbf{V}\in\mathcal{A}_{f\mathrm{uc}}} \left\{\mathbf{V}^H\mathbf{V}\right\} = \max_{\mathbf{V}_f\in\mathcal{A}_{f\mathrm{c}}} \left\{\mathrm{Trace}\left(\mathbf{V}_{if}\mathbf{V}_{if}^H\right) + \mathrm{Trace}\left(\mathbf{V}_{jf}\mathbf{V}_{jf}^H\right)\right\}$$
$$\max_{\mathbf{V}\in\mathcal{A}_{m\mathrm{uc}}} \left\{\mathbf{V}^H\mathbf{V}\right\} = \max_{\mathbf{V}\in\mathcal{A}_{m\mathrm{c}}} \left\{\mathrm{Trace}\left(\mathbf{V}\mathbf{V}^H\right)\right\}.$$

Now we posses all the ingredients necessary to define the non-cooperative games, $\mathtt{G}_1$ and $\mathtt{G}_2$. The uncoordinated game is give by the tuple $\mathtt{G}_1 \triangleq \left\langle \mathcal{N}, \mathcal{A}_{\mathrm{uc}}, \left\{R_{\mathrm{uc}}^{m}, R_{\mathrm{uc}}^{f}\right\}\right\rangle$. The game when the two systems are in coordination is $\mathtt{G}_2 \triangleq \left\langle \mathcal{N}, \mathcal{A}_{\mathrm{c}}, \left\{R_{\mathrm{c}}^{m}, R_{\mathrm{c}}^{f}\right\}\right\rangle$.

Let us set aside the above defined two games for a moment, we come back to them shortly. To analyze the coordinated system we must utilize coalitional games from the cooperative game theory. The most widely used solution concept in coalitional games is the *core.* In order for the two BSs to coordinate the core of the coalition game must be nonempty. A nonempty core implies that the grand coalition, which includes all the players, has a value which is divisible among the players so that no other partition of subsets of players can give a better value to any of the players. The analysis of the core requires that the cooperative game has TU which means that the sum utility of the coalition (the two cells in this case) is able to be shared between the members [156]. But we observe from the system model that the sum rate of the coordinated system is not arbitrarily transferable between the two players. Therefore we follow a usual trick employed in such situations, introduce a monitory transfer i.e., payment, between the macro and femto systems. It is imperative to understand that such a monitory transfer is not merely a tool to make the problem amenable to core analysis, but also has an important engineering aspect: coordination between the systems require sharing power with external users and communication of symbol information and channel state information (CSI) between the BSs. Such transactions have to be compensated in any practical system in order to provide an incentive to take part in CoMP. After introducing the payment c, the utility of MBS, U_{c}^{m}, and FBS, U_{c}^{f}, is given by (7.9). The payment is of units of rate, which can be interpreted in monitory terms as applicable.

$$U_{\mathrm{c}}^{m} \triangleq R_{\mathrm{c}}^{m} - c,\; U_{\mathrm{c}}^{f} \triangleq R_{\mathrm{c}}^{f} + c. \tag{7.9}$$

A coalitional game in characteristic form requires a set of players and a value function [157]. In our model the set of players is $\mathcal{N}$, which has three nonempty subsets.

To define the value function we revisit the games $\mathtt{G}_1$ and $\mathtt{G}_2$. There are multiple definitions of equilibria for non-cooperative games. In this research we are interested in CE which is a generalization of NE [157].

Correlated equilibria of the game $\mathtt{G}_1$ is a probability distribution $\tilde{p}_{\text{uc}}(\cdot)$ on the joint action space $\mathcal{A}_{\text{uc}}$ such that $\forall\ \mathbf{V} \in \mathcal{A}_{\text{uc}}$, $\forall\ \mathbf{V}'_m \in \mathcal{A}_{m\text{uc}}$, and $\forall\ \mathbf{V}'_f \in \mathcal{A}_{f\text{uc}}$

$$\sum_{\mathbf{V}:\mathbf{V}_f \in \mathcal{A}_{f\text{uc}}} \tilde{p}_{\text{uc}}(\mathbf{V})\, R^m_{\text{uc}}(\mathbf{V}) \geq \sum_{\mathbf{V}:\mathbf{V}_f \in \mathcal{A}_{f\text{uc}}} \tilde{p}_{\text{uc}}(\mathbf{V})\, R^m_{\text{uc}}\left(\mathbf{V}'_m, \mathbf{V}_f\right), \tag{7.10}$$

$$\sum_{\mathbf{V}:\mathbf{V}_m \in \mathcal{A}_{m\text{uc}}} \tilde{p}_{\text{uc}}(\mathbf{V})\, R^f_{\text{uc}}(\mathbf{V}) \geq \sum_{\mathbf{V}:\mathbf{V}_m \in \mathcal{A}_{m\text{uc}}} \tilde{p}_{\text{uc}}(\mathbf{V})\, R^f_{\text{uc}}\left(\mathbf{V}'_f, \mathbf{V}_m\right). \tag{7.11}$$

Similarly we define the CE of the game $\mathtt{G}_2$, the probability distribution $\tilde{p}_{\text{c}}(\cdot)$ on the action space $\mathcal{A}_{\text{c}}$, which satisfies $\forall\ \mathbf{V} \in \mathcal{A}_{\text{c}}$, $\forall\, \mathbf{V}'_m \in \mathcal{A}_{m\text{c}}$, and $\forall\, \mathbf{V}'_f \in \mathcal{A}_{f\text{c}}$

$$\sum_{\mathbf{V}:\mathbf{V}_f \in \mathcal{A}_{f\text{c}}} \tilde{p}_{\text{c}}(\mathbf{V})\, R^m_{\text{c}}(\mathbf{V}) \geq \sum_{\mathbf{V}:\mathbf{V}_f \in \mathcal{A}_{f\text{c}}} \tilde{p}_{\text{c}}(\mathbf{V})\, R^m_{\text{c}}\left(\mathbf{V}'_m, \mathbf{V}_f\right), \tag{7.12}$$

$$\sum_{\mathbf{V}:\mathbf{V}_m \in \mathcal{A}_{m\text{c}}} \tilde{p}_{\text{c}}(\mathbf{V})\, R^f_{\text{c}}(\mathbf{V}) \geq \sum_{\mathbf{V}:\mathbf{V}_m \in \mathcal{A}_{m\text{c}}} \tilde{p}_{\text{c}}(\mathbf{V})\, R^f_{\text{c}}\left(\mathbf{V}'_f, \mathbf{V}_m\right). \tag{7.13}$$

While a finite game is guaranteed to have at least one CE [157], in most cases we find that there are an infinite set of CE. Out of this set of CE we choose the equilibrium which maximizes the expected sum rate. The *maximum expected sum rate correlated equilibrium* (MESR-CE) of game $\mathtt{G}_1$ is the probability distribution obtained through solving the following linear system;

$$\begin{aligned}
&\underset{\mathbf{p}_{\text{uc}}}{\text{maximize}} \sum_{\mathbf{V}\in\mathcal{A}_{\text{uc}}} p_{\text{uc}}(\mathbf{V}) \left(R^m_{\text{uc}}(\mathbf{V}) + R^f_{\text{uc}}(\mathbf{V})\right) \\
&\text{subject to}\,(7.10)\,,\,(7.11) \\
&\qquad \sum_{\mathbf{V}\in\mathcal{A}_{\text{uc}}} p_{\text{uc}}(\mathbf{V}) = 1 \\
&\qquad p_{\text{uc}}(\mathbf{V}) \geq 0,\ \forall\, \mathbf{V} \in \mathcal{A}_{\text{uc}},
\end{aligned} \tag{7.14}$$

where $p_{\text{uc}}(\mathbf{V})$ is the probability of joint action $\mathbf{V} \in \mathcal{A}_{\text{uc}}$ and $\mathbf{p}_{\text{uc}} \triangleq \left(p_{\text{uc}}(\mathbf{V})\right)_{\mathbf{v}\in\mathcal{A}_{\text{uc}}}$. The expected rate of each player at CE of $\mathtt{G}_1$ is

$$R^m_{\text{uc,cor}} \triangleq \sum_{\mathbf{v}\in\mathcal{A}_{\text{uc}}} \tilde{p}_{\text{uc}}(\mathbf{V})\, R^m_{\text{uc}}(\mathbf{V}), \tag{7.15}$$

$$R^f_{\text{uc,cor}} \triangleq \sum_{\mathbf{v}\in\mathcal{A}_{\text{uc}}} \tilde{p}_{\text{uc}}(\mathbf{V})\, R^f_{\text{uc}}(\mathbf{V}), \tag{7.16}$$

where $\tilde{p}_{\text{uc}}(\cdot)$ is the MESR-CE solution of the linear program (7.14).

Analogously we obtain the MESR-CE of game $\mathtt{G}_2$ as the solution to the following linear system;

$$\begin{aligned} R_{\text{c, cor}} \triangleq \underset{\mathbf{p}_{\text{c}}}{\text{maximize}} & \sum_{\mathbf{V}\in\mathcal{A}_{\text{c}}} p_{\text{c}}(\mathbf{V}) \left(R_{\text{c}}^{m}(\mathbf{V}) + R_{\text{c}}^{f}(\mathbf{V}) \right) \\ \text{subject to} & \,(7.12)\,,\,(7.13) \\ & \sum_{\mathbf{V}\in\mathcal{A}_{\text{c}}} p_{\text{c}}(\mathbf{V}) = 1 \\ & p_{\text{c}}(\mathbf{V}) \geq 0,\, \forall\, \mathbf{V} \in \mathcal{A}_{\text{c}}. \end{aligned} \tag{7.17}$$

where $\mathbf{p}_{\text{c}} \triangleq (p_{\text{c}}(\mathbf{V}))_{\mathbf{V}\in\mathcal{A}_{\text{c}}}$. Let $\tilde{p}_{\text{c}}(\cdot)$ be the MESR-CE distribution of game $\mathtt{G}_2$. The expected rate of each player at CE of $\mathtt{G}_2$ is

$$R_{\text{c,cor}}^{m} \triangleq \sum_{\mathbf{V}\in\mathcal{A}_{\text{c}}} \tilde{p}_{\text{c}}(\mathbf{V})\, R_{\text{c}}^{m}(\mathbf{V})\,, \tag{7.18}$$

$$R_{\text{c,cor}}^{f} \triangleq \sum_{\mathbf{V}\in\mathcal{A}_{\text{c}}} \tilde{p}_{\text{c}}(\mathbf{V})\, R_{\text{c}}^{f}(\mathbf{V})\,. \tag{7.19}$$

Now we define the value function $v(\cdot)$ of the coalition game as follows;

$$v(\mathcal{S}) \triangleq \begin{cases} R_{\text{uc,cor}}^{m} & \mathcal{S} = \{\text{MBS}\}\,, \\ R_{\text{uc, cor}}^{f} & \mathcal{S} = \{\text{FBS}\}\,, \\ R_{\text{c, cor}} & \mathcal{S} = \mathcal{N}. \end{cases} \tag{7.20}$$

Here we recap the development so far of this section: in the above definition of the value function $v(\mathcal{S})$, $R_{\text{uc,cor}}^{m}$ in (7.15) (resp. $R_{\text{uc, cor}}^{f}$ in (7.16)) is the expected rate obtained by the macro system (resp. femto system) while playing the MESR-CE in $\mathtt{G}_1$. On the other hand the value of the grand coalition, $R_{\text{c, cor}}$ in (7.17), is the MESR of the two BSs while playing the MESR-CE in $\mathtt{G}_2$. Then the coalitional game in characteristic form is defined by the tuple $\mathtt{G}_3 \triangleq \langle \mathcal{N}, v(\cdot) \rangle$.

Definition 2. The core is the set of allocations such that no subgroup within the coalition can do better by leaving [157].

In our game the set of allocations are U_{c}^{m} and U_{c}^{f} in (7.9), such that $U_{\text{c}}^{m} + U_{\text{c}}^{f} = R_{\text{c, cor}}$.

Region of Coordination As MUE moves closer to FBS, signal level drops and interference level rises, hence one expects cooperation with FBS to be preferable to MBS. Since the sum rate can be apportioned between the two systems through the monitory transfer,

one expects to find a c, at which the core is non empty. The region where the core is non empty is called, the *region of coordination* or identically *CoMP region.* In a single input single output (SISO) system a signal to interference plus noise ratio (SINR) based argument easily demonstrates the existence of a core but the argument for MIMO requires a bit more analysis.

Proposition 1. $v(\mathcal{N}) \geq v(\text{MBS}) + v(\text{FBS})$ if and only if there exists a payment c such that $U_c^m \geq R_{uc,cor}^m$ and $U_c^f \geq R_{uc,cor}^f$.

Proof: We provide a constructive proof. By (7.9) and while $\mathtt{G}_2$ system is in CE the utilities are $U_{\text{c}}^m = R_{\text{c,cor}}^m - c$ and $U_{\text{c}}^f = R_{\text{c,cor}}^m + c$. Let us consider the LHS of *iff*, which is equivalent to $R_{\text{c, cor}} \geq R_{\text{uc,cor}}^m + R_{\text{uc,cor}}^f$, which implies either $R_{\text{c,cor}}^m \geq R_{\text{uc,cor}}^m$ or $R_{\text{c,cor}}^f \geq R_{\text{uc,cor}}^f$ or both. Let us take the case where $R_{\text{c,cor}}^m \geq R_{\text{uc,cor}}^m$ and $R_{\text{c,cor}}^f \leq R_{\text{uc,cor}}^f$, all other cases can be similarly proven. Then there always exists a positive constant c such that $\left(R_{\text{c,cor}}^m - c\right) = U_{\text{c}}^m \geq R_{\text{uc,cor}}^m$ and $\left(R_{\text{c,cor}}^f + c\right) = U_{\text{c}}^f \geq R_{\text{uc,cor}}^f$ since $\left(R_{\text{c,cor}}^m - c\right) + \left(R_{\text{c,cor}}^f + c\right) \geq R_{\text{uc,cor}}^m + R_{\text{uc,cor}}^f$. The converse (RHS $\Longrightarrow$ LHS) is proven simply by summing the two inequalities $U_c^m \geq R_{uc,cor}^m$ *and* $U_c^f \geq R_{c,cor}^f$. This completes the proof.

Proposition 1. claims that $R_{\text{c, cor}} \geq R_{\text{uc,cor}}^m + R_{\text{uc,cor}}^m$ is a necessary and sufficient condition for the core to be nonempty.

In order to establish the final result we need the following propositions.

Proposition 2. R_{uc}^m is non-increasing in d_{im} and monotonically increasing in d_{if}.

Proof: The proof depends on Loewner ordering of positive semidefinite (PSD) matrices ([158] 7.7.1). For two PSD matrices $\mathbf{A}$, $\mathbf{B}$, we write $\mathbf{A} \succeq \mathbf{B}$ (resp. $\mathbf{A} \succ \mathbf{B}$) if $\mathbf{A} - \mathbf{B}$ is PSD (resp. $\mathbf{A} \succ \mathbf{B}$ positive definite (PD)). Let $\mathbf{A} \triangleq \mathbf{H}_{im}\mathbf{V}_m\mathbf{V}_m^H\mathbf{H}_{im}^H$, $\mathbf{B} \triangleq \mathbf{H}_{if}\mathbf{V}_f\mathbf{V}_f^H\mathbf{H}_{if}^H$ and $\mathbf{C} \triangleq \sigma^2\mathbf{I}_R$. $\mathbf{A}$, $\mathbf{B}$ are PSD and $\mathbf{C}$ is PD, also $d_{if}^{-2\alpha}\mathbf{B} + \mathbf{C}$ is PD. Then the capacity of maro-system (7.3) can be reformulated as

$$R_{\text{uc}}^m = \log\det\left(\mathbf{I}_R + d_{im}^{-2\alpha}\left(d_{if}^{-2\alpha}\mathbf{B} + \mathbf{C}\right)^{\frac{-1}{2}}\mathbf{A}\left(d_{if}^{-2\alpha}\mathbf{B} + \mathbf{C}\right)^{\frac{-1}{2}}\right).$$

Let $0 < d_{im} < d'_{im}$, so (7.21) holds, with strict inequality if $\mathbf{A}$ is invertible (according to the properties of PD matrix). Therefore the determinant of (7.23) is no less than (7.22) ([158] 7.7.4), which implies that the determinant is non-increasing in d_{im}.

$$\mathbf{0} \prec \mathbf{I}_R + d_{im}'^{-2\alpha}\left(d_{if}^{-2\alpha}\mathbf{B} + \mathbf{C}\right)^{\frac{-1}{2}}\mathbf{A}\left(d_{if}^{-2\alpha}\mathbf{B} + \mathbf{C}\right)^{\frac{-1}{2}} \preceq \mathbf{I}_R + d_{im}^{-2\alpha}\left(d_{if}^{-2\alpha}\mathbf{B} + \mathbf{C}\right)^{\frac{-1}{2}}\mathbf{A}\left(d_{if}^{-2\alpha}\mathbf{B} + \mathbf{C}\right)^{\frac{-1}{2}}, \tag{7.21}$$

$$\mathbf{I}_R + d_{im}'^{-2\alpha}\left(d_{if}^{-2\alpha}\mathbf{B} + \mathbf{C}\right)^{\frac{-1}{2}}\mathbf{A}\left(d_{if}^{-2\alpha}\mathbf{B} + \mathbf{C}\right)^{\frac{-1}{2}} \tag{7.22}$$

$$\mathbf{I}_R + d_{im}^{-2\alpha}\left(d_{if}^{-2\alpha}\mathbf{B} + \mathbf{C}\right)^{\frac{-1}{2}}\mathbf{A}\left(d_{if}^{-2\alpha}\mathbf{B} + \mathbf{C}\right)^{\frac{-1}{2}} \tag{7.23}$$

Next we reformulate (7.3),

$$R_{\text{uc}}^{m} = \log\det\left(\mathbf{I}_R + d_{im}^{-2\alpha}\mathbf{A}^{\frac{1}{2}}\left(d_{if}^{-2\alpha}\mathbf{B}+\mathbf{C}\right)^{-1}\mathbf{A}^{\frac{1}{2}}\right),$$

and let $0 < d_{if} < d'_{if}$. Then (7.24) holds and by a similar argument to above we have that the determinant is increasing in d_{if}. This completes the proof.

$$0 \prec d_{im}^{-2\alpha}\mathbf{A}^{\frac{1}{2}}\left(d_{if}^{-2\alpha}\mathbf{B}+\mathbf{C}\right)^{-1}\mathbf{A}^{\frac{1}{2}} \prec d_{im}^{-2\alpha}\mathbf{A}^{\frac{1}{2}}\left(d_{if}'^{-2\alpha}\mathbf{B}+\mathbf{C}\right)^{-1}\mathbf{A}^{\frac{1}{2}}. \tag{7.24}$$

Now we consider the properties of R_c^m.

Proposition 3. $R_c^m(\cdot)$ is monotonically increasing in $d_{if}^{-2\alpha}$ and $d_{im}^{-2\alpha}$ and is bounded from below by

$$\gamma^m\left(d_{if}, \mathbf{V}_{if}\right) \triangleq \log\det\left(\mathbf{I}_R + \frac{1}{\sigma^2}d_{if}^{-\alpha}\mathbf{H}_{if}\mathbf{V}_{if}\mathbf{V}_{if}^H\mathbf{H}_{if}^H\right).$$

Proof: The proof utilizes Weyl's inequality for Hermitian matrices [160]. Let us first consider $d_{if}^{-2\alpha}$. Suppose $\mathbf{X}$, $\mathbf{Y}$ are positive semidefinite (PSD) note that the inequality reduces to

$\lambda_i(\mathbf{X}) + \lambda_n(\mathbf{Y}) \leq \lambda_i(\mathbf{X}+\mathbf{Y}) \leq \lambda_i(\mathbf{X}) + \lambda_1(\mathbf{Y}),\ i = 1, \ldots, n,$

where $\lambda_i(\mathbf{X})$ is the i^{th} largest eigenvalue of $\mathbf{X}$, i.e., largest eigenvalue is $\lambda_1(\mathbf{X})$ and smallest is $\lambda_n(\mathbf{X})$. If $\mathbf{X}$, $\mathbf{Y}$ are positive semidefinite (PSD) note that the inequality reduces to

$0 \leq \lambda_i(\mathbf{X}) \leq \lambda_i(\mathbf{X}+\mathbf{Y}) \leq \lambda_i(\mathbf{X}) + \lambda_1(\mathbf{Y}),\ i = 1, \ldots, n.$

Let $\mathbf{X} = \mathbf{I}_R + \frac{d_{im}^{-2\alpha}}{\sigma^2}\mathbf{H}_{im}\mathbf{V}_m\mathbf{V}_m^H\mathbf{H}_{im}^H + \frac{d_{if}^{-2\alpha}}{\sigma^2}\mathbf{H}_{if}\mathbf{V}_{if}\mathbf{V}_{if}^H\mathbf{H}_{if}^H$ and $\mathbf{Y} = \frac{\delta}{\sigma^2}\mathbf{H}_{if}\mathbf{V}_{if}\mathbf{V}_{if}^H\mathbf{H}_{if}^H$ where $\delta \in \mathbb{R}_+$. Then monotonicity in $d_{if}^{-2\alpha}$ follows from

$$0 < \det(\mathbf{X}) = \prod_i \lambda_i(\mathbf{X}) \leq \det(\mathbf{X}+\mathbf{Y}) = \prod_i \lambda_i(\mathbf{X}+\mathbf{Y}).$$

Similarly the proof extends to $d_{im}^{-2\alpha}$. Then setting $d_{im}^{-2\alpha} = 0$ the lower bound is achieved.

Theorem 1. *For some $d > 0$, $\exists$ d_{th} such that for $d_{if} \leq d_{\text{th}}$, the region of cooperation is nonempty. Proof:* Let $\mathbf{V} = (\mathbf{V}_{if}, \mathbf{V}_{jf}) \in \mathcal{A}_{\text{c}}$, $\mathbf{V}' \in \mathcal{A}_{\text{uc}}$ be any two actions from the respective spaces and let the location of the FUE be fixed relative to the FBS at $\left(\bar{d}_{jf}, \bar{\theta}_j\right)$. Then $R_{\text{c}}^f(\mathbf{V})$ and $R_{\text{uc}}^f(\mathbf{V}')$ are constants irrespective of location of MUE. Now consider that MUE moves along a trajectory with decreasing d_{if} and increasing d_{jm}. By Proposition 2, $R_{\text{uc}}^m(\mathbf{V}')$ is decreasing. As $d_{if} \to 0$, by Proposition 3, $R^m(d_{if}, \cdot) \to \infty$. Therefore there must exist $d_{if} \leq d_{\text{th}}$, such that $R_{\text{c}}^m(d_{if}, \cdot) + R_{\text{c}}^f(\mathbf{V}) \geq R_{\text{uc}}^m(\mathbf{V}') + R_{uc}^f(\mathbf{V}')$. Since the action choice was arbitrary $\exists d_{th}$ such that, $\min_{\mathbf{v}\in\mathcal{A}_{\text{uc}}}(R_{\text{c}}^m(\mathbf{V}) + R_{\text{c}}^f(\mathbf{V})) \geq \max_{\mathbf{v}\in\mathcal{A}_{\text{uc}}}(R_{uc}^m(\mathbf{V}) + R_{uc}^f(\mathbf{V}))$.

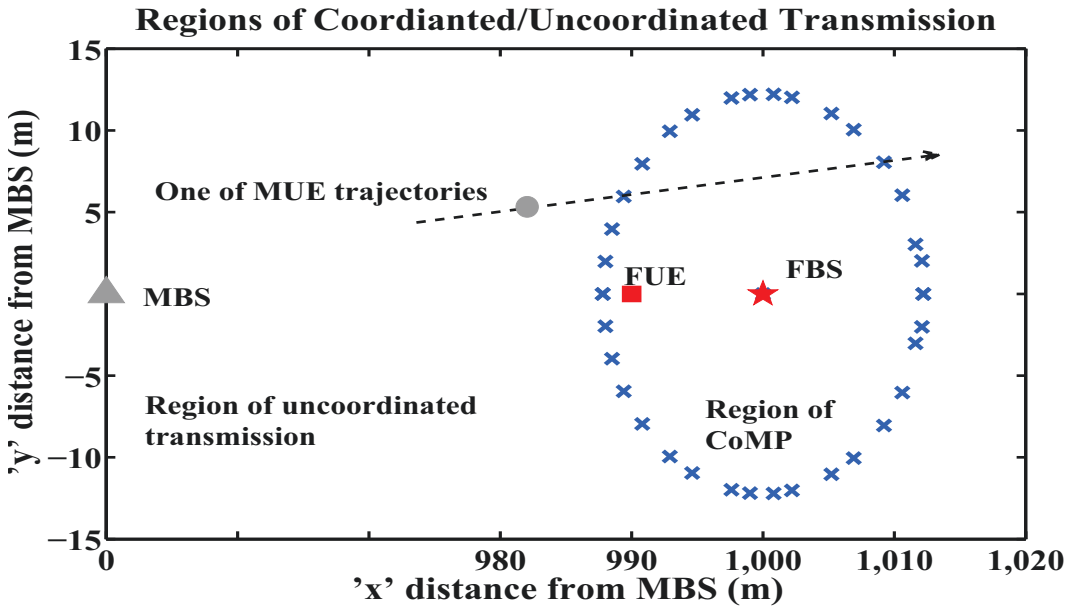

Figure 7.2: Region of coordination.

Therefore $\forall$ probability distributions $\tilde{p}_{\text{uc}}$ and $\tilde{p}_{\text{c}}$ we have $\sum_{\mathbf{v}\in\mathcal{A}_{\text{c}}} \tilde{p}_{\text{c}}(\mathbf{V}) \left(R_{\text{c}}^{m}(\mathbf{V}) + R_{\text{c}}^{f}(\mathbf{V})\right) \geq \sum_{\mathbf{v}\in\mathcal{A}_{\text{uc}}} \tilde{p}_{\text{uc}}(\mathbf{V}) \left(R_{\text{uc}}^{m}(\mathbf{V}) + R_{\text{uc}}^{f}(\mathbf{V})\right)$. This completes the proof.

Theorem 1. together with Proposition 1 suggests the existence of a region around the FBS where the core is nonempty. Thus we establish the rationality of CoMP scheme JT.

7.3 Numerical Results

The distances are measured in meters (m), we locate MBS at $(0, 0)$, FBS at $(1000, 0)$, and FUE $(990, 0)$. Unless otherwise stated, the default maximum transmit power of MBS is 5 W and of FBS is 1 W. The two BSs each has 4 antennas and each UE has 2 antennas. In the coordinated mode of transmission, by default FBS distributes the power evenly among FUE and MUE. The AWGN power is set at 10^{-4} W. In the Fig. 7.2 MUE moves from far negative x region towards the FBS in linear trajectories. One such trajectory is shown in the figure. We mark the region where coordination is preferred over uncoordinated transmission. The symmetry in the region is due to the use of symmetric channel matrices on either side of the FBS in simulation.

In the rest of the figures the trajectory of the MUE is on the x axis (y coordinate is 0). Fig. 7.3 denotes the expansion of the CoMP region as the FBS transmit power increases. We also see from the figure that $R_{\text{c, cor}}$ far exceeds $R_{\text{uc, cor}}$ as MUE approaches FBS inside the region of coordination. In Fig. 7.4 we show on the plan of (x, y) the value of the

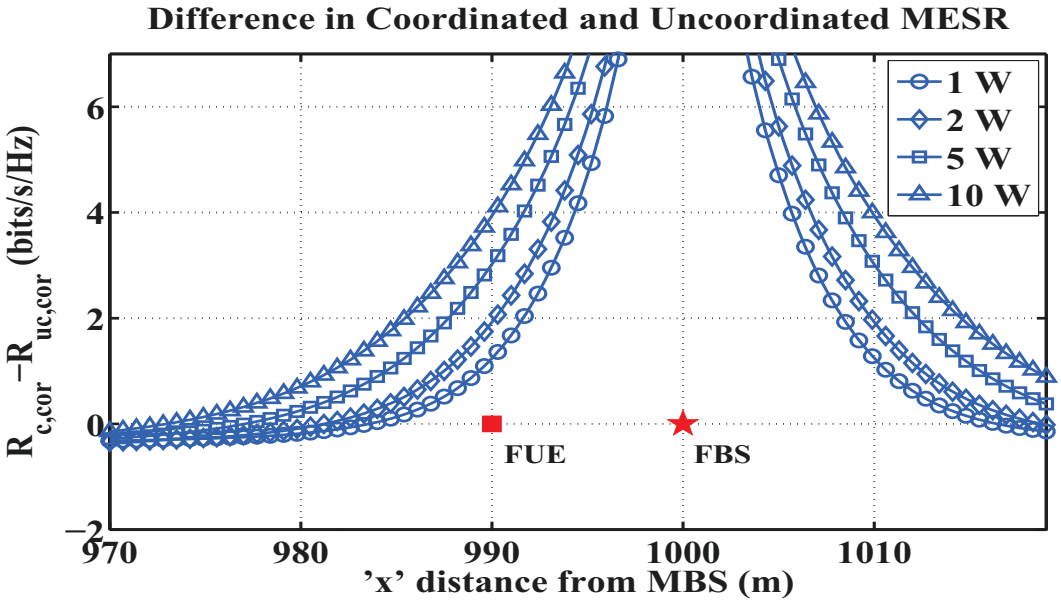

Figure 7.3: Dependence of CoMP region on FBS transmit power.

coalition over the value of uncoordinated system.

In Fig. 7.5 we demonstrate that as the amount of power allocated to MUE increases the *diameter* of the coordination region shrinks. The term diameter is loosely used to mean the distance between the entry point and exit point of CoMP region when the MUE's trajectory is on x axis (y coordinate 0). Consider the two MUE power ratios of a and c such that $c > a$. Then the explanation for the phenomenon seen in Fig. 7.5 is that while operating at ratio c if the FBS switches to CoMP at the coordination boundary of the ratio a then the reduction of FUE rate is higher than the increase in MUE rate as still MUE is further away from FBS than FUE, thus discouraging the formation of the coalition till MUE moves closer to FBS than before.

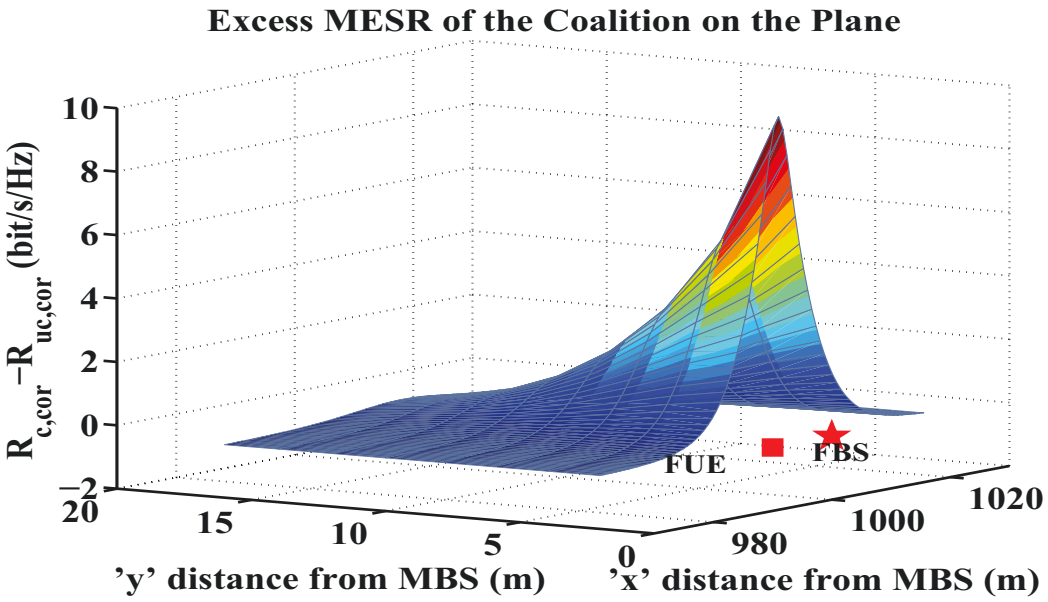

Figure 7.4: Geometric distribution of value of coalition, $v(\mathcal{N})$, over uncoordinated system.

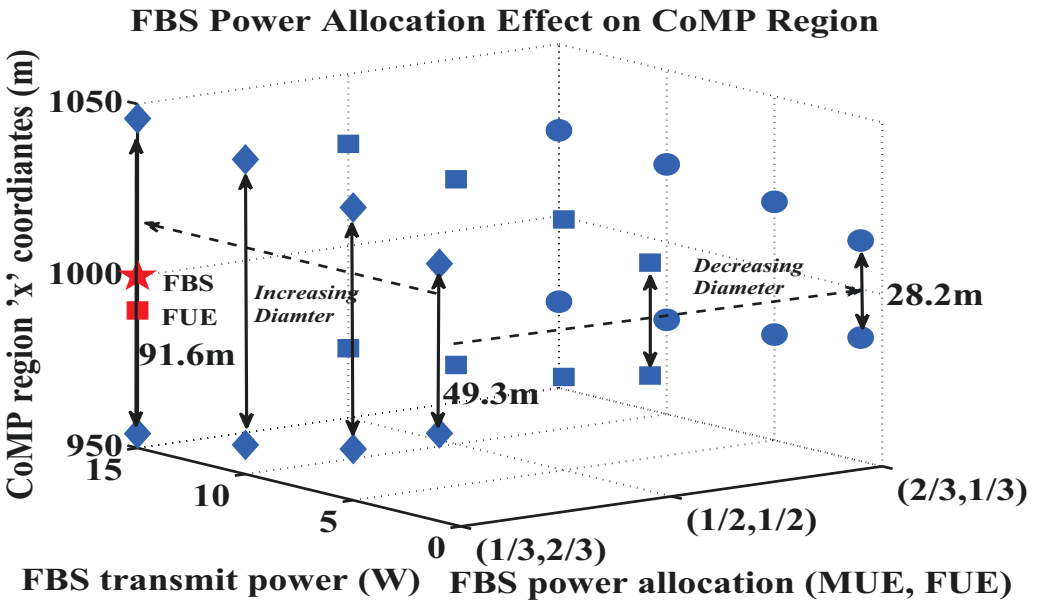

Figure 7.5: The variation of the diameter of the CoMP region with FBS power allocation ratio (a, b).
Here (a, b) implies a, b fractions of power are assigned to MUE and FUE respectively.

Chapter 8

Conclusion

In this thesis, we investigated the problem of resource allocation, routing, beamforming and determing the number of transmit antennas for multicarrier modulation based CR networks. We introduce the resource allocation and routing problem to MIMO-WPM CR ad-hoc networks and give a solution which gives the consideration to the features of BD-GMD in MIMO systems and PUs' priority in CR networks. We validate our proposed scheme by observing average throughput generated by our proposed scheme using three different types of CSI. Additionally we compare the contribution of each method in our proposed scheme to throughput enhancement by designing different test schemes. We address the user scheduling and CSIT feedback problem in network MIMO systems. We propose a two-stage CSIT feedback mechanism and user scheduling methods based on the ergodic rate taking into account the large-scale fading and channel variation. The numerical results indicate that the proposed scheduling methods achieve high user spectral efficiency and fairness with much lower feedback overhead. A linear precoder design which aims at alleviating the interference at PR for OSTBC based CR has been introduced. One of the principal contributions is to endow the conventional prefiltering technique with the excellent features of OSTBC in the context of CR. The prefiltering technique has been optimized for the purpose of maximizing the SNR at SR on the premise that the orthogonality of OSTBC is kept, the interference introduced to PL by SL is maintained under a tolerable level and the total transmitted power constraint is satisfied. Numeral Results have shown that polarization diversity contributes to achieve better SNR at SR, moreover, the increase in number of antennas will significantly delay the arrival of the saturation point for the SNR at SR. In regard to design issues in CSCS, we put forward practical propositions for determining the number of transmit antennas and controlling downlink inter-sub-small cell interference. We found how the factors influence the number of concurrent sojourners

and further impact the number of transmit antennas on sub-small cell APs. We proved and verified that *BDBF* performs better than the interference controller using optimal BF alone for gaining more capacity within a bearably large radius of uncertainty region. We considered the MIMO downlink of a HetNet consisting of a maro- and a femtocell. We devised two non-cooperative games. The first game we considered, $\mathtt{G}_1$, had the two cells in non-CoMP. In the second game $\mathtt{G}_2$ the cells were in CoMP. Then we let each cell work in the respective MESR-CE in each game. Now we defined a third game $\mathtt{G}_3$, which is coalition game in characteristic form with TU. In $\mathtt{G}_3$ the value of the coalition is allowed to be arbitrarily transferred between the two cells via a payment. We use solution mechanism of core to analyze $\mathtt{G}_3$. Then we proved there exists a region where the core of the game $\mathtt{G}_3$ is nonempty. Our results demonstrate that JT is a rational decision in some regions. CoMP decision is reduced to identifying a geographical region defined by threshold d_{th}. Such decision mechanisms for CoMP schemes other than JT and for different channel models can be considered in future work.

Bibliography

[1] J. Mitola III and G. Q. Maguire, Jr., "Cognitive radios: making software radio more personal," *IEEE Pers. Commun.*, vol. 6, no. 4, pp. 13–18, Aug. 1999.

[2] S. Haykin, "Cognitive radios: brain-empowered wireless communications," *IEEE J. Sel. Areas Commu.*, vol. 23, no. 2, pp. 201–220, Feb. 2005.

[3] B. Kouassi, L. Deneire, B. Zayen, R. Knopp, F. Kaltenberger, F. Negro, D. Slock, and I. Ghaur, "Design and implementation of spatial interweave LTE-TDD cognitive radio communication on an experimental platform," *IEEE Wireless Communications,* vol. 20, no. 2, pp. 60-67, Apr. 2013.

[4] J. Xiao, R. Q. Hu, Y. Qian, L. Gong and B. Wang, "Expanding LTE network spectrum with cognitive radios: From concept to implementation," *IEEE Wireless Commun.,* vol. 20, no. 2, pp. 12-19, Apr. 2013.

[5] L. Ding, T. Melodia, S.N. Batalama, J.D. Matyjas, M.J. Medley, "Cross-Layer Routing and Dynamic Spectrum Allocation in Cognitive Radio Ad Hoc Networks," *IEEE Trans. Vehi. Tech.,* vol. 59, no. 4, pp. 1969-1979, May 2010.

[6] Y. Zhang; C. Leung, "A Distributed Algorithm for Resource Allocation in OFDM Cognitive Radio Systems," *IEEE Trans. Vehi. Tech.,*, vol.60, no.2, pp. 546-554, Feb. 2011.

[7] Q. Qu, L.B. Milstein, D.R. Vaman, "Cognitive Radio Based Multi-User Resource Allocation in Mobile Ad Hoc Networks Using Multi-Carrier CDMA Modulation," *IEEE J. Sel. Areas in Commun.*, vol. 26, no. 1, pp. 70-82, Jan. 2008.

[8] S. Kim, G. B. Giannakis, "Optimal Resource Allocation for MIMO Ad Hoc Cognitive Radio Networks," *IEEE Trans. Info. Theory*, vol. 57, no. 5, pp. 3117-3131, May 2011.

[9] C. Gao, Y. Shi, Y. T. Hou, S. Kompella, "On the Throughput of MIMO-Empowered Multihop Cognitive Radio Networks," *IEEE Trans. Mobile Computing*, vol. 10, no. 11, pp. 1505-1519, Nov. 2011.

[10] S. Gao, L. Qian, D. R. Vaman, "Distributed energy efficient spectrum access in cognitive radio wireless ad hoc networks," *IEEE Trans. Wireless Commun.*, vol. 8, no. 10, pp. 5202-5213, October 2009.

[11] Y. Xue, B. Li, K. Nahrstedt, "Optimal resource allocation in wireless ad hoc networks: a price-based approach," *IEEE Trans. Mobile Computing*, vol. 5, no. 4, pp. 347-364, April 2006.

[12] G. Scutari, D. Palomar, and S. Barbarossa, "Competitive Design of Multiuser MIMO Systems Based on Game Theory: A Unied View," *IEEE J. Sel. Areas Commun.*, vol. 26, no. 7, pp. 1089-1103, Sep. 2008.

[13] S. Ye and R. S. Blum, "Optimized Signaling for MIMO Interference Systems With Feedback," *IEEE Trans. Signal Process.*, vol. 51, no. 11, pp. 2839-2848, Nov. 2003.

[14] Rui Zhang, "Cooperative Multi-Cell Block Diagonalization with Per-Base-Station Power Constraints," *IEEE J. Sel. Areas Commun.*, vol. 28, no. 9, pp. 1435-1445, Dec. 2010.

[15] L. Liang, W. Xu, X. Dong, "Limited Feedback-Based Multi-Antenna Relay Broadcast Channels with Block Diagonalization," *IEEE Trans. Wireless Commun.*, vol. 12, no. 8, pp. 4092-4101, Aug. 2013.

[16] X. Zhang, J. Xing, W. Wang, "Outage Analysis of Orthogonal Space–Time Block Code Transmission in Cognitive Relay Networks With Multiple Antennas," *IEEE Trans. Vehi. Tech.*, vol. 62, no. 7, pp. 3503-3508, Sep. 2013.

[17] Wei Ni, I.B. Collings, "A New Adaptive Small-Cell Architecture," *IEEE J. Sel. Areas Commu.*, vol. 31, no. 5, pp. 829-839, May 2013.

[18] W. Wang, G. Yu, A. Huang, "Cognitive radio enhanced interference coordination for femtocell networks," *IEEE Commun. Mag.*, vol. 51, no. 6, pp. 37-43, Jun. 2013.

[19] M. Haddad, S. E. Elayoubi, E. Altman, Z. Altman, "A Hybrid Approach for Radio Resource Management in Heterogeneous Cognitive Networks," *IEEE J. Sel. Areas Commun.*, vol. 29, no. 4, pp. 831-842, Apr. 2011.

[20] M. Wildemeersch, T. Q. S. Quek, C. H. Slump, A. Rabbachin, "Cognitive Small Cell Networks: Energy Efficiency and Trade-Offs," *IEEE Trans. Commun.*, vol. 61, no. 9, pp. 4016-4029, Sep. 2013.

[21] S. Sardellitti, S. Barbarossa, "Joint Optimization of Collaborative Sensing and Radio Resource Allocation in Small-Cell Networks," *IEEE Trans. Signal Process.*, vol. 61, no. 18, pp. 4506-4520, Sep.15, 2013.

[22] F. Pantisano, M. Bennis, W. Saad, M. Debbah, M. Latva-aho, "Interference Alignment for Cooperative Femtocell Networks: A Game-Theoretic Approach," *IEEE Trans. Mobile Computing*, vol. 12, no. 11, pp. 2233-2246, Nov. 2013.

[23] F. Pantisano, M. Bennis, W. Saad, M. Debbah, "Spectrum Leasing as an Incentive Towards Uplink Macrocell and Femtocell Cooperation," *IEEE J. Sel. Areas Commu.*, vol. 30, no. 3, pp. 617-630, Apr. 2012.

[24] C. H. M. de Lima, M. Bennis, M. Latva-aho, "Coordination Mechanisms for Self-Organizing Femtocells in Two-Tier Coexistence Scenarios," *IEEE Trans. Wireless Commun.*, vol. 11, no. 6, pp. 2212-2223, Jun. 2012.

[25] S. Guruacharya, D. Niyato, M. Bennis, D. I. Kim, "Dynamic Coalition Formation for Network MIMO in Small Cell Networks," *IEEE Trans. Wireless Commun.*, vol. 12, no. 10, pp. 5360-5372, Oct. 2013.

[26] Xin Jin, Abdelwaheb Marzouki, Djamal Zeghlache, and Mathew Goonewardena, "Resource Allocation and Routing in MIMO-WPM Cognitive Radio Ad-Hoc Networks," in *Proc. IEEE Vehicular Technology Conference (VTC)-Fall*, Quebec City, Canada, Sep. 2012, pp. 1-5.

[27] Li-Chuan Tseng, Xin Jin, Abdelwaheb Marzouki, and ChingYao Huang, "Downlink Scheduling in Network MIMO Using Two-Stage Channel State Feedback," in *Proc. IEEE Vehicular Technology Conference (VTC)-Fall*, Quebec City, Canada, Sep. 2012, pp. 1-5.

[28] Abdelwaheb Marzouki and Xin Jin, "Precoder Design for Orthogonal Space-Time Block Coding based Cognitive Radio with Polarized Antennas," in *Proc. IEEE International Symposium on Wireless Communication Systems (ISWCS)*, Paris, France, Aug. 2012, pp. 691-695.

[29] Mathew Goonewardena, Xin Jin, Wessam Ajib, and Halima Elbiazey, "Competition vs. Cooperation: A Game-Theoretic Decision Analysis for MIMO HetNets," in *Proc.*

IEEE International Conference on Communications (ICC), Sydney, Australia, Jun. 2014, accepted.

[30] FCC, ET Docket No 03-222 Notice of proposed rule making and order, December 2003.

[31] I. Akyildiz, L. Won-Yeol, M.C. Vuran, and S. Mohanty, "NeXt generation/dynamic spectrum access/cognitive radio wireless networks: A survey," *Computer Networks*, vol. 50, no. 13, pp. 2127 – 2159, 2006.

[32] V. Chakravarthy, X. Li, Z. Wu, M. A. Temple, F. Garber, R. Kannan and A. V. Vasilakos, "Novel overlay/underlay cognitive radio waveforms using SD-SMSE framework to enhance spectrum efficiency-part i: theoretical framework and analysis in AWGN channel," *IEEE Trans. Commun.*, vol. 57, no. 12, pp. 3794-3804, Dec. 2009.

[33] S. Senthuran, A. Anpalagan, and O. Das, "Throughput Analysis of Opportunistic Access Strategies in Hybrid Underlay-Overlay Cognitive Radio Networks," *IEEE Trans. Wireless Commun.*, vol. 11, no. 6, Jun. 2012.

[34] J. Oh and W. Choi, "A Hybrid Cognitive Radio System: A Combination of Underlay and Overlay Approaches," in *Proc. IEEE Vehicular Technology Conference Fall*, pp. 1-5, 6-9 Sep. 2010.

[35] D. Cabric, S. M. Mishra and R.W. Brodersen, "Implementation issues in spectrum sensing for cognitive radio", in Conference Record of the Thirty-Eighth Asilomar Conference on Signals, Systems and Computers, 2004, vol. 1, pp. 772-776, 7-10 Nov. 2004.

[36] G. Bansal, M. J. Hossain, P. Kaligineedi, H. Mercier, C. Nicola, U. Phuyal, M. M. Rashid, K. C. Wavegedara, Z. Hasan, M. Khabbazian, and V. K. Bhargava, "Some research issues in cognitive radio networks," in *Proc. IEEE AFRICON*, Windhoek, Namibia, Sep. 2007, pp. 1–7.

[37] D. Cabric, A. Tkachenko, and R. W. Brodersen, "Experimental study of spectrum sensing based on energy detection and network cooperation," in *Proc. IEEE MILCOM*, 2006.

[38] B. Wang and K. J. R. Liu, "Advances in cognitive radio networks: A survey," *IEEE J. Sel. Topics Signal Process.*, vol. 5, no. 1, pp. 5–23, Jan. 2011.

[39] D.-C. Oh and Y.-H. Lee, "Energy detection based spectrum sensing for sensing error minimization in cognitive radio networks," *Int. J. Commun. Netw. Inf. Security (IJCNIS)*, vol. 1, no. 1, Apr. 2009.

[40] W. A. Gardner, "Exploitation of spectral redundancy in cyclostationary signals," *IEEE Signal Process. Mag.*, vol. 8, no. 2, pp. 14–36, Apr. 1991.

[41] K. Kim, I. A. Akbar, K. K. Bae, J.-S. Um, C. M. Spooner, and J. H. Reed, "Cyclostationary approaches to signal detection and classification in cognitive radio," in *DySPAN 2007*, pp. 212-215, Apr. 2007.

[42] J. Lunden, V. Koivunen, A. Huttunen, and H. V. Poor, "Collaborative cyclostationary spectrum sensing for cognitive radio systems," *IEEE Trans. Signal Process.*, vol. 57, no. 11, pp. 4182–4195, Nov. 2009.

[43] H. Mahmoud, T. Yucek, and H. Arslan, "OFDM for cognitive radio: merits and challenges," *IEEE Wireless Commun.*, vol. 16, no. 2, pp. 6-14, Apr. 2009.

[44] Y. Zhang and L. C., "Resource allocation in an OFDM-based cognitive radio system," *IEEE Trans. Commun.*, vol. 57, no. 7, pp. 1928-1931, Jul. 2009.

[45] S. Wang, M. Ge, W. Zhao, "Energy-Efficient Resource Allocation for OFDM-Based Cognitive Radio Networks," *IEEE Trans. Commun.*, vol. 61, no. 8, pp. 3181-3191, Aug. 2013.

[46] S. Wang, "Efficient resource allocation algorithm for cognitive OFDM systems," *IEEE Commun. Lett.*, vol. 14, no. 8, pp. 725-727, Aug. 2010.

[47] D. Ngo, C. Tellumbra, and H. H. Nguyen, "Resource allocation for OFDM-based cognitive radio multicast networks," in *Proc. IEEE Wireless Commun. and Networking Conf.*, pp. 1–6, Apr. 2009

[48] Z. Hasan, G. Bansal, E. Hossain, V. K. Bhargava, "Energy-efficient power allocation in OFDM-based cognitive radio systems: A risk-return model," *IEEE Trans. Wireless Commun.*, vol. 8, no. 12, pp. 6078-6088, Dec. 2009.

[49] Y. Huang, Q. Li, W.-K. Ma, and S. Zhang, "Robust multicast beamforming for spectrum sharing-based cognitive radios," *IEEE Trans. Signal Process.*, vol. 60, no. 1, pp. 527–533, Jan. 2012.

[50] E. Gharavol, Y.-C. Liang, and K. Mouthaan, "Robust downlink beamforming in multiuser MISO cognitive radio networks with imperfect channel-state information," *IEEE Trans. Veh. Technol.*, vol. 59, no. 6, pp. 2852–2860, Jul. 2010.

[51] Y. Zhang, E. Dall'Anese, and G. B. Giannakis, "Distributed optimal beamformers for cognitive radios robust to channel uncertainties," *IEEE Trans. Signal Process.*, vol. 60, no. 12, pp. 6495–6508, Dec. 2012.

[52] E. Stathakis, M. Skoglund, L.K. Rasmussen, "On Beamforming and Orthogonal Space-Time Coding in Cognitive Networks with Partial CSI," *IEEE Trans. Commu.*, vol. 61, no. 3, pp. 961-972, Mar. 2013.

[53] V. Bohara, S. H. Ting, Y. Han, and A. Pandharipande, "Interferencefree overlay cognitive radio network based on cooperative space time coding," in *Proc. 5th Int. Conf. Cognitive Radio Oriented Wireless Netw. Commun. (CROWNCOM)*, Cannes, France, Jun. 2010, pp. 1–5.

[54] S.-J. Kim and G. B. Giannakis, "Optimal Resource Allocation for MIMO Ad Hoc Cognitive Radio Networks," in *Proceedings of the 46th Annual Allerton Conference on Communication*, Control, and Computing, 2008, pp. 39–45.

[55] F. Huang, S. Wang, and S. Du, "Resource allocation in OFDM-based multi-cell cognitive radio systems," in *Proc. Annual Wireless and Optical Communications Conference (WOCC)*, 2011, pp. 1–5.

[56] S. Wang, Z. Zhou, M. Ge, and C. Wang, "Resource Allocation for Heterogeneous Cognitive Radio Networks with Imperfect Spectrum Sensing," *IEEE J. Sel. Areas Commun.*, vol. 31, no. 3, pp. 464-475, Mar. 2013.

[57] R. Xie, F. Yu, H. Ji, and Y. Li, "Energy-efficient resource allocation for heterogeneous cognitive radio networks with femtocells," *IEEE Trans. Wireless Commun.*, vol. 11, no. 11, pp. 3910–3920, Nov. 2012.

[58] L.M. Cortes-Pena, "MIMO Space-Time Block Coding (STBC): Simulation and Results," EC6604 *Personal and Mobile Communications Presented to Dr. Gorden stuber*, apr.-2009.

[59] D. Gesbert, M. Shafi, D. Shiu, P. Smith, and A. Naguib, "From theory to practice: an overview of MIMO space-time coded wireless systems," *IEEE J. Sel. Areas Commun.*, vol. 21, no. 3, pp. 281–302, 2003.

[60] D. Tse and P. Viswanath, *Fundamentals of Wireless Communication*. Cambridge University Press, 2005.

[61] I. Telatar, "Capacity of multi-antenna Gaussian channels," Eur. Trans. Telecommun., vol. 10, no. 6, pp. 585–595, Nov./Dec. 1999.

[62] A. Goldsmith, *Wireless Communications*. Cambridge University Press, 2005.

[63] V. Bohara, S. H. Ting, Y. Han, and A. Pandharipande, "Interferencefree overlay cognitive radio network based on cooperative space time coding," in *Proc. 5th Int. Conf. Cognitive Radio Oriented Wireless Netw. Commun. (CROWNCOM)*, Cannes, France, Jun. 2010, pp. 1–5.

[64] M. Hoch, "Comparsion of ConvOFDM and Wavelet-OFDM for Narrow-Band Powerline Communications," in *Proc. of 15th International OFDM Workshop*, Hamburg, Germany, September 2010, pp. 190–194.

[65] M. K. Lakshmanan, H. Nikookar, "A review of wavelets for digital wireless communication," *Wireless Personal Communications, Springer Netherlands*, Volume 37, No. 3-4, May 2006, pp. 387-420.

[66] U. Khan, S. Baig and M. J. Mughal, "Performance Comparison of Wavelet Packet Modulation and OFDM over Multipath Wireless Channel with Narrowband Interference," *International Journal of Electrical and Computer Sciences*, vol. 9, no. 9, pp. 17-18, Feb., 2009.

[67] M. Oltean, M. Nafornita, "Efficient Pulse Shaping and Robust Data Transmission Using Wavelets", in *Proc. 2007 IEEE International Symposium on Intelligent Signal Processing*, Oct. 3-5, pp. 43-48, ISBN: 1-4244-0829-6.

[68] S. Tripathi, A. Rastogi, K. Sachdeva, M. Sharma, P. Sharma, "PAPR Reduction in OFDM System using DWT with Non linear High Power Amplifier," *International Journal of Innovative Technology and Exploring Engineering (IJITEE)* ISSN: 2278-3075, Volume-2, Issue-5, April 2013.

[69] M. LALLART, K. E. NOLAN, P. SUTTON, and L. E. DOYLE, "On-The-Fly Synchronization Using Wavelet and Wavelet Packet OFDM," In Proc. PIMRC 2008.

[70] I. I. Anusha and P. Mullick, *Multicarrier Modulation for Wireless Communication using Wavelet Packets*. Ethesis@nitr, 2012.

[71] H. J. Taha and M. F. M. Salleh, "Performance Comparison of Wavelet Packet Transform (WPT) and FFT-OFDM System Based on QAM Modulation Parameters in Fading Channels," *WSEAS Transactions on Communications*, vol. 9, no. 8, Aug. 2010.

[72] P. P. Vaidyanathan, *Multirate Systems and Filter Banks*. Prentice Hall, 1993.

[73] A. Jamin and P. Mahonen, "Wavelet packet modulation for wireless communications," *Wireless Communications and Mobile Computing Journal*, vol.5, no. 2, Mar. 2005.

[74] D. Karamehmedovic, M.K.Lakshmanan, and H.Nikookar, "Optimal Wavelet Design for Multicarrier Modulation with Time Synchronization Error," in *Proc. IEEE GLOBECOM'09*, Nov. 30 2009-Dec. 4 2009.

[75] T.S. Rappaport, *Wireless Communications*. Prentice Hall, 2002.

[76] V. Brik, S. Rayanchu, S. Saha, S. Sen, V. Shrivastava, and S. Banerjee, "A measurement study of a commercial-grade urban WiFi mesh," in *Proc. ACM/USENIX IMC*, Oct. 2008, pp. 111-124.

[77] *Fading Channels, Communications system Toolbox, MathWorks.*

[78] M. K. Lakshmanan, I. Budiarjo, and H. Nikookar, " Wavelet packet multicarrier modulation based spectrum pooling systems with low mutual interference," in *Proc. IEEE VTC'09*, Sep. 2009.

[79] A. Jamin and P. Mahonen, "Wavelet packet modulation for wireless communications," *Wireless Commun. and Mobile Computing*, vol.5, no.2, pp.123–137, Mar. 2005.

[80] M. K. Lakshmanan, I. Budiarjo and H. Nikookar, "Wavelet Packet Multi-carrier Modulation MIMO Based Cognitive Radio Systems with VBLAST Receiver Architecture," in *Proc. IEEE WCNC'08*, Mar. 31 2008–Apr. 3 2008.

[81] S. Lin, Winston. W. L. Ho and Y. C. Liang, "Block Diagonal Geometric Mean Decomposition (BD-GMD) for MIMO Broadcast Channels," *IEEE Trans. Wireless Commun.*, vol. 7, no. 7, pp. 2778–2789, Jul. 2008.

[82] Simon Haykin. Adaptive Filter Theory. Prentice-Hall, Inc, 1996.

[83] S. Coleri, M. Ergen, A. Puri, and A. Baha, "Channel Estimation Techniques Based on Pilot Arrangement in OFDM Systems," *IEEE Trans. Broadcasting*, vol. 48, no. 3, pp. 223–229, Sep. 2002

[84] Ed. W.C. Jakes, Jr. *Microwave Mobile Communications*. New York: Wiley, 1974.

[85] Z. R. Zaidi and B. L. Mark, "Mobility Tracking Based on Autoregressive Models," *IEEE Trans. Mobile computing*, vol. 10, no. 1, pp. 32–43, Jan. 2011.

[86] H. Hijazi and L. Ros, "Joint data QR-detection and Kalman estimation for OFDM time-varying Rayleigh channel complex gains," *IEEE Trans. Commun.*, vol. 58, no. 1, pp. 170–178, 2010.

[87] L. Ying, S. Shakkottai and A. Reddy, "On Combining Shortest-Path and Back-Pressure Routing Over Multihop Wireless Networks," in *Proc. IEEE INFOCOM'09*, Apr. 19-25 2009.

[88] Q. H. Spencer, A. L. Swindlehurst, and M. Haardt, "Zero-forcing methods for downlink spatial multiplexing in multiuser MIMO channels," *IEEE Trans. Signal Processing.*, vol. 52, no. 2, pp. 461–471, 2004.

[89] J. Zhang, R. Chen, J. Andrews, A. Ghosh, and R. Heath, "Networked mimo with clustered linear precoding," *IEEE Trans. Wireless Commun.*, vol. 8, no. 4, pp. 1910–1921, 2009.

[90] Z. Shen, R. Chen, J. G. Andrews, R. W. Heath, and B. L. Evans, "Low complexity user selection algorithms for multiuser mimo systems with block diagonalization," *IEEE Trans. Signal Process.*, vol. 54, no. 9, pp. 3658–3663, 2006.

[91] S. Sigdel and W. Krzymien, "User scheduling for network mimo systems with successive zero-forcing precoding," in *Proc. IEEE Vehicular Technology Conference (VTC)'10–Fall*, 2010, pp. 1-6.

[92] J. Zhang, J. Andrews, and R. Heath, "Block diagonalization in the mimo broadcast channel with delayed csit," in *Proc. IEEE Global Telecommunications Conference (GLOBECOM)'09*, 2009, pp. 1-6.

[93] H. Shirani-Mehr, G. Caire, and M. J. Neely, "MIMO downlink scheduling with non-perfect channel state knowledge," *IEEE Trans. Commun.*, vol. 58, no. 7, pp. 2055–2066, 2010.

[94] C. Min, N. Chang, J. Cha, and J. Kang, "Mimo-ofdm downlink channel prediction for ieee802.16e systems using kalman filter," in *Proc. IEEE Wireless Communications and Networking Conference (WCNC)'07*, pp.942-946, 2007.

[95] A. Lozano and A. M. Tulino, "Capacity of multiple-transmit multiplereceive antenna architectures," *IEEE Trans. Information Theory.*, vol. 48, no. 12, pp. 3117–3128, 2002.

[96] J. Wishart, "The generalised product moment distribution in samples from a normal multivariate population," *Biometrika 20A (1-2): 32-52*, 1928.

[97] A. Gupta and D. Nagar, *Matrix variate distributions*. Chapman & Hall/CRC, 2000, vol. 104.

[98] H. G. Borgos, "Partitioning of a line segment," 1997.

[99] R. Jain, D. Chiu, and W. Hawe, "A quantitative measure of fairness and discrimination for resource allocation in shared computer systems," *DEC Research Report TR-301*, 1984.

[100] Y.-C. Liang, K.-C. Chen, G.-Y. Li, P. Mahonen, "Cognitive Radio Networking and Communications: An Overview," *IEEE Trans. Vehicular Technology*, vol. 60, no. 7, pp. 3386-3407, Sept. 2011.

[101] A. Hoang, Y. Liang, and M. Islam, "Power control and channel allocation in cognitive radio networks with primary users' cooperation," *IEEE Trans. Mobile Comput.*, vol. 9, no. 3, pp. 348–360, Mar. 2010.

[102] R.-C. Xie, F.-R. Yu, H. Ji, "Dynamic Resource Allocation for Heterogeneous Services in Cognitive Radio Networks With Imperfect Channel Sensing," *IEEE Trans. Vehicular Technology*, vol. 61, no. 2, pp. 770–780, Feb. 2012.

[103] R. Prasad and A. Chockalingam, "Precoder Optimization in Cognitive Radio with Interference Constraints," in *Proc. IEEE ICC* 2011.

[104] M. Jung, K. Hwang, and S. Choi, "Interference Minimization Approach to Precoding Scheme in MIMO-Based Cognitive Radio Networks," *IEEE Commun. Lett.*, vol. 15, no. 8, pp. 789–791, Aug. 2011.

[105] K. T. Phan, S. A. Vorobyov, N. D. Sidiropoulos, and C. Tellambura, "Spectrum sharing in wireless networks: A QoS-aware secondary multicast approach with worst user performance optimization," in *Proc. IEEE SAM'08*, pp. 23–27, Jul. 2008.

[106] A. Punchihewa, V.-K. Bhargava, C. Despins, "Linear Precoding for Orthogonal Space-Time Block Coded MIMO-OFDM Cognitive Radio," *IEEE Trans. Commun.*, vol. 59, no. 3, pp. 767–779, Mar. 2011.

[107] S. Shahbazpanahi, M. Beheshti, A. B. Gershman, M. GharaviAlkhansari, and K. M. Wong, "Minimum variance linear receivers for multiaccess MIMO wireless systems with space–time block coding," *IEEE Trans. Signal Process.*, vol. 52, no. 12, pp. 3306–3313, Dec. 2004.

[108] R. G. Lorenz and S. P. Boyd, "Robust minimum variance beamforming," *IEEE Trans. Signal Process.*, vol. 53, no. 5, pp. 1684–1696, May 2005.

[109] C. D. Richmond, "Capon algorithm mean squared error threshold SNR prediction and probability of resolution," *IEEE Trans. Signal Process.*, vol. 53, no. 8, pp. 2748–2764, Aug. 2005

[110] 3GPP TR 25.996 V10.0.0, "Spatial channel model for MIMO simulations," www.3gpp.org, Mar. 2011.

[111] R. L. G. Cavalcante and I. Yamada, "Multiaccess interference suppression in OSTBC-MIMO systems by adaptive projected subgradient method," *IEEE Trans. Signal Process.*, vol. 56, no. 3, pp. 1028–1042, Mar. 2008.

[112] M. Gharavi-Alkhansari and A. B. Gershman, "Constellation space invariance of orthogonal space–time block codes," *IEEE Trans. Inf. Theory*, vol. 51, no. 1, pp. 331–334, Jan. 2005.

[113] S. M. Alamouti, "A simple transmit diversity technique for wireless communications," *IEEE J. Sel. Areas Commun.*, vol. 16, no. 8, pp. 1451–1458, Oct. 1998.

[114] V. Tarokh, H. Javarkhani and Calderbank, "Space-time block codes from orthogonal designs," *IEEE Transactions on Information Theory*, vol. 45, no. 5, July 1999, pp. 1456-1467.

[115] J. Hoydis, M. Kobayashi, and M. Debbah, "Green Small-Cell Networks," *IEEE Veh. Technol. Mag.*, vol. 6, no. 1, pp. 37-43, 2011.

[116] I. Ashraf, F. Boccardi and L. Ho, "Sleep mode techniques for small cell deployment," *IEEE Comm. Mag.*, vol. 49, no. 8, pp. 72-79, Aug 2011.

[117] Q. Li, G. Li, W. Lee, M. il Lee, D. Mazzarese, B. Clerckx, and Z. Li, "MIMO techniques in WiMAX and LTE: a feature overview," *IEEE Comm. Mag.*, vol. 48, no. 5, pp. 86–92, May. 2010.

[118] J. Lee, J.-K. Han *et al.*, "MIMO Technologies in 3GPP LTE and LTE-Advanced," *EURASIP Journal on Wireless Communications and Networking*, vol. 2009, 2009.

[119] H. Sung, S.-R. Lee, and I. Lee, "Generalized channel inversion methods for multiuser MIMO systems," *IEEE Trans. Commun.*, vol. 57, Nov. 2009.

[120] R. Chen, Z. Shen, J. G. Andrews, and R. W. Heath, "Multimode transmission for multiuser MIMO systems with block diagonalization," *IEEE Trans. Signal Process.*, vol. 56, no. 7, pp. 3294–3302, Jul. 2008.

[121] L. Liu, R. Chen, S. Geirhofer, K. Sayana, Z. Shi and Y. Zhou, "Downlink MIMO in LTE-Advanced: SU-MIMO vs. MU-MIMO," *IEEE Comm. Mag.*, vol. 50, no.2, pp.140-147, February 2012.

[122] M. Costa, "Writing on dirty paper," *IEEE Trans. Inf. Theory*, vol. 29, no. 3, pp. 439–441, May 1983.

[123] A. Khina and U. Erez, "On the robustness of dirty paper coding," *IEEE Trans. Commun.*, vol. 58, no. 5, pp. 1437 –1446, May 2010.

[124] N. Jindal, W. Rhee, S. Vishwanath, S. A. Jafar, and A. Goldsmith, "Sum power iterative water-filling for multi-antenna Gaussian broadcast channels," *IEEE Trans. Info. Theory*, vol. 51, no. 4, pp. 1570–1580, Apr. 2005.

[125] Z. Hasan, H. Boostanimehr, and V. K. Bhargava, "Green cellular networks: A survey, some research issues and challenges," *IEEE Commun. Surveys Tuts.*, vol. 13, no. 4, pp. 524–540, Fourth Quarter, 2011.

[126] V. Chakravarthy, Z. Wu, M. Temple, F. Garber, R. Kannan, and A. Vasilakos, "Novel overlay/underlay cognitive radio waveforms using SD-SMSE framework to enhance spectrum efficiency–part I: theoretical framework and analysis in AWGN channel," *IEEE Trans. Commun.*, vol. 57, Dec. 2009.

[127] Z. Shen, R. Chen, J. G. Andrews, R. W. Heath Jr., and B. L. Evans, "Low complexity user selection algorithms for multiuser MIMO systems with block diagonalization," *IEEE Trans. Signal Processing*, vol. 54, no. 9, pp. 3658–3663, Sept. 2006.

[128] S. Sigdel and W. A. Krzymien, "Simplified fair scheduling and antenna selection algorithms for multiuser MIMO orthogonal space division multiplexing downlink," *IEEE Trans. Veh. Technol.*, vol.58, no.3, pp.1329–1344, March 2009.

[129] F. Bause and G. Horvath, "Fitting Markovian Arrival Processes by Incorporating Correlation into Phase Type Renewal Processes," in *Proc. of the 7th International Conference on Quantitative Evaluation of SysTems (QEST 2010)*, pages 97,Äì106. IEEE Computer Society, 2010.

[130] A. Ghosh, R. Jana, V. Ramaswami, J. Rowland, and N. Shankaranarayanan, "Modeling and characterization of large-scale Wi-Fi traffic in public hot-spots," in *Proc. of IEEE INFOCOM*, Shanghai, China, Apr. 2011.

[131] Q. Zhao and B. M. Sadler, "A survey of dynamic spectrum access," *IEEE Sig. Proc. Mag.*, vol.24, no.3, pp.79–89, May 2007.

[132] Y. Zhang, E. Dall'Anese, and G. B. Giannakis, "Distributed Optimal Beamformers for Cognitive Radios Robust to Channel Uncertainties," *IEEE Trans. Sig. Proc.*, vol.60, no.12, pp.6495-6508, Dec. 2012.

[133] T. Al-Khasib, M. Shenouda, and L. Lampee, "Dynamic spectrum management for multiple-antenna cognitive radio systems: Designs with imperfect CSI," *IEEE Trans. Wireless Commun.*, vol.10, no.9, pp.2850–2859, Sep. 2011.

[134] S. Ekin, M. M. Abdallah, K. A. Qaraqe, E. Serpedin, "Random Subcarrier Allocation in OFDM-Based Cognitive Radio Networks," *IEEE Trans. Sig. Proc.*, vol. 60, no.9, pp.4758-4774, Sep. 2012.

[135] G. Zheng, K.-K. Wong, and B. Ottersten, "Robust cognitive beamforming with bounded channel uncertainties," *IEEE Trans. Sig. Proc.*, vol.57, no.12, pp.4871–4881, Dec. 2009.

[136] V. A. Yakubovich, "S-procedure in nonlinear control theory," *Vestnik Leningrad Univ.*, vol.4, no.1, pp.73–93, 1977.

[137] S. Boyd and L. Vandenberghe, *Convex Optimization*. Cambridge University Press, 2004.

[138] M. Grant and S. Boyd, "CVX: Matlab software for disciplined convex programming, version 1.21," http://cvxr.com/cvx, Apr. 2011.

[139] S. Asmussen, O. Nerman, and M. Olsson, "Fitting Phase-Type Distributions via the EM Algorithm," *Scandinavian Journal of Statistics*, vol. 23, no. 4, pp. 419-441, 1996.

[140] EMpht, http://home.imf.au.dk/asmus/pspapers.html.

[141] J. Andrews, H. Claussen, M. Dohler, S. Rangan, and M. Reed, "Femtocells: Past, present, and future," *IEEE J. Sel. Areas Commun.*, vol. 30, no. 3, pp. 497–508, 2012.

[142] T. Zahir, K. Arshad, A. Nakata, and K. Moessner, "Interference management in femtocells," *IEEE Commun. Surveys Tuts.*, vol. 15, no. 1, pp. 293–311, 2013.

[143] M. Sawahashi, Y. Kishiyama, A. Morimoto, D. Nishikawa, and M. Tanno, "Coordinated multipoint transmission/reception techniques for lte-advanced [coordinated and distributed mimo]," *IEEE Wireless Commun. Mag.*, vol. 17, no. 3, pp. 26–34, 2010.

[144] X. Kang, R. Zhang, and M. Motani, "Price-based resource allocation for spectrum-sharing femtocell networks: A stackelberg game approach," *IEEE J. Sel. Areas Commun.*, vol. 30, no. 3, pp. 538–549, 2012.

[145] S. Buzzi, G. Colavolpe, D. Saturnino, and A. Zappone, "Potential games for energy-efficient power control and subcarrier allocation in uplink multicell ofdma systems," *IEEE J. Sel. Topics Signal Process.*, vol. 6, no. 2, pp. 89–103, 2012.

[146] J. Huang and V. Krishnamurthy, "Cognitive base stations in lte/3gpp femtocells: A correlated equilibrium game-theoretic approach," *IEEE Trans. Commun.*, vol. 59, no. 12, pp. 3485–3493, 2011.

[147] M. Bennis, S. M. Perlaza, and M. Debbah, "Learning coarse correlated equilibria in two-tier wireless networks," in *Proc. IEEE International Conference on Communications (ICC)*, 2012, pp. 1592–1596.

[148] W.-S. Lai, M.-E. Chiang, S.-C. Lee, and T.-S. Lee, "Game theoretic distributed dynamic resource allocation with interference avoidance in cognitive femtocell networks," in *Proc. IEEE Wireless Communications and Networking Conference (WCNC)*, 2013, pp. 3364–3369.

[149] F. Pantisano, M. Bennis, W. Saad, R. Verdone, and M. Latva-aho, "Coalition formation games for femtocell interference management: A recursive core approach," in *Proc. IEEE Wireless Communications and Networking Conference (WCNC)*, 2011, pp. 1161–1166.

[150] Z. Zhang, L. Song, Z. Han, W. Saad, and Z. Lu, "Overlapping coalition formation games for cooperative interference management in small cell networks," in *Proc. IEEE Wireless Communications and Networking Conference (WCNC)*, 2013, pp. 643–648.

[151] F. Pantisano, M. Bennis, W. Saad, and M. Debbah, "Spectrum leasing as an incentive towards uplink macrocell and femtocell cooperation," *IEEE J. Sel. Areas Commun.*, vol. 30, no. 3, pp. 617–630, 2012.

[152] B. Ma, M. Cheung, and W. V.W.S., "Interference management for multimedia femtocell networks with coalition formation game," in *Proc. IEEE International Conference on Communications (ICC)*, 2013, pp. 4705–4710.

[153] S. Mathur, L. Sankar, and N. B. Mandayam, "Coalitions in cooperative wireless networks," *IEEE J. Sel. Areas Commun.*, vol. 26, no. 7, pp. 1104–1115, 2008.

[154] D. Gesbert, H. Bolcskei, D. Gore, and A. Paulraj, "Outdoor mimo wireless channels: models and performance prediction," *IEEE Trans. Commun.*, vol. 50, no. 12, pp. 1926–1934, 2002.

[155] S. Christensen, R. Agarwal, E. Carvalho, and J. Cioffi, "Weighted sumrate maximization using weighted mmse for mimo-bc beamforming design," *IEEE Trans. Wireless Commun.*, vol. 7, no. 12, pp. 4792–4799, 2008.

[156] W. Saad, Z. Han, M. Debbah, A. Hjorungnes, and T. Basar, "Coalitional game theory for communication networks," *IEEE Signal Process. Mag.*, vol. 26, no. 5, pp. 77–97, 2009.

[157] N. Nisan, T. Roughgarden, E. Tardos, and V. V. Vazirani, *Algorithmic game theory*. Cambridge University Press, 2007.

[158] R. Horn and C. Johnson, *Matrix Analysis*. Cambridge University Press, 2012.

[159] Y.-H. Nam, L. Liu, Y. Wang, C. Zhang, J. Cho, and J.-K. Han, "Cooperative communication technologies for lte-advanced," in *Proc. IEEE International Conference on Acoustics Speech and Signal Processing (ICASSP)*, 2010, pp. 5610–5613.

[160] J. Franklin, *Matrix Theory*, ser. Dover Books on Mathematics. Dover Publications, 2000.

List of f gures

List of tables